5-2014

Characterization of Eocene-Oligocene Depocenters in Prydz Bay, East Antarctica : A Lithostratigraphic Correlation of ODP Sites 739, 742, and 1166

Daniel James Ciarletta

MONTCLAIR STATE UNIVERSITY

Characterization of Eocene-Oligocene Depocenters in Prydz Bay, East Antarctica: A Lithostratigraphic Correlation of ODP Sites 739, 742, and 1166

By

Daniel James Ciarletta

A Master's Thesis Submitted to the Faculty of

Montclair State University

In Partial Fulfillment of the Requirements

For the Degree of

Master of Science

May 2014

School College of Science and Mathematics

Department Earth & Environmental Studies

Thesis Committee:

[redacted]

Thesis Sponsor: Dr. Sandra Passchier

[redacted]

Committee Member: Dr. Tanya Blacic

[redacted]

Committee Member: Dr. Josh Galster

ABSTRACT

The Eocene-Oligocene transition (EOT) marked a profound shift in the Earth's climate, as the global greenhouse of the early Cenozoic gave way to 'icehouse' conditions, or a climatic regime influenced by the waxing and waning of glacial ice. Antarctica was dramatically altered during this time; its formerly cool temperate ecosystems nearly obliterated by the first major episode of continental glaciation. A record of this transition appears to be partly preserved in approximately half a kilometer of sediments recovered from three holes (at ODP Sites 739, 742, and 1166) bored in the continental margin at Prydz Bay, an embayment of the East Antarctic coast. Until recently, these holes were never completely described with common nomenclature and analysis. This study re-evaluated these cores under a unified regime, using a laser particle sizer to generate matrix grain size distribution profiles for 253 samples collected from the combined sediment column. Additional analysis of select samples was performed with a scanning electron microscope to classify grain textures, as well as ICP-OES to provide geochemical information. The results of this study support stratigraphic relationships between the ODP sites that were previously only inferred through seismic acquisition. This provides a much more complete picture of the sedimentation processes occurring through the EOT. Chemical and microtextural weathering signals also provide a new window into the environment of Prydz Bay during the EOT. These signals seem to confirm hypotheses from previous researches that the site featured a cool/temperate environment with tidewater glacial systems in the late Eocene that transitioned into near polar glacier conditions dominated by ice sheet growth by the early Oligocene. Crucially, the results of this investigation suggest that enhanced glaciation of the Prydz Bay region was already occurring before the start of the Oligocene, which suggests that an initial step down in global temperature during the late Eocene (proxied from the foraminiferal oxygen isotope record) may be directly related to the initiation of continental ice expansion.

CHARACTERIZATION OF EOCENE-OLIGOCENE DEPOCENTERS IN PRYDZ BAY, EAST ANTARCTICA: A LITHOSTRATIGRAPHIC CORRELATION OF ODP SITES 739, 742, AND 1166

A THESIS

Submitted in partial fulfillment of the requirements

For the degree of Master of Science

By

Daniel James Ciarletta

Montclair State University

Montclair, NJ

May 2014

ACKNOWLEDGEMENTS

Foremost, I would like to thank Dr. Sandra Passchier for giving me the opportunity work on this investigation, as well as my thesis committee members, Dr. Tanya Blacic and Dr. Josh Galster, for offering their time and input. I would like to thank the National Science Foundation for financially supporting this investigation, as well as all previous investigators who contributed to the study of Prydz Bay, who have built up a collective pool of knowledge I strive to contribute something meaningful to. I would also like to thank all the students of the graduate office for their exceptional camaraderie over the course of this investigation and during my studies at Montclair State University. And I would especially like to thank my family and friends for all their support, as well as my girlfriend, Kim, whose love and wittiness has made this past year outstanding.

TABLE OF CONTENTS

FIGURES

TABLES

1. INTRODUCTION

1.1 Overview

The aim of this investigation is to characterize the sediment depocenters active during the Eocene-Oligocene transition (EOT) between approximately 33.7 and 33.9 million year ago (mya) at the mouth of Prydz Bay, a major embayment of the East Antarctic coast lying within the Australian Sector. The EOT is thought to be a time of profound change on the Antarctic continent, marking the demise of greenhouse conditions and the first shift to 'icehouse' conditions, or a climatic regime influenced by the waxing and waning of glacial ice (Kennett, 1977). The understanding of this time period within the realm of Antarctica is confined to several boreholes drilled in the margin of the continent, three of which were drilled into the continental shelf at the mouth of Prydz Bay. Currently, sedimentological analysis of cores recovered from these holes leaves many uncertainties regarding the geologic history of the region. One of the most important questions is how the strata drilled by these cores relate to each other spatially and temporally. By re-examining the cores in greater detail, this project hopes to determine to what degree the cores interact with a horizontally continuous sequence of sedimentary units, attempting to at least partially reconstruct the temporal and spatial components of depocenter succession.

This investigation also seeks to evaluate the extent to which the sedimentary record reflects changes in ice growth, particularly in relation to two positive oxygen isotope excursion events, EOT-1 and Oi-1, which are thought to define the onset of the icehouse (Coxall et al., 2005). Whether ice growth occurred in a stepwise process or was more gradual or abrupt remains a significant question. Understanding the timing and duration of suspected growth events as interpreted from the sediment cores will likely

have a significant impact on ice and climate modeling across the EOT (Stocchi et al., 2013).

1.2 Geologic Setting of Prydz Bay

1.2.1 Structural History

Prydz Bay is a major embayment of the Indian Ocean-fronting portion of East Antarctica, lying within the Australian Sector. This deep and extensive incision into the hinterlands of the continent is thought to be several orders of age older than the earliest known continental scale glaciations and may be the longest lived drainage system of the East Antarctic Ice Sheet (Harrowfield et al., 2005, Taylor et al., 2004).

The origins of Prydz Bay lie in the formation of the Lambert Graben, the tectonic structure which underlies the topographic depression. The Lambert Graben is described as an aulacogen in an intra-continental rift system that existed during Permian time between present day East Antarctica and India-Australia (Whitehead et al., 2006, Cooper et al., 1991). This failed rift was subsequently filled in by a thick sequence of Permian through Cenozoic sediment, estimated to be at least 5 km thick (Cooper et al., 1991, Harrowfield et al., 2005).

Harrowfield et al. (2005) elaborate on the Permian rifting, suggesting a greater than 6000 km long shelf parallel basin was created, compartmentalized by multiple cross-basin accommodation zones. These accommodation zones are thought to have exhibited increasingly transtensional characteristics towards southern Africa, and it is suspected that one of these zones was responsible for the creation of the Lambert Graben (Harrowfield et al., 2005). Subsequent rifting from late Cretaceous time into the Paleogene eventually resulted in the full breakup of India-Australia from the Antarctic continent, isolating the Lambert Graben (Cande, 2004).

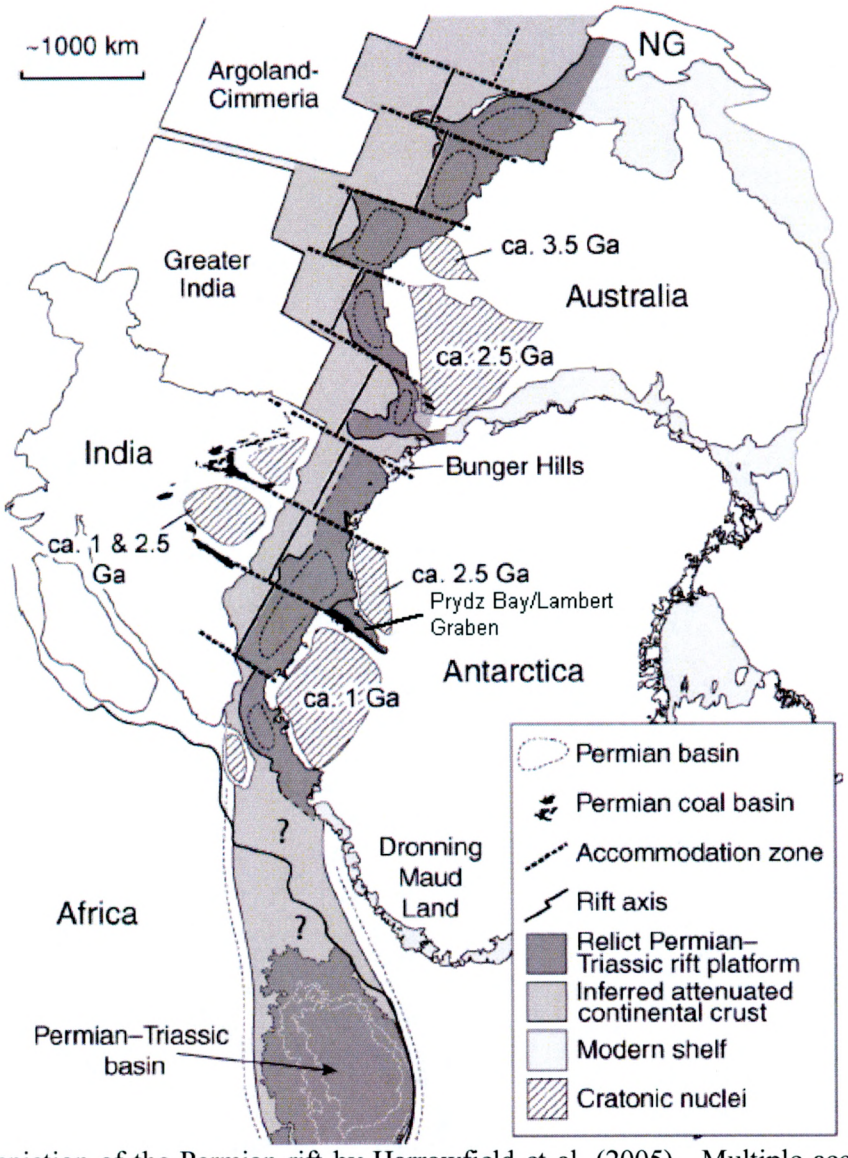

Figure 1. Depiction of the Permian rift by Harrowfield et al. (2005). Multiple accommodation zones offset the rift perpendicular to the direction of extension. Note that Prydz Bay/Lambert Graben has been labeled in the central area of the map.

1.2.2 Pre-Cenozoic Sedimentary Geology

From the late Paleozoic through the Triassic, the more inland portions of the Lambert Graben received sediments that would ultimately form the rocks of the Amery Group (Harrowfield et al., 2005). These rocks are today exposed within the Prince Charles Mountains, which flank the western side of the graben, comprising what is believed to be the greatest exposure of rock in the eastern part of the continent (Holdgate et al., 2005).

The Amery Group is described by Holdgate et al. (2005) as consisting of at least 3000 meters of carbonaceous sandstones, siltstones, and conglomerates believed to have been deposited in alluvial through lacustrine environments. Approximately 1000 meters of the Amery Group are associated with the Permian Bainmedart Coal Measures, which are composed of fluvial deposits featuring over a hundred known coal seams. Some of these seams are as much as 10 meters in thickness (Holdgate et al., 2005).

1.3 Climate History

1.3.1 Cretaceous to Eocene

Based on pollen and spores recovered from Cretaceous units, the climate of Prydz Bay during the latest Mesozoic is inferred to have been substantially milder than today. The environment during this time is described by Macphail & Truswell (2004) as being non-marine or marginally marine, primarily constituting Austral conifer woodland. The contemporary climate associated with this particular biome is cited as being moderately humid and temperate, although given the high latitude at Prydz Bay the local plant community would have been additionally subjected to substantial periods of low light and cold temperatures that would have likely produced conditions similar to those experienced in forests growing near the tree line in the modern day northern hemisphere (Macphail & Truswell, 2004).

By the late Eocene, conditions that had existed during Cretaceous time had not drastically changed at Prydz Bay. Using fossil plant remains, pollen, spores, and dinocysts recovered from relevant stratigraphic units, Macphail & Truswell (2004) were able to approximate that the environment during this period was a coastal cool-temperate rainforest. The plant community is specifically cited as being composed of Southern

Beech (*Nothofagus*), coniferous *Araucariaceae* and *Podocarpaceae* trees/scrub, and many species of low-growing flowering plants (Cantrill & Poole, 2012, Macphail & Truswell, 2004). Mean annual temperature is thought to have averaged less than 12 °C, with freezing winters, and rainfall estimated to have been as much as 1200 to 1500 mm per year, with generally high humidity (Cantrill & Poole, 2012).

1.3.2 Eocene-Oligocene Transition

During the Eocene-Oligocene transition (EOT), significant changes in climate are inferred to have affected the Antarctic continent, substantially impacting local geological processes and radically altering terrestrial ecosystems. Starting at about 33.9 million years ago, the ratio of oxygen-18 versus oxygen-16, or $\delta^{18}O$, analyzed from benthic foraminifera (a proxy for ice growth since oxygen-16 is more abundantly incorporated into ice derived from meteoric water) begins to show a significant positive excursion (Coxall et al., 2005, DeConto et al., 2008). This first excursion event is referred to as the EOT-1 and may coincide with global ocean cooling of approximately 2.5 °C, along with enhanced glaciation on land (Lear et al., 2007). The second event, the Oi-1, which occurred about 200,000 years later, is a much larger $\delta^{18}O$ excursion and may have coincided with the widespread continental glaciation on Antarctica. (Figure 2 demonstrates the aforementioned change in $\delta^{18}O$ from ODP Site 1218, which is located in the central Pacific Ocean.) Foraminiferal $\delta^{18}O$ from ODP Site 738, which was drilled into the Kerguelen Plateau opposite Prydz Bay, shows this event is consistent with a large increase in ice rafted debris (IRD) at that location, which may be indicative of substantial ice sheet growth on the order of tens of thousands of years (Scher et al., 2011).

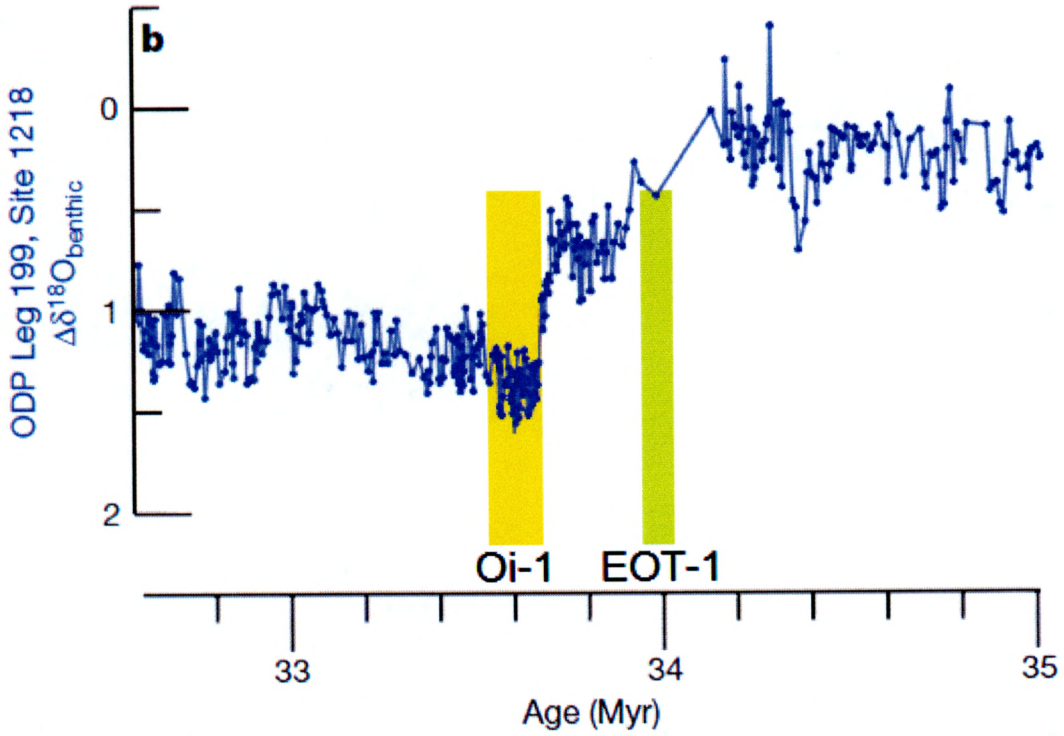

Figure 2. Change in foraminiferal $\delta^{18}O$ from ODP Site 1218 in the central Pacific. Note the double step in positive changes starting around 34 mya. The green bar highlights the position of the EOT-1 event, while the yellow bar highlights the position of the Oi-1 event. Figure modified from DeConto et al. (2008), original credit to Coxall et al. (2005).

1.4 Study Locations and Interpretations from Drilling Legs

Knowledge of the geologic record regarding the EOT in the southern high latitudes leaves much to be desired. This is primarily because there are only a handful of drill sites that have been explored on the Antarctic margin (in particular the East Antarctic margin) with recovered cores spanning this period of time. Three of these borehole locations lie along the continental shelf at the mouth of Prydz Bay. These are Sites 739 (Hole C) and 742 (Hole A), which were visited during Ocean Drilling Program (ODP) Leg 119, and Site 1166 (Hole A), which was visited during ODP Leg 188. (See Figure 3)

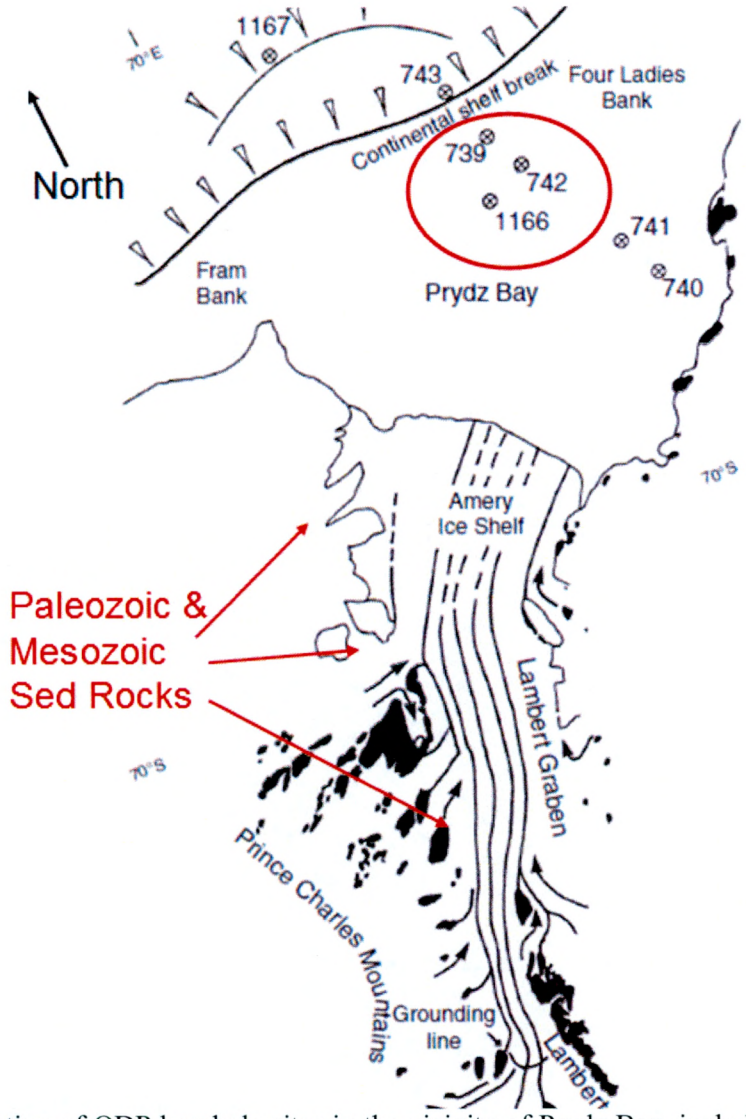

Figure 3. Location of ODP borehole sites in the vicinity of Prydz Bay, including Sites 739, 742, and 1166, highlighted by red circle. Nearby boreholes outside the red circle (which do not penetrate EOT stratigraphy) and location of Amery Group Paleozoic and Mesozoic sedimentary rocks are also indicated. Dark shaded regions represent portions of the Prince Charles Mountains exposed above contemporary ice cover. Figure modified from Erohina et al. (2004) with original credit to Hambrey & McKelvey (2000).

The history of these borings, which are suspected to partly span the EOT, has already been explored to some degree, but much work still remains to be done in order to more effectively ascertain their temporal and lithologic relationships. Presently, much of what is known about the lithology and stratigraphy of these sites is derived from seismic acquisition, shipboard logs, and reports associated with the drilling expeditions.

Sediments thought to have been deposited at the time of the EOT at sites 742 and 739 are suspected as being at least partly glaciogenic by Cooper et al. (1991) and Hambrey et al. (1991) in the Leg 119 reports. This suspicion is described, citing other work by Cooper & Webb (1990) and Webb (1990), as partly from a result of a comprehensive review of Antarctic and global climate proxies up to 1991. At that time, according to the aforementioned works, glacial conditions in Antarctica by the earliest Oligocene had already been inferred as a possibility from climate isotopic records. The general observation that stratigraphic units on the Antarctic shelf (that had been dated with palynology) also displayed alternating steeply dipping foresets and topsets was further equated with glacial activity (Webb, 1990). Additionally, Cooper & Webb (1990) cite work by LeMasurier (1970) who found evidence of volcanic rock in contact with ice during the Eocene in Marie Byrd Land, suggesting that glacial conditions at that location might be indicative of glacial conditions elsewhere on the continent at the time.

Thus, when sediments were recovered in Leg 119 that visually appeared to be glacial diamictites (Barron et al., 1989), this was believed to bolster existing inferences from proxies. In the analysis of the sediment by Hambrey et al. (1991), mechanical grain size analysis generally showed that EOT material from Site 742 contained clay-silt-sand fractions of 20-35% clay, 20-25% silt, and 40-50% sand, while material from Site 739 was approximately in the range of 20-25% clay, 20-50% silt, and 20-50% sand. With these fractions, Hambrey et al. (1991) agreed with the visual analysis that the sediments were actually diamictites. Hambrey et al. (1991) further note that visual estimation of the gravel component for both sites primarily fluctuated between 1-5% for the relevant stratigraphic sections.

Subsequent later drilling at Site 1166 during Leg 188 penetrated deeper into the stratigraphy of Prydz Bay than previously achieved during Leg 119, attempting to core suspected pre-glacial/glacial transition units (O'Brien et al., 2001). Much of the mid-late Eocene and EOT cores recovered at this site (stratigraphically below the intervals at Sites 742 and 739 per Erohina et al. [2004]) contained poorly sorted coarse to very coarse sands with plant/organic fragments, based on visual logging. This lithology, on the assumption that it was indicative of a transition to possible glacial conditions inferred from overlying stratigraphy, was described as being indicative of a pre-glacial alluvial environment and/or a glacial outwash complex (O'Brien et al., 2001). Later work by Strand et al. (2003) examining quartz grain microtextures with scanning electron microscope found evidence of both fluvial and glacial modification of grain surfaces in the mid-late Eocene and EOT cores of Site 1166, potentially corroborating the interpretations of O'Brien et al. (2001) in the Leg 188 reports.

This study seeks to update the aforementioned existing knowledge base by performing analyses that were never accomplished on the Prydz Bay core sections when they recovered a decade or more ago. Given the great expense and planning necessary to recover and store sediments from the EOT units around the continent, it is imperative that the maximum amount of information be derived from the relevant drill sites. Primary sampling and sedimentological description using a standardized sediment classification scheme for the Leg 188 and Leg 119 core sections has for the most part not occurred since around the time of the 1988 and 2001 expeditions. Thus, re-examining cores from Holes 1166A, 742A, and 739C, may yield new and valuable data, potentially offering insights and research directions that were not manifest in investigations tied to the drilling operations.

1.5 Age Model

Much of what is understood about the ages of the Prydz Bay cores is broadly applied, with the age of material in sections loosely constrained based on studies accomplished in tandem with the drilling operation. However, some additional development has been made recently, particularly with regard to placing the Oi-1 event. Houben et al. (2013) provided a dinoflagellate cyst datum, constrained by *Malvinia escutiana*, which was found to not exist before the onset of the Oligocene. Cysts of this species were subsequently identified in a core section of Hole 739C at 310.73 meters below seafloor (mbsf). On the basis of other Oligocene taxa found above this position (up to 169.0 mbsf), as well as Eocene taxa observed below this point (to bottom of hole), it was suggested that this location marks the Oi-1 event in the Prydz Bay cores (Houben et al., 2011). Above 169.0 mbsf, a shift in diatom assemblages with an associated change in lithology suggests a Miocene age (Baldauf & Barron, 1991).

For Hole 742A, recovery of palynomorphs (dinocysts, pollen, spores, etc) was sparse, but the majority of material found between 171.3 and 315.0 mbsf has been dated to the Eocene (Truswell, 1991). However, Truswell (1991) noted several intervals below 190.0 mbsf that contained pollen from the Permian. On the basis of Permian pollen that had previously been recovered from the onshore Amery Group, pollen from Site 742 was inferred by Truswell to have been recycled from material derived from the Prince Charles Mountains and is not indicative of the true age of the unit. Seismic analysis indicates the topmost portion of Hole 742A in its EOT section (171.3 to ~230 mbsf) may partly overlap the same units preserved in the bottom of Hole 739C (Cooper et al., 1991).

The lowermost two meters below seafloor in Hole 742A (313.0 to 315.0 mbsf) were noted to contain an abundance of Cretaceous palynomorphs (lacking Eocene

material), with no dinocysts or other marine microfossils present, suggesting a terrestrial origin (Truswell, 1991). This was initially inferred to mean the section might be of Cretaceous age, but analysis of seismic data by Erohina et al. (2004) strongly suggests that this material is above the Cretaceous unconformity underlying the Cenozoic sediments of Prydz Bay. More likely, this particular section is composed of terrestrial material recycled from the Cretaceous. Hambrey (1991) also mentions that there are plant remains in this section, but they cannot be conclusively dated.

In Hole 1166A, all sediment between 142.5 mbsf and the bottom of hole (266.8 mbsf) contained palynomorphs that dated to the Eocene, with an abundance of dinocysts and diatoms in the upper part of the hole (142.5 to 220.85 mbsf) and a relative paucity in the lower section (below 220.85 mbsf). This suggests a transition from a marginal marine/terrestrial environment to an open marine setting (Macphail & Truswell, 2004). Additionally, Macphail & Truswell (2004) note that some Cretaceous palynomorphs are present in the lowermost part of 1166A, but they suggest these are recycled, existing in clasts from that time period. Interestingly, Erohina et al. (2004) infers based on seismic interpretation that the very bottom of Hole 742A might penetrate the same unit as the lower part of Hole 1166A, which suggests that recycled Cretaceous material in both holes may be of shared depositional lineage. Erohina et al. (2004) also notes that a probable unconformity divides the Eocene material at Site 1166. (This surface may therefore be present at Site 742 if the aforementioned stratigraphic relation to Site 1166 can be established.) Figure, 4, at the end of this section, illustrates the location of this and other significant unconformities, and Table 1 indicates the relative ages of the sediment intervals they divide.

Unlike Holes 739C and 742A, Hole 1166A actually contains a potentially interpretable magnetic signature in the top of its uppermost section (135.41 to 148.0 mbsf) (Florindo et al., 2003). This interval contains a reverse polarity inclination down to 136.2 mbsf, followed by normal polarity inclination to 148.0 mbsf. On the basis of biostratigraphy, Florindo et al. (2004) suggested this interval may record chron 13n with chron 12r (earliest Oligocene, ~30.9 to 33.5 mya). However, chron 15n with 13r (primarily late Eocene, ~33.5 to 34.8 mya) and 17n with 16r (late Eocene ~36.3 to 37.4 mya) are also equally if not more probable, particularly since diatom evidence does not support an Oligocene age (Florindo et al., 2004). It is therefore suspected that the upper EOT unit at Site 1166 actually records an interval of time prior to the Oi-1 event. (Additionally, depending on what chrons are used in interpretation, the upper unit may be at least partly older than the EOT-1.)

How much further back in time the lowermost part of Hole 1166A extends into the Eocene remains unknown. Macphail & Truswell (2004) note that some of the few dinocysts recovered from the lower interval of 1166A are associated with "trans-antarctic flora", which ranged between approximately the late early Eocene to Oligocene. Based on this, Macphail & Truswell (2004) estimated this lowermost section of 1166A to be middle to late Eocene in age, with a much broader margin of approximation than overlying material.

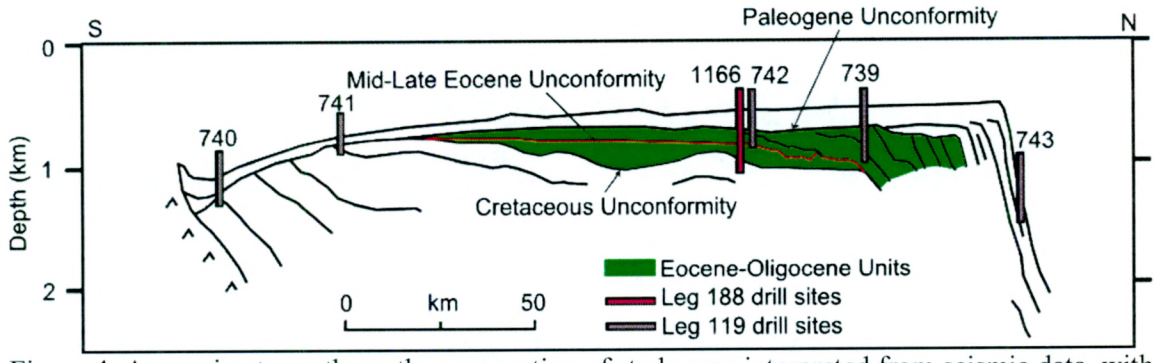

Figure 4. Approximate north-south cross section of study area interpreted from seismic data, with locations of drill sites from Legs 188 and 119. Intervals believed to span the middle-late Eocene and early Oligocene are colored in green. Significant unconformities seen in the seismic data and recognized from biostratigraphy include a Cretaceous unconformity, which underlies the middle-late Eocene (pre-EOT) sediment, a middle-late Eocene unconformity, which is overlain by latest Eocene to Early Oligocene (EOT) sediments, and a Paleogene unconformity, above which all sediment is thought to have been deposited post-Oligocene. Figure is modified from Erohina et al. (2004), with original credit to Cooper et al. (1991).

Table 1. Age model for Sites 1166, 742, and 739, based on biological/magnetic control, and featuring correlations from seismic interpretation.

Site 1166	Site 742	Site 739
Palynomoprhs found between 142.5 and 266.8 mbsf dated to Eocene. Taxa above this interval are post-Oligocene, and taxa below date to Cretaceous. (Macphail & Truswell, 2004)	Seismic analysis indicates the topmost portion of Site 742 in its Eocene section (171.3 to ~230 mbsf) may partly overlap the same units preserved in the bottom of Site 739. (Cooper et al., 1991)	Shift in diatom assemblages above 169.0 mbsf suggest Miocene age. (Baldauf & Barron, 1991)
Magnetics, correlated with biostratigraphy, suggest chrons 15n/13r or 17n/16r may be present between 135.41 and 148.0 mbsf. This would equate to late Eocene age, possibly post EOT-1. (Florindo et al., 2004)	Palynomoprhs found between 171.3 and 315.0 mbsf dated to Eocene. Overlying units post-Oligocene. (Truswell, 1991)	*Malvinia escutiana* dinocyst appearance at 310.73 mbsf indicates probable onset of Oligocene. Eocene dinocyst taxa located below this level extend to bottom of hole. (Houben et al., 2011)
Some dinocysts recovered below 220.0 mbsf, down to 266.8 mbsf, are part of the "trans-antarctic flora" and could be as old as middle Eocene. (Macphail & Truswell, 2004)	Seismic analysis indicates bottom few meters of Site 742 may be part of same unit as lowest Eocene interval of Site 1166. Despite presence of Cretaceous palynomoprhs noted by Truswell (1991), seismic indicates all cores from Site 742 above Cretaceous unconformity. (Erohina et al., 2004)	

Key
Biological Control
Magnetic Control
Seismic Correlation

2. METHODS

2.1 Overview

Investigation of the study area and drill sites was divided into multiple components. These included seismic interpretation, updated logging of core sections, laser particle sizer derived grain size analysis, scanning electron microscope assisted grain surface texture analysis, and use of Inductively Coupled Plasma Optical Emissions Spectrometer (ICP-OES) to derive chemical index of alteration (CIA) and various geochemical ratios.

2.2 Seismic Interpretation

Prior to physical analysis of the core sections, a seismic investigation of Prydz Bay was performed using multi-channel seismic profiles available from the Antarctic Seismic Data Library System (SDLS). Seismic lines were originally collected by the Australian Bureau of Mineral Resources (BMR) Expedition 33 in 1982 (Stagg, 1985) and later uploaded in digital format to SDLS, accessible in both processed/pre-filtered TIFF and raw SEGY formats. The former was viewable in GeoMapApp software, a package developed and sustained by Lamont-Doherty Earth Observatory and the U.S. National Science Foundation backed Integrated Earth Data Applications (Ryan et al., 2009).

Using GeoMapApp, major reflectors were traced across the Expedition 33 seismic lines and exported in point ASCII format. Previous seismic interpretations (with correlation to sediment cores) performed by Cooper et al. (1991) and Erohina et al. (2004) were consulted during and after the tracing process to compare results. Traced reflectors were subsequently correlated with each other using cross lines and grouped together to create a loose reflector surface. These were then used to create reflector grids in Golden Software's Surfer program using nearest neighbor interpolation at 0.04 degree

spacing. (Note that grids were created as square grids, so the narrowing effect of longitude at higher latitude actually enhances cell resolution slightly in the south.)

Using Surfer, subtraction was performed between reflector grids, generating the thickness intervals or *isopachs* of intervening sedimentary units. For the purpose of interpretation within the focus of this investigation, two isopach maps were generated. One shows the thickness of the middle-late Eocene (pre-EOT) sediment identified in the age model, and the other displays the thickness of overlying late Eocene-Oligocene (EOT) sediment laid down above the middle-late Eocene unconformity. The reflectors used to derive these maps additionally constitute a lowermost unconformity between the middle-late Eocene interval and underlying Cretaceous sediments and another unconformity between the EOT interval and overlying suspected Miocene units (Erohina et al., 2004, Cooper et al., 1991). See Figure 4, in Age Model, section 1.5, for illustration.

2.3 Core Logging and Grain Size Analysis

The Eocene-Oligocene sections of cores recovered from ODP Sites 1166, 742, and 739 were re-examined at the Gulf Coast Repository at Texas A&M University, College Station, Texas in July, 2013. Cores were visually re-described and photographed for the first time since their initial logging by the shipboard scientific party during expeditions in 1988 (739, 742) and 2001 (1166). (Re-description was deemed necessary, as the expeditions used different classification schemes during the initial logging.) More importantly, core sections were sampled for investigation. Visual core description summaries are included in Appendix B.

Samples from the cores were purposefully taken to provide a high level of detail across the Eocene-Oligocene boundary. Each individual core section was sampled at least once, however, additional samples were procured from individual sections if sufficient changes in the lithologic character were noted. A total of 253 samples covering a combined drilled interval of 584.39 meters were extracted from these Prydz Bay cores.

A Malvern Mastersizer 2000 laser particle sizer was used to measure the matrix grain sizes in the aforementioned sediment samples, with particle size detection in the range 0.02 to 2000 μm. (Gravel fraction was recorded separately based on visual logging in Appendix B.) Like a mechanical sieve stack, this machine partitions grain diameter, however, it accomplishes this by quantifying the diameter of each grain size class using laser diffractometry. The specific diffraction theory used to determine the grain size is Mie theory, which estimates grain diameter via extinction efficiency, which is described as an effect of scatter and absorption (Sperazza et al., 2004).

The laser particle sizer is purported to have a very high level of instrumental precision, reported by Sperazza et al. (2004) to generate an uncertainty of approximately 1%. However, the accuracy of results is subject to two major parameters, namely pump speed and obscuration. Obscuration is related to the quantity of material in suspension, being a function of the ability of light to pass through aliquot material loaded in the instrument. In order to produce consistent precision, Sperazza et al. (2004) suggested the optimal working obscuration was between 15-20% for fine grain sediments. Coarser sediments, however, were observed to have more consistent precision at higher obscurations, near 25% (Sperazza et al., 2004). For pump speed, best results are suggested to occur between 1800 to 2300 rpm, with lower speeds not sufficient to evenly

suspend coarse particles, and higher speeds causing excessive reading of the fine fraction (Sperazza et al., 2004).

For analysis of the Prydz Bay samples, pump speeds and obscurations followed the standard operating procedure for measuring sediments. This method utilizes a pump speed of 2200 rpm, with a default acceptable 'green line' obscuration range of 10-20%. However, given the coarseness of the samples from the cores (which were observed to have significant fractions in the coarse to very coarse sand range), the optimal obscuration was expected to occur at a higher range. Thus, the optimal obscuration was inferred to be 20-30%, with a minimum-maximum possible range of approximately 10-40%.

Pre-treatment of samples for the laser particle sizer followed the *Sample Pretreatment for Sediments with Negligible Biogenic Silica* and *Sample Pretreatment for Sediments with Small Amounts of Biogenic Silica*, part of the standard operating procedure approved by Montclair State University for using the laser particle sizer. These treatments are based on the work of Konert & Vandenberghe (1997). They are similar, except that removal of biogenic silica includes some additional steps. (See Appendix A for detailed sample preparation.) The determination to use one method or the other was based on whether silica/opal or diatoms had been reported at or near the sample location. For cores from Sites 742 and 739, opal content was approximated by Hambrey et al. (1991) using diatoms found in smear slides. For cores from Site 1166, silica was estimated by the shipboard scientific party per O'Brien et al. (2001) from interstitial water geochemistry, which was correlated to diatom abundance.

Post-processing of laser particle sizer results converted raw particle sizes (as percentage of volume) into visual grain size distributions using Excel spreadsheets.

Grain size statistics were also computed for each sample, comprising mean grain size (in terms of ϕ), standard deviation, skew, and kurtosis. Calculations used to generate these statistics were derived from Blott & Pye (2001) in their description of GRADISTAT, a grain size statistics calculation package. The particular method utilized for this analysis followed the logarithmic methods of moments, which was updated from Folk (1974).

2.4 Scanning Electron Microscope – Microtexture Analysis

Surface textures of sediment grains as viewed via SEM, specifically quartz grains, have proven useful for identifying the environments that a grain has been subjected to (Krinsley & Doornkamp, 1973). This environmental history can often be complex, with multiple generations of textures present. For example, grains that have been subjected to glacial weathering may display conchoidal fracturing. If these grains also display gouges and abrasions superimposed on these fractures, it may be indicative of further reworking (Margolis & Kennet, 1970).

For this investigation, a Hitachi S-3400N scanning electron microscope (SEM) was used to analyze the surface textures of sediment grains sampled from Sites 739, 742, and 1166 to determine their environmental origin and weathering state. This was not performed on all 253 samples used for grain size, but rather a subset of these indicative of seven distinct sedimentological units identified from the laser particle analysis. Specific microtexture classifications were derived from Krinsley & Doornkamp (1973) and Mahaney et al. (1996).

Grains with a diameter of 63 μm to 2000 μm were taken randomly from each sample in order to provide an approximation of the grain textures for corresponding intervals. These were initially separated from the main sample mass by wet screening

through a 63 μm mesh. (The fine fraction <63 μm was separately collected and stored for ICP analysis). Grains were then washed with Millipore filtered water (not with SnCl as per Strand et al. [2003] and others) in order to preserve surface features. They were then dried in a drying oven at 75°C and stored in a labeled dish. Forty quartz grains were tentatively selected from each sample using fine tweezers under magnification. They were later mounted for SEM analysis on an aluminum stub using carbon adhesive. (Composition of the grains was subsequently verified using a Bruker AXS Xflash X-Ray Detector [XRD].)

To obtain the SEM imagery, micrographs derived from secondary electron emission were utilized in conjunction with gold coating of the aforementioned grains. This is the process that has been used throughout multiple quartz grain texture studies dating from the early 1970s to the present. The accelerating voltages utilized in these investigations have varied slightly, for example, with 15 kV used by Helland et al. (1997) and 12 kV used by Strand et al. (2003). In the course of this investigation, accelerating voltages between 12 and 15 kV were utilized, owing to subjectivity in producing adequate imagery. Slight variations in settings were logged during micrograph acquisition to ensure the imaging process is replicable by future investigators.

The process of describing and quantifying grain textures utilized a system of abundance ranks and descriptive metrics to classify the incidence of specific textures. During acquisition, frequency and presence of microtextures were ranked according to Newsome & Ladd (1999), which divided abundance into four classes: <2% surface area = not present, 2-25% surface area = present, 25-50% surface area = abundant, and >75% = very abundant. Sphericity and roundness of individual particles were quantified using the Powers (1953) scale. Processed textural abundances were subsequently brought into

the PAST statistics software (Hammer et al., 2001) in order to compare samples against each other. The software was utilized to generate a correlation table, as well as a principal component analysis, using surface microtextures to differentiate the samples.

2.5 ICP-OES – Geochemistry

A Horiba Jobin-Yvon Ultima Inductively Coupled Plasma Optical Emission Spectrometer (ICP-OES) was utilized to derive major and trace element abundance for the fine fraction (<63 μm) of the subset of samples selected previously for SEM texture analysis. This was used to calculate the chemical index of alteration (CIA), as well as determine several geochemical ratios, including Al/Ti, Fe/Ti, K/Na, Al/Na, Zr/Sc, and Sr/Ba. Guidelines for preparing samples for ICP-OES generally followed the setup of Murray et al. (2000), although the process in this case closely mirrors the previous work performed on glacial sediments at Montclair State University by Hansen (2011). As part of this method, multiple replicates of one of the samples and a rock standard were run in order to establish accuracy and precision for the instrument. (The accuracy and precision analysis is included in Appendix C.) Processed geochemical ratios and CIA were later brought into the PAST software to create a principal component analysis in order to determine the degree of separation amongst the samples.

Of the geochemical metrics mentioned, perhaps the most useful in differentiating the samples is the CIA, which was first proposed by Nesbitt and Young (1982). Calculating this parameter potentially allows for two inferences. First, the purpose of the CIA is to determine weathering history. This means differences and similarities in the weathering environment that produced the samples should be quantifiable. Second, changes in environment could be correlated to changes in other geochemical ratios,

which might further bolster the notion of a shift in sediment supply. This last point is particularly relevant if glacial activity is reworking material deposited at an earlier time. This would also have implications for SEM textures, perhaps being able to help distinguish the ordering of texture events and vice versa.

The Al/Ti ratio is useful due to its potential to in some ways distinguish the source of sediments based on the titanium and aluminum content of parent material. Specifically, the ratio considers the variation of titanium and aluminum between mafic, intermediate, and felsic rock sources, with lower ratios suggestive of a mafic source and higher ratios coincident with a felsic source (Taylor and McLennan, 1985). By tracking changes in this ratio through the range of samples, subsequent changes in sediment supply might be inferred.

The other geochemical ratios are primarily useful for determining weathering state. Fe/Ti (using the oxide states), for instance, may be useful because iron has been demonstrated to leach out of detrital rocks faster than titanium, particularly under conditions where substantial quantities of ilmenite grains are present (Morad, 1986) (Force, 1991). Weibel (2003) more explicitly defines the leaching environment, stating removal of iron probably occurs mostly in the saturated zone of soils. Here, iron is oxidized from ilmenite grains and is likely removed through diffusion, with the process potentially being enhanced by the presence of organic acids in groundwater. This process can create detrital rutiles –titanium oxide minerals. It is important to note that Weibel's analysis, however, focused on sandstones, while this investigation uses the mud fraction for the geochemistry. While this would seem to present an issue, Morad (1986) incorporated shales into his analysis and presented similar results, suggesting that mudrocks can be similarly depleted in iron content.

K/Na and Al/Na are similar to Fe/Ti in the sense that sodium is more reactive (and thus, more easily removed during chemical alteration) than either potassium or aluminum, which makes these ratios useful for determining weathering state (Yang et al., 2006). This is bolstered by Yang et al. (2004), who noted that both the K/Na and Al/Na ratios had a significant degree of correlation with the CIA in their study of Chinese river sediments. How well these ratios respond with CIA in a high latitude climate with potential marine influence remains to be seen, although the inclusion of these ratios in the investigation is seen as useful, since a greater quantity of variables in a multi-variate analysis should enhance statistical differentiation.

Another ratio included in this analysis is Sr/Ba, which follows this same trend as K/Na, Al/Na, and Fe/Ti, with strontium being the more reactive component in this ratio. (Yang et al., 2006) However, Sun et al. (2005), citing earlier work under Sun et al. (2000), notes that Sr/Ba is also sensitive to marine versus terrestrial deposition. Sun does not go on to define exactly why this is true, but a possibility is that this has to do with seawater being enriched in strontium relative to meteoric water (Burton, 1990). This would imply the presence of authigenic minerals, perhaps some form of carbonate with strontium substituted for calcium. How this ratio works with sediments from this study is not entirely clear, as Sun et al. (2005) do not define how this ratio responds to other environmental factors, or if it is subjective of particle size or biogenic influences. (In the Sun et al. [2005] study, grains were ground to ~75 μm for ICP analysis rather than being sieved.) However, as with the other weathering ratios, this ratio is included for the sake of increasing the number of variables in the geochemistry analysis.

3. RESULTS

3.1 Laser Particle Sizer

Grain size distribution curves (size ϕ versus percent volume of sample) and a complete table of grain size statistics for all samples, including clay-silt-sand fraction, mean ϕ, skew, standard deviation, and kurtosis (and interpretation of values for skew, standard deviation, and kurtosis) are presented separately in Appendix A. Below is shown a comparison of the Eocene-Oligocene sections of all three sites, based on average matrix grain size determined by the laser particle sizer (Figure 5, next page). Note that all core sections averaged in the silt range, although with variations from coarse to very fine silt. An observation from visual logging, the presence of coal clasts, is also included in this figure, indicated by gray shading. Coal clasts were seen throughout 1166A, as well as the lower part of 742A. Another figure is shown below the first, illustrating each hole with accompanying area plot of percentage clay-silt-sand fraction, as well as bar graphs of standard deviation and kurtosis (Figure 6).

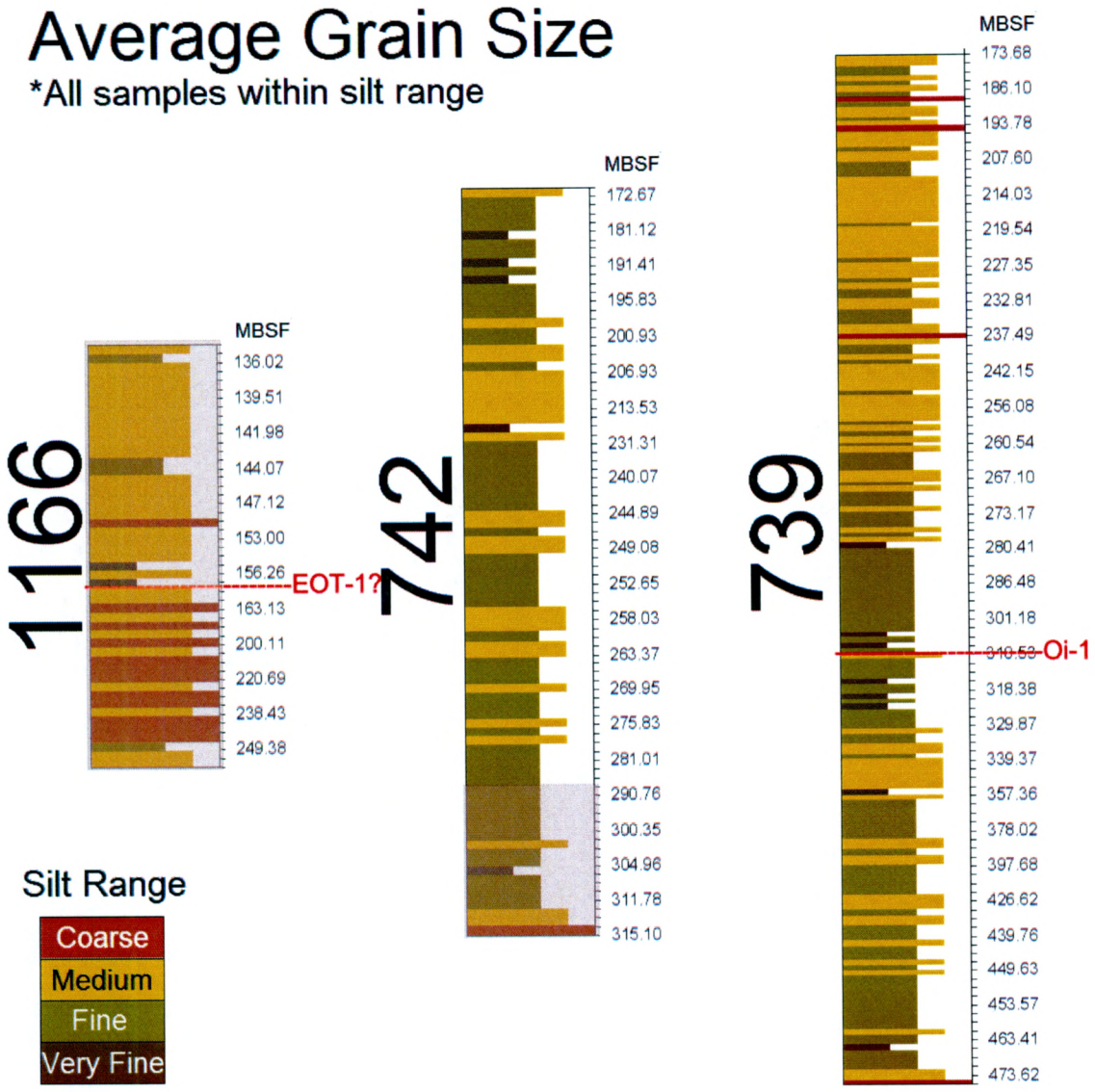

Figure 5. Eocene-Oligocene cores from Holes 1166A, 742A, and 739C, shown side by side with laser particle sizer derived average matrix grain sizes for each sample (253 samples in total). All average grain sizes were within the silt range. Depth in meters below seafloor (aligned to middle of each sample increment) is shown to the right of each core. A key is provided, color coding the average grain sizes for categories of coarse, medium, fine, and very fine silt. Possible position of EOT-1 is based on magnetics from Florindo et al. (2003) and palynology from Macphail & Truswell (2004). Oi-1 placement is per Houben et al. (2011). Also shown is observation of coal clasts from visual logging of lithology, indicated by sections highlighted in gray.

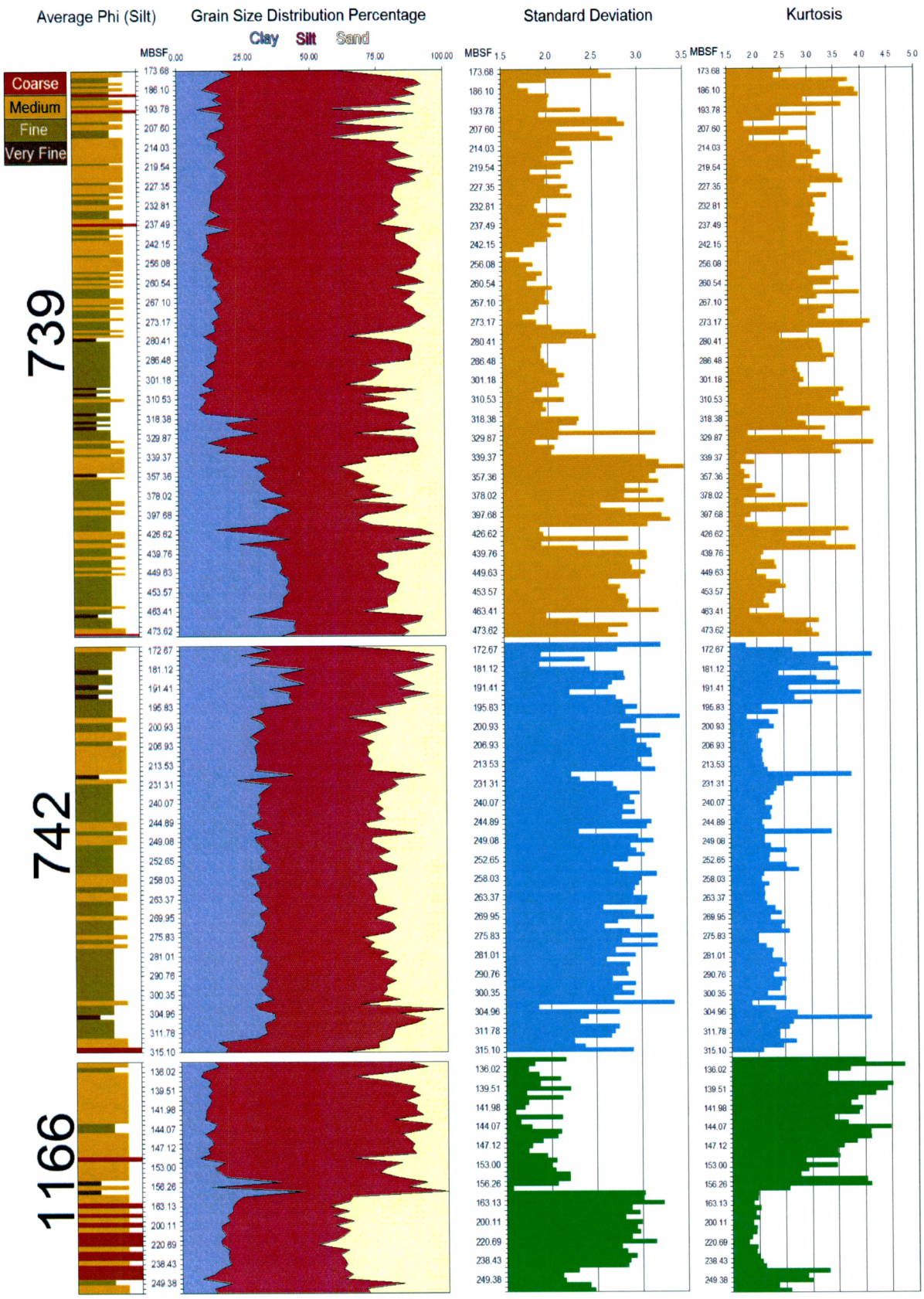

Figure 6. Eocene-Oligocene core sections from Holes 1166A, 742A, and 739C displayed stacked on top of each other (not to imply stratigraphic relation), with accompanying percentage of matrix clay-silt-sand, and graphs of kurtosis and standard deviation.

Comparing average grain size with clay-silt-sand percentage, standard deviation, and kurtosis in Figure 6, it is possible to identify two broad intervals in the Eocene-Oligocene core sections from Hole 1166A, divided at approximately 158.0 mbsf. The lower unit is enriched in sand sized particles relative to the upper unit, as well as featuring a higher standard deviation and lower kurtosis. Values for the latter two metrics describe this lower interval as being both very poorly sorted and well graded (primarily platykurtic distribution of grain sizes). The upper interval, conversely, is less poorly sorted, with reduced grading, owing to high kurtosis values that give samples in this interval primarily mesokurtic and leptokurtic distributions.

In the Eocene-Oligocene core sections from Hole 742A, three intervals can be identified, divided at approximately 305.0 mbsf and approximately 200.0 mbsf. The lowermost interval is in its bottommost section enriched in sand, with very poor sorting and broad sediment distributions similar to the lower interval of 1166A. It grades towards less sand, slightly improved sorting, and slightly reduced grading, before the middle interval is reached, above approximately 305.0 mbsf. Values for standard deviation increase into the middle unit, making the unit more poorly sorted than immediately below in the lower interval. Kurtosis values also reduce slightly, and all distributions in the middle interval become predominantly platykurtic, indicating well graded grain size distributions. Above 200.0 mbsf, standard deviation values begin to fall, and kurtosis values begin to increase (with predominantly leptokurtic and mesokurtic distributions towards the top of the core), indicating a slight improvement in sorting and a decrease in grading.

The Eocene-Oligocene core sections from Hole 739C are partitioned into two intervals similarly to 1166A, divided at approximately 319.0 mbsf. Relative to the upper

interval of 739C, the lower interval is much more poorly sorted and well graded, with primarily platykurtic to mesokurtic grain size distributions. Above 319.0 mbsf, sorting improves and grain size distributions become much less graded, featuring mesokurtic to leptokurtic distributions. The silt fraction of the gravel-free matrix also increases in the upper part of 739C, being about 70% of the sediment matrix volume in the upper interval compared to about 45% in the lower interval.

As described in the Methods, samples for microtexture and geochemical analysis were taken from the cores based on the laser particle sizer analysis and core descriptions. The seven intervals divided amongst the three sites were the basis of this sampling, and care was taken to take material from each interval that was representative of the majority of the material within each of the units. (No special sampling preference for finer or coarser grained units was necessary, since the majority of core material contained sufficient grain size fractions for both microtexture and grain size analysis.) The exact samples (IODP description) are stated below, along with accompanying shorthand, for ease of identification in figures (Table 2). Shorthand descriptions are condensed to site number and "U", "M", and "L", indicating "upper", "middle", and "lower", corresponding to the location of the interval in the Eocene-Oligocene sections of each site. Locations of samples in drill holes are graphically depicted in Figure 7, next page.

Table 2. Microtexture and Geochemical Sample Depth, IODP Sample Name, and Shorthand Labels

Depth	IODP Sample Name	Shorthand Label
MBSF	Core.Section.Location (cm)	Core.Relative Interval
242.09	739 32R1 99-101	739U
450.5	739 55R2 10-12	739L
193.23	742 22R2 103-105	742U
249.08	742 28R1 58-60	742M
314.52	742 34R6 72-74	742L
143.24	1166 16R1 104-106	1166U
220.49	1166 24R2 29-31	1166L

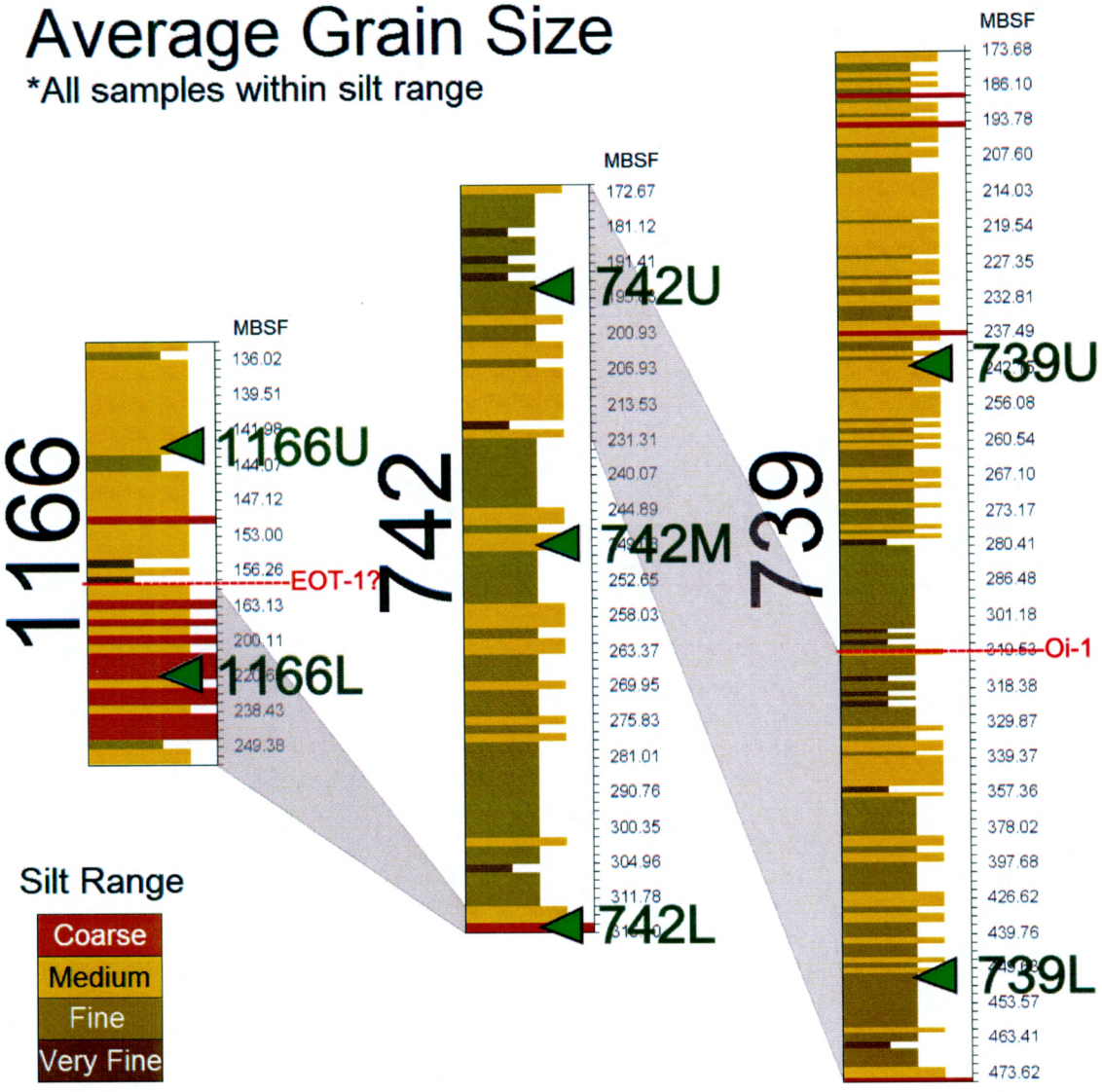

Figure 7. Sample locations used for geochemical and microtextural analysis are indicated on core sections with green dots and labeled with core number and "U", "M", and "L", indicating "upper", "middle", and "lower" section of the core for ease of reading. Exact sample location, including IODP section number and location within section are noted in Table 2.

3.2 Microtexture Analysis

Raw ranking of textures and qualification of sphericity/roundness are included in Appendix D. As mentioned in the methods, ranks for textures were based on abundance classes. However, to produce meaningful statistics, ranks were converted to a simple 'present' and 'not present' scheme for each microtexture. The percentage of grains per sample featuring a given texture was then calculated. This was used to construct Table 3, below, which shows the overall abundance of mechanical and chemical microtextures for each sample based on their appearance on the surface of individual grains. The table has been color coded to show trends in abundances, with a key provided beneath.

Table 3. Percent abundance of individual mechanical and chemical textures.

	Mechanical Textures													Chemical Textures			
	small conchoidal fractures	large conchoidal fractures	straight steps	arcuate steps	large breakage blocks	fractured plates	edge abrasion	mechanical/impact pits	straight grooves	curved grooves	irregular depressions	cracks	rounded edges	solution pits	adhering particles	silica precipitation	overgrowths
1166L	70	70	53	50	48	13	53	70	58	48	70	58	85	85	95	88	35
1166U	78	65	45	58	33	23	38	75	30	28	53	25	95	100	98	100	53
742L	75	55	45	43	63	30	60	83	43	30	83	43	88	98	98	100	38
742M	85	73	48	25	65	70	55	100	78	45	55	88	95	100	80	100	20
742U	85	76	32	38	29	71	62	100	47	3	56	85	100	100	100	100	56
739L	65	63	35	43	53	70	93	100	78	50	70	78	88	100	95	100	50
739U	82	64	59	59	77	90	97	100	100	59	100	92	95	100	90	100	79

Key
<25%
25-75%
>75%

Table 3 indicates that there is very little difference in chemical texture between the samples, although 739U features a significantly greater abundance of overgrowths than the other samples. In terms of mechanical textures, there appears to be a trend moving from sample 1166L to 739U (essentially, upward in the stratigraphy). Towards sample

739U, the abundance of nearly all the mechanical textures seems to increase. This can be seen simply by observing the number of green cells (>75% abundance) near the bottom of the table as compared to the top.

The abundance values from Table 3 were brought into the PAST statistics package to produce a correlation table and principal component analysis (PCA). However, due to the lack of differences in the chemical textures, statistics were only meaningful for the mechanical textures. Figure 8 shows the results of the PCA with bivariate plot and minimum span tree. Nearly all of the mechanical textures graph on one side of the plot, with a group of samples on side, and another group on the other. This strongly implies that the mechanism driving the difference between the two groups is predominantly the general abundance of the mechanical textures, rather than variations in individual textures. The PCA therefore seems to confirm the previously noted observations of Table 3, since the group which features the greatest abundance of mechanical textures consists of 742M, 742U, 739L, and 739U, while the group which features the least abundance is composed of 1166L, 742L, and 1166U.

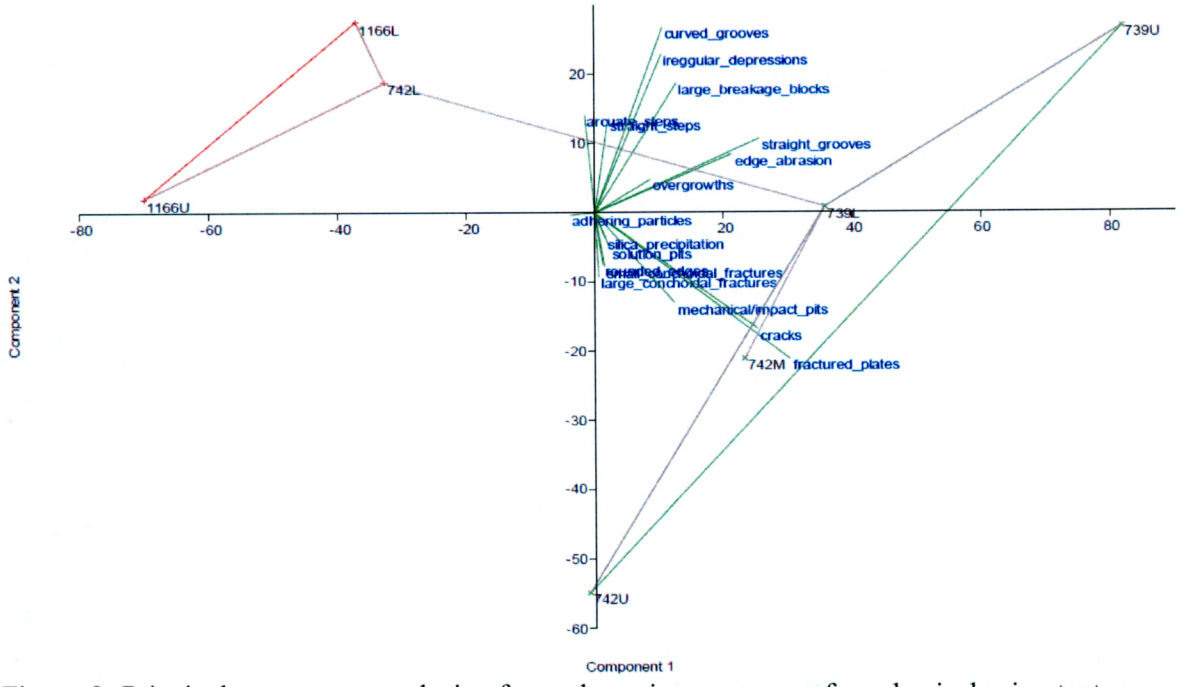

Figure 8. Principal component analysis of samples using presence of mechanical microtextures. Samples 1166L, 1166U, and 742L plot together in one group, while the remaining samples plot in a separate group. The primary difference between the two groups appears to be driven by the abundance of the mechanical textures.

The difference in the groups is further noted in the correlation table generated by PAST, based on the mechanical textures (Table 4, next page). Samples 1166L, 1166U, and 742L are more than 75% correlated amongst each other, while correlation to the remaining samples is in the range of 7% to 58%. In the second group, samples 742M, 742U, and 739L are all more than 70% correlated amongst each other. 739U is 87% correlated to 739L, although only 60 to 63% correlated to 742M and 742U, which suggests that it forms a smaller subgroup of similarity within the second group. The greatest difference between any samples generally occurs between the 1166 samples and the 739 samples, which are only 7 to 33% correlated.

Table 4. Correlation table displaying % similarity of samples based on presence of mechanical textures

	1166L	1166U	742L	742M	742U	739L	739U
1166L		76%	77%	42%	44%	33%	20%
1166U	76%		78%	37%	58%	25%	7%
742L	77%	78%		49%	58%	50%	49%
742M	42%	37%	49%		80%	71%	63%
742U	44%	58%	58%	80%		73%	60%
739L	33%	25%	50%	71%	73%		87%
739U	20%	7%	49%	63%	60%	87%	

Key
<40%
40-70%
>70%

3.3 Geochemical Analysis

Raw normalized weight % and element abundances in ppm for individual sample runs on the ICP-OES are included in Appendix C. Table 5, below, displays the final geochemical ratios calculated from the average elemental abundances produced by the ICP-OES for the seven samples.

Table 5. Geochemical ratios for major and trace elements

	1166L	**1166U**	**742L**	**742M**	**742U**	**739L**	**739U**
CIA	79.86	79.44	81.20	70.53	74.23	54.38	63.03
Zr/Sc ratio	24.07	11.55	24.49	24.50	18.20	19.98	18.40
Sr/Ba ratio	0.18	0.24	0.17	0.18	0.18	0.11	0.23
Fe/Ti ratio	3.60	7.07	3.47	5.49	6.10	7.14	7.21
K/Na ratio	12.18	4.89	11.33	5.83	6.67	6.24	2.76
Al/Na ratio	64.04	34.69	65.61	22.58	29.96	26.69	11.27
Al/Ti ratio	28.50	24.21	24.72	18.59	20.38	19.70	18.62

Generally, the CIA shows a trend of decreasing weathering signal from 1166 to 739, with values close to 80 for 1166L, 1166U, and 742L, values near 70 for the remainder of 742, and values near 60 for 739L and 739U. Parallel trends appear to be reflected in the other geochemical ratios, although there is inconsistency when comparing 1166U to 1166L and 742L. Figure 9, below, shows the results of principal component analysis performed by PAST, using the geochemical ratios shown above. The same groupings present from the microtextural analysis appear again, although in this case the similarities and differences

in the group of 1166L, 1166U, and 742L are somewhat modified. Since individual ratios in the bivariate plot extend to one side of the component plot, and since the groups are divided between two sides of the plot, an inference can be made that the primary element differentiating the two groups is the degree of weathering of the sample sediment. This is because, with the partial exception of Al/Ti ratio, all of the ratios are dependent to some degree on weathering history.

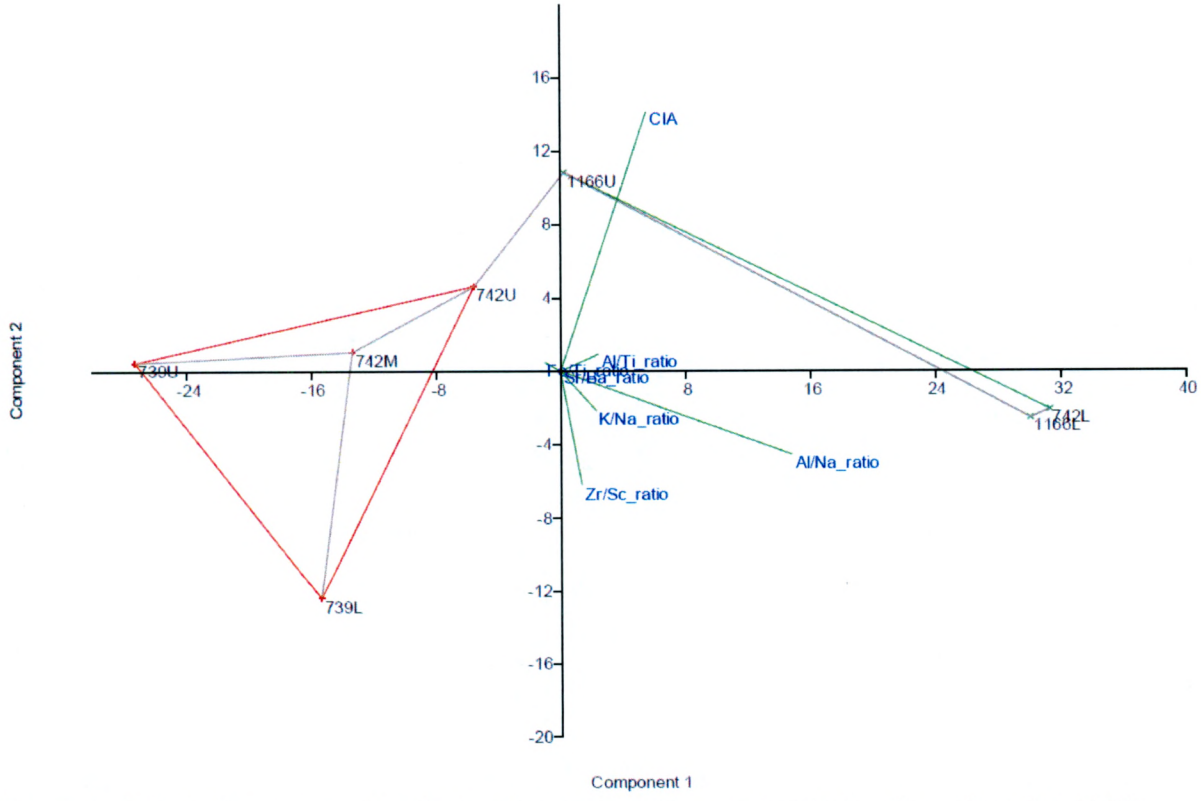

Figure 9. Principal component analysis of samples using geochemical ratios. Samples 1166L, 1166U, and 742L plot together in one group, while the remaining samples plot in a separate group that is especially well differentiated with respect to samples 1166L and 742L. The in-group relationship between 1166L/742L and 1166U is not as well defined as the relationship between 1166L and 742L, which plot nearly on top of each other, indicating a very high degree of geochemical similarity.

3.4 Seismic

As described in the Methods, isopach thickness maps using two-way travel time were generated for the suspected middle-late Eocene (pre-EOT) interval and the overlying late Eocene-Oligocene (EOT) interval. These maps are shown below, oriented north up, using square grids (Figure 10). Note the longitudinal lines (x-axis), which are depicted as perpendicular to latitude, would in reality be compressed towards to south to compensate for the curvature of the Earth. Thus, what is shown below is actually stretched relative to the true dimensions of the mapped area, similar to what a Mercator map projection might look like at high latitudes.

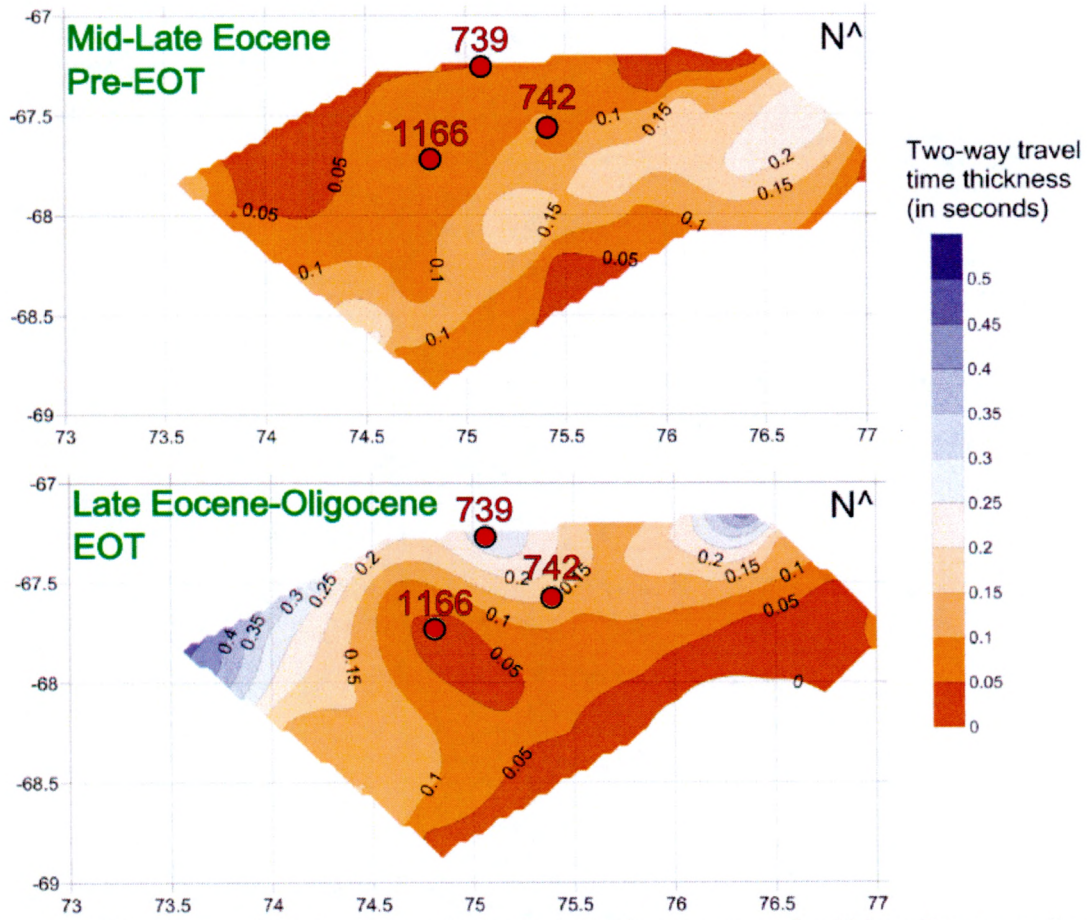

Figure 10. North-up oriented square grid isopach thickness maps of mid-late Eocene sediment, top, and late Eocene-Oligocene (EOT) sediment, bottom. Thickness is two-way travel time in seconds. X-axis is degrees east longitude, Y-axis is degrees south latitude.

4. DISCUSSION

4.1 Sedimentology

Core sections from Site 1166 are perhaps the easiest to interpret from the results of the current investigation because the differences in the upper and lower sections are fairly dramatic. As noted in the results, there is a marked increase in matrix sorting towards the upper interval of Hole 1166A (above 158.0 mbsf), as well as fining up of sediment, with the lower interval of 1166A being composed of beds with mean matrix grain sizes in the range of coarse to medium silts while beds in the upper interval are in the range of medium to fine silt (Figure 6, Results). The sand fraction of the matrix in the upper interval of 1166A (~15-20% of total matrix volume) is also approximately half of the fraction noted in the lower interval (~35-40% of total matrix volume).

Visual logging of cores from 1166A (see Appendix B) follows the upper/lower dichotomy from the particle sizer, with the lower interval of 1166A featuring abundant massively bedded gray sand/sandstone with yellowish to brownish stains suggestive of soil horizons, while the upper interval of 1166A features olive gray silty claystone/mudstone with extensive bioturbation/burrowing, a few shell fragments, and frequent interlamination. Taken together with the particle sizer results, the visual logging agrees with the palynological assessment of Macphail & Truswell (2004) that the upper interval represents a marine environment, while the lower interval is indicative of a more terrestrial setting.

In cores from Hole 742A, the lowermost section (described visually as interlaminated sandstone/siltstone) features clay-silt-sand fractions that are superficially similar to the lower sand/sandstone interval of 1166A, although the matrix sand fraction grows progressively smaller up core before shifting abruptly at 305.0 msbf. The sorting in

the lowermost portion of 742A is also comparable to the lower interval of 1166A (very poorly sorted), and both intervals were noted in visual core descriptions to contain contorted bedding near their bases. Based on processes occurring in modern glacial environments, the origin of this contorted bedding is suspected to be indicative of marginal glacial processes occurring in a fluvioglacial setting per Benn et al. (2003) –this will be discussed in more detail in the Synthesis (sections 4.5) of the Discussion.

The middle section of 742A between 305.0 and ~200.0 mbsf, while deposited above the Mid-Late Eocene unconformity, is lithologically dissimilar from the likely similarly stratigraphically positioned upper interval of 1166A. This section is described primarily as a non-bioturbated gray sandy siltstone and silty sandstone, while the upper interval of 1166A is described as olive gray bioturbated claystone/mudstone. In the visual logs, the bedding tends be frequently massive, although there are significant interbeds of both silt and sand. Clay-silt-sand is close to 30%-45%-25% total volume, nearly evenly mixed (as would be expected in the matrix component of a true diamictite, especially given the massive bedding), which is much different than the upper section of 1166A, which is predominantly a silt matrix (~70%). No bioturbation and shell fragments are noted, and as Truswell (1991) notes, palynomorphs are scarce. This may imply that the material was laid down relatively fast, or perhaps in an environment that was not conducive to preservation of palynomorphs, such as a subglacial or very close proximity proglacial setting, assuming glacial conditions predominated.

The upper section of 742A, above ~200 mbsf is visually similar to the middle section (described as a gray sandy mudstone and muddy sandstone compared to the gray sandy siltstone and silty sandstone of the middle section), although from matrix grain size analysis the clay fraction increases to approximately 40% of total volume at the expense

of the sand fraction. A jump up in kurtosis values and a decrease in standard deviation shows that this section also becomes more sorted than the middle section. Like the middle interval of 742A, the upper interval of 742A similarly lacks palynomorphs (Truswell, 1991). This implies there may have been some similarities in the environmental conditions between the two intervals (possibly glacial conditions owing to the diamictite-like matrix grain size distributions of the middle interval), although different enough that deposited sediment became slightly more sorted and finer up core. This slight difference may be indicative of a subglacial environment transitioning to a proglacial environment. The lower section of Hole 739C (below 319.0 mbsf) both visually from core logging (described as a gray-brownish gray clayey silty sand and a sandy diamictite), and in terms of clay-silt-sand fraction, appears very similar to the upper section of Hole 742A. While the lower part of 739C is slightly more platykurtic overall than the upper interval of 742A, they have similar kurtosis values, overlapping in the mesokurtic range. The clay-silt-sand fraction in both intervals is more or less identical, being about 40%-45%-15% of total volume. From visual core logs, it is notable that both units also contain no shell fragments or any other macroscopic marine features.

The upper section of Hole 739C (above 319.0 mbsf), features a marked improvement in sorting and decrease in grading over the interval below, have mesokurtic to leptokurtic distributions. Its clay-silt-sand fraction is about 15%-70%-15%, which is very similar to upper section of 1166A, which is suggested from this investigation to have been deposited in a marine environment. Given the presence of shell fragments and a few worm tubes noted in the visual core logs, and factoring in the presence of marine dinocysts per Houben et al. (2011) and Baldauf & Barron (1991), it therefore seems very likely that this interval was similarly laid down in a marine setting.

4.2 Microtexture Analysis

From the Results section, the PCA analysis and correlation table of grain microtextures (see Figure 8 and Table 3) show that sediment samples 1166L, 1166U, and 742L form one distinct group, while 742M, 742U, 739L, and 739U form another distinct group. The primary feature driving the difference between these two groups is the simple abundance of mechanical microtextures, with the presence of individual textures significantly enhanced in the group containing samples from Site 739 versus the group containing samples from Site 1166.

Interestingly, while the two groups have very similar chemical texture abundances, it was noted while examining grains from Hole 1166A that there were instances of double overprinting. That is to say, some grains appeared to have mechanical textures that were overprinted with two different generations of chemical textures. There are two possibilities to explain this. The first possibility is that the 1166 group (per the results, the lower part of 742 is included in this group, although it was not directly noted to feature double overprinting) features two generations of weathering events, while the group of 742M, 742U, 739L, and 739U feature only one generation of weathering. The other option is that all of the grains across all cores feature prominent diagenetic alteration, but only the material from the 1166 group has a pre-diagenetic weathering signal. Regardless of origin, since this signal was not properly accounted for in SEM analysis, this aspect of double/pre-diagenetic weathering is believed to manifest as a decrease in the abundance of mechanical textures in the 1166 group. The implication is that a sizable portion of mechanical textures in this group might have been obliterated or obscured by an initial round of chemical weathering that did not occur for the 739 group. (See Figures 11, 12,

and 13 for examples of double overprinting, and Figure 14 for a contrast in grades of chemical alteration, below)

Additionally, it is particularly interesting that 1166U is similar to 1166L and 742L, and that 742M is similar to 742U, 739L, and 739U. Both the upper part of 1166 and middle part of 742 appear to have been laid down above the middle-late Eocene unconformity, but only 1166U appears to feature signs of surface weathering. This implies a separation in time and/or space of these samples. Potentially, the interval containing 1166U could have been laid down prior to the interval containing 742M, with a notable change in environmental conditions occurring in Prydz Bay during the intervening time. This change is reinforced by the geochemistry, which suggests the shift in environmental conditions may be the result of enhanced glaciation.

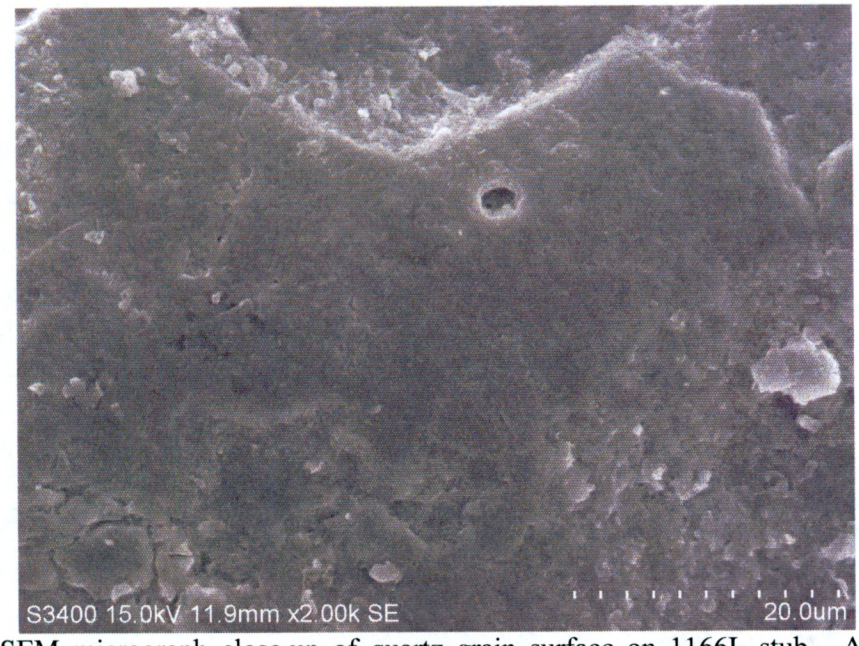

Figure 11. SEM micrograph close-up of quartz grain surface on 1166L stub. A solution pit (towards the upper middle-right of image) can be seen in an already precipitated/dissolved terrain, printed over an area of possible fractured plates/breakage.

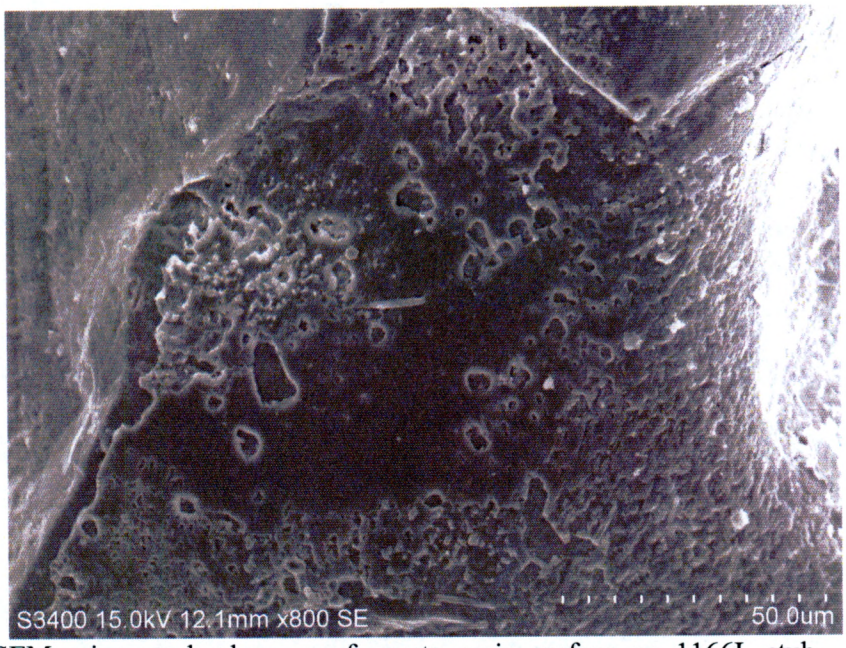

Figure 12. SEM micrograph close-up of quartz grain surface on 1166L stub. A "skin" of precipitation appears to show evidence of being dissolved, and the precipitation itself appears to potentially overly an existing chemically weathered surface, suggesting multiple generations of weathering or a combination of weathering and diagenetic alteration.

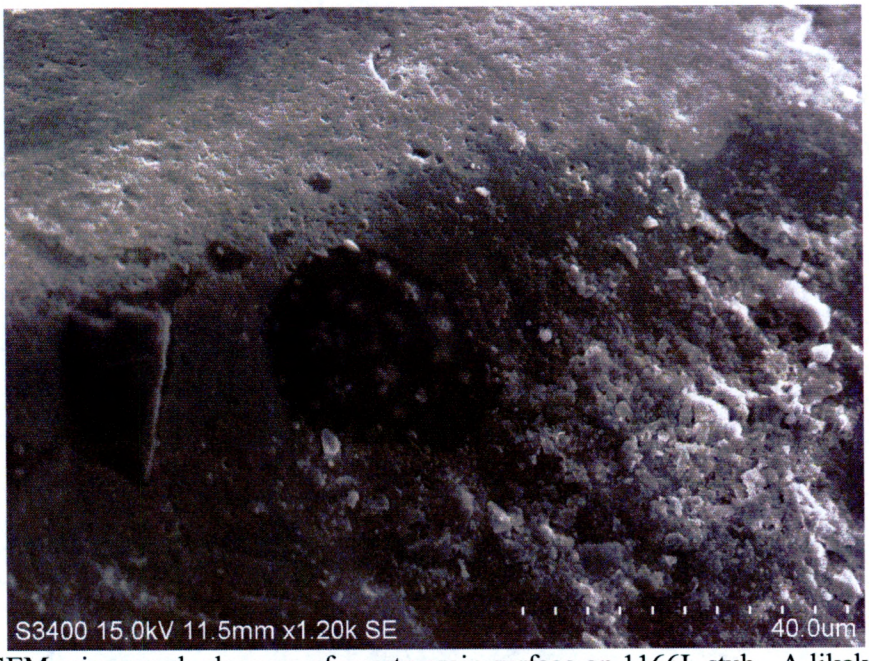

Figure 13. SEM micrograph close-up of quartz grain surface on 1166L stub. A likely conchoidal fracture area (lower left) is overprinted by partly dissolved terrain, which is further overprinted by two different types of growth (a smooth "dark" growth near middle of image, and a rough "bright" growth/precipitation [itself possibly partly dissolved] at lower right).

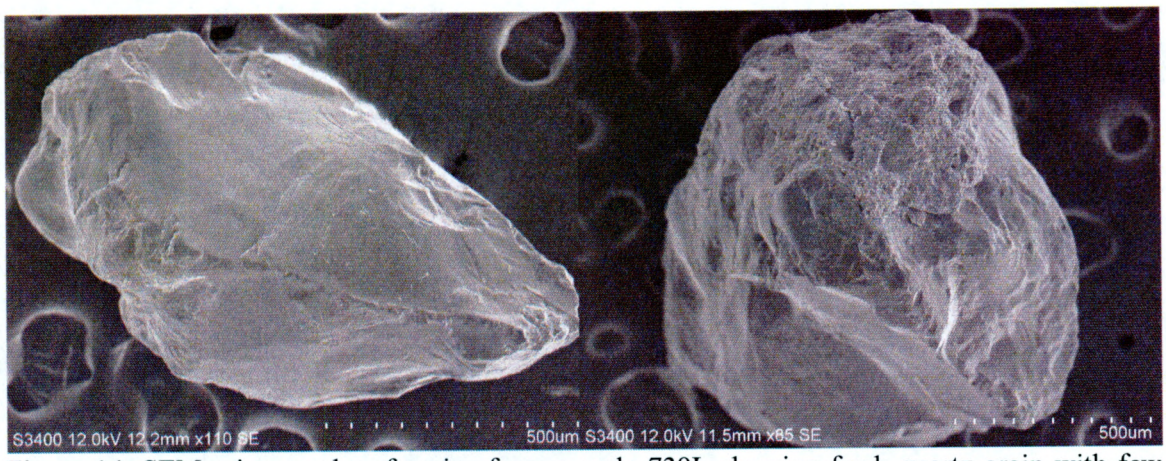

Figure 14. SEM micrographs of grains from sample 739L showing fresh quartz grain with few chemical textures present (left), as well as another grain with close to 50% of surface covered by precipitation, obliterating portion of mechanical textures (right).

4.3 Geochemistry

The results of the geochemistry strongly support the results of the microtextural analysis to a degree much greater than could have been anticipated in the early stages of investigation. To this end, the most correlative geochemical metrics are the CIA and the Al/Ti ratio. The combination of samples 1166L, 1166U, and 742L all feature CIA values near 80 and Al/Ti ratios in the range of 24-29. Alternatively, the group of 742M, 742U, 739L, and 739U all feature Al/Ti ratios near 20, with the CIA for 742M/742U close to 70, and the CIA for 739L/739U close to 60.

The higher CIA values for the group with 1166 samples implies a strong chemical weathering signal (Nesbitt & Young, 1982). Coincidentally, the lower cores from Hole 742A and a wide distribution of cores from Hole 1166A were noted in visual core logging to contain abundant coal clasts. These clasts do not appear in the upper cores of Hole 742A and are extremely rare in Hole 739C, comprising only two isolated instances of granule size fragments. As coal seams are predominant in the Amery Group (Holdgate et

al., 2005), this implies that the material may have been sourced locally in the Prince Charles Mountains along the western margin of Prydz Bay.

That the 739 samples feature lower CIA values (close to fresh granite, according to Nesbitt and Young [1982)]) likely means that the material in these samples were derived under fully glacial erosion conditions, with a lack of chemical modification. The in-between CIA values for the middle and upper part of Hole 742A may therefore signify some transition in climate, with temperate conditions potentially giving way to colder, polar conditions. This possible change in climate/weathering conditions appears to coincide with a potential change in sourcing, as no coal clasts are seen in the middle of Hole 742A, and clasts are absent to extremely rare at points further up in the stratigraphic column.

That the Al/Ti ratios for 1166A and the lower part of 742A are so similar seems to confirm they are likely sourced from the same region. The same is true for the other core sections, which all have Al/Ti values very close to 20. This difference affirms there was a significant change in the source areas feeding sediment into Prydz Bay in the late Eocene. If fully glacial conditions began to occur in the area of Prydz Bay by the time the middle interval of 742A was laid down, the change might well be attributable to the demise of local wet based glaciation and the onset of ice sheet advance –this could explain the drop off in coal clasts, assuming this attribute is truly indicative of local sourcing versus sourcing from the hinterlands.

The other ratios, being proxies for weathering conditions, similarly support the CIA, although 1166U in these ratios appears much less weathered than 1166L and 742L. Examining the PCA plot (Figure 9, section 3.3 in the Results) 1166U actually graphs much further apart from 1166L and 742L than in the microtextural analysis. Similarly,

this same inconsistency with the geochemical ratios occurs for sample 739U, which also appears to be less weathered than its counterpart in 739L. This is particularly true when regarding 739U's K/Na and Al/Na, which are smaller relative to 739L, despite 739U having a CIA that is actually slightly higher than that of 739L. Notably, dinocyst/diatom assemblages for the sections containing 1166U (Macphail & Truswell, 2004) and 739U (Baldauf & Barron, 1991) suggest these have an open marine influence, which is not apparent in the other relevant core sections. From a cursory perspective, this could be interpreted to suggest that some aspect of the marine environment might be altering the non-CIA weathering ratios in these sections. However, it is equally probable that the effect may actually be the result of processes that do not necessarily coincide with marine deposition. Further investigation will be required to determine the causative agents responsible for this inconsistency.

Regarding the PCA analysis of the geochemistry, which corroborates the groupings of the microtextural analysis, it is notable that 1166L and 742L graph nearly on top of each other. If the PAST software is asked to provide a correlation number for these two samples, it returns a value of 0.99868, or a 99.8% probability of similarity. Thus, geochemically speaking, the lower part of Hole 1166A and lower part of Hole 742A are virtually identical based on the limited sample set presented here. However, to determine the reliability of this relationship more samples will need to be taken across all core sections in order to amplify the statistical differences between units.

4.4 Seismic

The results of the seismic investigation seem to reveal a dramatic shift in sedimentation during the Eocene into the early Oligocene. Coincident with the suspected middle-late

Eocene (pre-EOT) section, there is a belt of relatively thick sediment that extends from southwest to northeast across the study area (Figure 10, in the Results). Reflector traces through the bottom contact of the belt (which corresponds to the Cretaceous unconformity), shows this swath of middle-late Eocene material exists inside of a valley-like trough structure.

Since the trough is coincident with the Cretaceous unconformity, it is somewhat certain that it is an erosional feature generated at some point between the late Cretaceous and the middle-late Eocene. This interpretation is supported by the investigation of Erohina et al. (2004), which notes that layered reflections in the Cretaceous interval are truncated southwest of Site 742, coincident with the area of the trough. Given the architecture of the Lambert Graben itself, which turns slightly northeast at its mouth along the shelf, it is probable that this trough may represent the axis of a large fluvial valley that drained Prydz Bay during the early Cenozoic. This would explain the downcutting into the Cretaceous sediment and would also imply a relative sea level fall in the area at the time of trough formation, with depocenters having migrated further offshore. The infilling of the trough with Eocene sediment implies that, if there was a relative decrease in sea level closer in time to the EOT, it may have been fairly short lived. To fill the trough with late Eocene sediment there are at least two possibilities (which may have occurred simultaneously). Either the offshore regions were sufficiently filled with sediment and deposition began to migrate back up the embayment, or relative sea level increased, which would have converted the trough into functional accommodation space.

Presumably, if inland erosion increased as a result of glacial action (as is implied by the CIA decrease previously mentioned), it could imply that offshore depocenters were overwhelmed during temporary stable stands of sea level. A model of glacial erosion by

Wilson et al. (2012) indicated that erosion of inland areas as a result of ice expansion during the Eocene-Oligocene may have been capable of filling the Lambert Graben to sea level, creating a terrestrial environment at the location of the drill sites. Wilson et al. (2012) further explains that post-Eocene erosion of the Lambert Graben occurred as ice radiated outward to the coast, deepening the basin significantly. Evidently, this later episode of erosion did not disrupt the Cretaceous unconformity in the vicinity of the drill sites, since the seismic data shows the middle-late Eocene interval fully blankets the area.

The suspected late Eocene-Oligocene (EOT) section above the middle-late Eocene sediments (Figure 10, in the Results) shows that deposition changed abruptly, no longer 'filling in the cracks', but actively expanding the depositional front seaward, as the thickest sequences in this interval are offshore, towards the outer continental shelf. If large-scale continental glaciation was occurring at this time, as is potentially suggested by the geochemical and quartz grain microtexture analyses referred to in the previous sections, relatively large volumes of sediment may have been transported to the shelf, which could have forced material to prograde at the shelf break.

4.5 Synthesis

4.5.1 Contemporary Analogy for Eocene Environment of Prydz Bay

The geochemical analysis, in conjunction with the microtextural analysis, suggest chemical weathering was significant at Prydz Bay when material recovered from Site 1166 and the lowest interval of Site 742 was deposited in the middle to late Eocene. Cantrill & Poole (2012) and Macphail & Truswell (2004) describe late Eocene conditions at Prydz Bay as being particularly wet, with forests present, which could have contributed organic acids to soils and runoff, enhancing chemical weathering. According to the

National Oceanic and Atmospheric Administration (NOAA) of the United States, there are four locations in northwestern North America that have a climate similar to the inferred climate of Prydz Bay in the Eocene. These are Annette, Juneau, Valdez, and Yakutat in the southeastern part of Alaska. Of the four, Juneau and Valdez are probably the most similar, especially since their annual precipitation is closer to Eocene Prydz Bay than the other two sites. A table is provided below, for comparison, using thirty year averages from NOAA (2012) and climate parameters for Eocene Prydz Bay from Cantrill & Poole (2012).

Table 6. Comparison of annual precipitation, temperature, and relative humidity (30-year averages) in southeastern Alaska compared to Eocene Prydz Bay

	Mean Temp (°C)	Mean Precip. (mm)	Rel. Humidity (%)
Prydz Bay	Less than 12	1200-1500	High
Annette	8.1	2580	High (73%)
Juneau	5.6	1580	High (71%)
Valdez	3.2	1803	High (69%)
Yakutat	4.6	3940	High (77%)

In contemporary southeastern Alaska, conditions are such that complex plant communities are capable of existing in close proximity to large temperate glaciers. An example occurs at the Malaspina Glacier, located near Yakutat at 60 degrees latitude (which is similar in latitude to Prydz Bay). This glacier is presently one of largest temperate/tidewater glaciers in the world, covering an area comparable to U.S. state of Rhode Island (Gustavson and Boothroyd, 1987). The glacier is sourced in the Chugach Mountains, which host one third of Alaska's glaciated landscape (Molnia, 2008). While these mountains abut what are described by Shulski and Wendler (2007) as some of the warmest parts of Alaska, they receive heavy snowfall, owing to their height and proximity to moisture laden air over the Gulf of Alaska. Shulski and Wendler (2007) note that

Thompson Pass, located in the Chugach Mountains near Valdez, consistently receives Alaska's highest recorded snowfall, averaging 1400 cm per year.

The presence of a tidewater glacier similar to the Malaspina Glacier would explain some of the features previously observed in sediments from Hole 1166A and the lower interval of Hole 742A. In terms of microtextures and CIA, a tidewater glacier in a warmer humid climate could explain how mechanical textures were potentially overprinted by chemical weathering, with grains being first worked by glacial action and then precipitated/dissolved by chemical action in fluvioglacial outwash. The Malaspina Glacier, for example, hosts an extensive system of island-like bars split by meltwater streams and covered with vegetation where it meets the sea (Gustavson and Boothroyd, 1987). The contorted bedding previously mentioned in the grain size analysis (section 4.1) could also be explained by a glacier similar to Malaspina. Contorted beds are often seen in areas where sediment is deposited over ice, typically along glacial margins. As ice melts and retreats, support is removed causing beds to sag erratically (Benn et al., 2003).

The source area for a possible tidewater glacier was probably in the Prince Charles Mountains over 200 km to the southwest. This is based on abundant coal clasts found in Hole 1166A and in the lowest interval of Hole 742A, which may be indicative of the Amery Group sediments retained in the mountain chain. While 200 km seems improbably distant, the Malaspina Glacier, for example, extends dozens of kilometers from its source mountains into the sea and coastal plain (Gustavson and Boothroyd, 1987).

4.5.2 Reconstruction of Sedimentation Based on Results of this Study

The combination of all four analyses undertaken during the course of this investigation, in tandem with past research efforts, provides for a reconstruction surrounding the depositional events of the EOT at Prydz Bay. Based on seismic investigation, sometime

before the middle-late Eocene (but after or during the late Cretaceous) a significant channel was eroded through a likely coastal plain setting composed of Cretaceous sediment at the mouth of Prydz Bay. By approximately late Eocene time, a tidewater glacial system, perhaps similar to the Malaspina Glacier in contemporary southeastern Alaska, was functioning in the area, recorded by the intervals present at the base of Holes 1166A and 742A.

Both of the aforementioned intervals grade upward from contorted bedded, poorly sorted silty sands and sandy silts to slightly better sorted material, with almost equal portions of matrix clay-silt-sand. At Site 1166, there is an abrupt transition through the relevant core sections at ~158.0 mbsf, and material further grades up into significantly better sorted and predominantly silty material based on matrix grain size analysis. This sequence may indicate a roll back of the tidewater glacial front. In this scenario, the earliest/lowest contorted beds are consistent with marginal glacial processes per Benn et al. (2003). As the glacier backed away, non-contorted but yet still poorly sorted sediment was deposited as outwash in front of the glacier, forming bars and channels similar to what is seen at the mouth of the present-day Malaspina Glacier. (Gustavson and Boothroyd, 1987)

Why the glacier backed away may have been a function of increasing relative sea level. The increase in sorting and coincident increase in silt matrix content in the upper part of Hole 1166A implies a less energetically dynamic environment replaced the pro-glacial outwash setting. This is likely consistent with a more marine setting (especially owing to the proximity this environment would have had relative to the previous outwash environment), and this is bolstered by the Macphail & Truswell (2004) palynological analysis, which indicates an abundance of marine taxa in relevant core sections.

Where the record continues in the middle cores of Hole 742A, significant environmental changes are inferred to have occurred at Prydz Bay. Al/Ti ratios show that a switch in sediment sourcing likely occurred, and CIA values begin to decrease up core, eventually becoming consistent with fresh material, indicating chemical weathering became less influential. PCA plots of geochemical and microtextural ratios show that all units stratigraphically above and including the middle interval of Hole 742A have greater abundance of mechanical textures and less weathering signal than underlying material. From visual core logs, coal clasts large enough to be identified by eye are no longer present in these units or are extremely rare, indicating nearby source regions (bearing Amery Group sediment) may have become secondary.

This information, combined with the grain size analysis of middle-upper 742A and lower 739C, which show a nearly even mix of clay-silt-sand matrix, as well as other observations from the visual logs (particularly, massively bedded sandy mudstone/muddy sandstone and diamictite with a lack of bioturbation) suggests subglacial or very proximal glacial conditions brought on by ice sheet expansion may have impacted Prydz Bay at the time the middle and upper intervals of Hole 742A and lower interval of Hole 739C were deposited. (The visual, grain size, and mechanical/geochemical similarity of the upper section of Hole 742A and the lower section of Hole 739A also suggest the two intervals are stratigraphically related.) It is notable that the subglacial/proximal glacial conditions consistent with ice sheet advance occur below the level of the Oi-1 event at Site 739.

In the upper part of 739C (primarily above Oi-1), an increase in sorting and matrix silt fraction (as well as the presence of bioturbation) similar to what is seen in the upper interval of 1166A occurs. This is again thought to be consistent with a marine environment, bolstered by the diatom/dinocyst analysis of Houben et al. (2011) and

Baldauf & Barron (1991). The low CIA values and highest noted abundance of mechanical textures implies sediment deposited in this interval is glaciomarine in origin, probably formed in a cold near-polar climate. This suggests some ice sheet retreat may have occurred, but a large ice sheet was still present in the area.

4.5.3 Modeling Implications

The sequence of events described above is similar to what is proposed in a model by Stocchi et al. (2013), although that is not to imply the timing of events as modeled is actually consistent with the reality of the deposition. One of the more interesting aspects of the Stocchi et al. (2013) model is the inclusion of crustal dynamics that occur with the outward migration of a forebulge from an advancing ice sheet. As the forebulge expands through the coast, it temporarily uplifts the terrain before lowering it below its starting elevation, owing to the crust sagging under the weight of the ice sheet. This would produce a slight relative sea level fall along the coast, followed by a larger rise as the forebulge passes through. This mechanism could therefore be responsible for the upward fining sequence at Site 1166, potentially resultant from the rolling back of a Malaspina-type glacier.

In the Stocchi et al. (2013) model, the abrupt transition in lithology at Site 1166 at ~158.0 mbsf is considered to be a transgressive surface coincident with flooding from the sea. This agrees with this investigation's interpretation of units above 158.0 mbsf having marine influence, particularly due to previously noted enhanced bioturbation and fining (both visually and from matrix grain size analysis) relative to underlying units. The transition is tied to the EOT-1 event in model time, but this is based on the boundary conditions of the model itself, so the basis in reality is tenuous. It is notable, however that this investigation indicates that approximately around the EOT-1 (based on the age model)

that a major ice sheet was not yet present at Prydz Bay, and humid and wet conditions prevailed owing to the high CIA values noted at Site 1166.

The model shows the ice sheet expanding across Prydz Bay post EOT-1, reaching just landward of Site 739 near the Oi-1. Based on the lithology from this investigation it is possible that the lower interval of Hole 739C (described by this investigation as a non-bioturbated muddy sand and diamictite) indicates the glacier overrode this location, but it may have been merely in very close proximity as well. Regardless, the model shows the ice sheet retreated noticeably in conjunction with the Oi-1. Stocchi et al. (2013) also moves the original Oi-1 location at 310.73 mbsf to 319.0 mbsf (the break between the upper and lower intervals of 739C identified by this investigation using laser particle sizer analysis). This was done because the break in lithology is thought by Stocchi et al. (2013) to be an unconformity consistent with transgression over the position of the previous ice front, associated with the Oi-1 event at Site 739 in model time.

Further evidence of ice sheet presence at Site 739, as indicated by investigation, results from low CIA values seen in sediment samples recovered from Hole 739C cores, as well as Al/Ti ratios that are different from Hole 1166A, implying a sediment source change. The lack of coal clasts in 739C, found previously in 1166A and thought to be an indicator of local sourcing, further backs the idea of a shift in sediment supply that may be consistent with ice sheet advance. One difference, however, between the model and this investigation, is that this investigation suggests near-polar glacial conditions may have began somewhat before Oi-1 (in late Eocene time), based on the biostratigraphy.

It is notable that at Site U1360, on the Wilkes Land margin, a similar early Oligocene interval is found, with the *Malvinia escutiana* dinocyst noted above the level of an underlying unconformity (Houben et al., 2011). The Stocchi et al. (2013) model shows

the underlying unconformity is consistent with Oi-1 at Site U1360 (similarly to Site 739), however, Houben (speaking about the same model two years prior to the Stocchi et al. [2013] paper being published) explicitly states this relationship is hypothetical.

4.5.4 Future Research

Perhaps the greatest implication of this investigation is that the sediments in cores from Sites 1166, 742, and 739 provide an almost complete record of the depositional conditions that occurred during the EOT at Prydz Bay, owing to the bolstering of previously inferred stratigraphic relations by geochemical and microtextural analysis. At the same time, this also creates opportunity for future research. The sampling for geochemical and microtextural analysis was very coarse, with only one sample taken per interval identified from grain size analysis. More samples will need to be taken from these intervals to refine the findings of this investigation. But more importantly, there is one area that was particularly under-sampled during this investigation, leaving a large hole of uncertainty in the summary of events described in the last section.

The lower part of the middle interval of Hole 742A has two features that have not been totally rectified. Firstly, Truswell (1991) notes the presence of Permian pollen below 190.0 mbsf in Hole 742A, which has been traced to the Amery Group. (This is separate from the observation of Cretaceous palynomorphs found in the lowermost cores in Hole 742A). This implies material sourced from the Prince Charles Mountains (the 'local' source) was still present throughout the middle interval of Hole 742A, despite that unit having Al/Ti ratios similar to those of Hole 739C. This may mean that the sole sample from middle interval of Hole 742A just happened to fall in a bed that was more remotely influenced than locally influenced as far as sourcing. (There is also some evidence of possible Amery Group sediment in cores from Hole 739C, according to Jenkins & Alibert

[1991], although perhaps not as significant when compared to Site 742 in the EOT core sections.)

Secondly, visual core logs show the lower part of the middle section of Hole 742A features potential Amery Group coal clasts between ~287.0 and ~305.0 mbsf, below the level where sample 742M was derived. This fact, combined with the aforementioned observation by Truswell (1991) strongly implies that the transition from a local glacier to an ice sheet was more gradual and probably more complex than outlined in this investigation. It also implies that the sediment record at Site 742 is more complete than realized.

Indeed, a very fine silt interval identified from grain size analysis at just below ~305.0 mbsf (also noted in visual core logs as an interlaminated sandstone/siltstone interval) may actually be the equivalent of the surface noted at Site 1166 at 158.0 mbsf (correlated with seismic at the middle-late Eocene unconformity). If this is true, the material above this surface, which contains coal clasts up to ~287.0 mbsf, might be an equivalent unit to the upper interval of Hole 1166A. Thus, extracting a geochemical/microtexture sample from this unit is essential for future investigation, as it may demonstrate that Site 742 features a nearly complete record of the Eocene-Oligocene transition, minus the uppermost portion near Oi-1. Additionally, if correlation with the upper interval of 1166A can be confirmed, age control for the sediment column at Site 742 would be greatly improved.

5. CONCLUSIONS

CIA values, weathering ratios, chemical/mechanical textures, grain size analysis, and visual core descriptions corroborate previous characterization of the late Eocene environment at Prydz Bay as a wet/temperate environment and suggest a coastal tidewater glacier system may have been active at this time. The same metrics suggest this environment was subsequently replaced by a more polar setting into Oligocene time, particularly since CIA values of sediment at Site 739 approach those of fresh rock. The combined analyses strongly indicate the presence of an ice sheet/enhanced glaciation at Prydz Bay before the Oi-1, with a sharp decline in chemical weathering through the latest Eocene.

Geochemical, microtextural, and matrix grain size analyses potentially confirm possible stratigraphic relationships inferred by previous research, suggesting the EOT record at Prydz Bay is more complete than previously realized. The results of this study strongly indicate Site 1166, Hole A, interval 158.0 to 266.8 mbsf, is likely the lithostratigraphic equivalent of Site 742, Hole A, interval ~305.0 to 315.0 mbsf. This investigation also suggests Site 742, Hole A, interval 171.3 to ~230 mbsf, is lithostratigraphically related to Site 739, Hole C, interval 319.0 to 482.6 mbsf. Figure 15 illustrates these relationships, also detailing weathering conditions associated with lithostratigraphic units identified from this investigation.

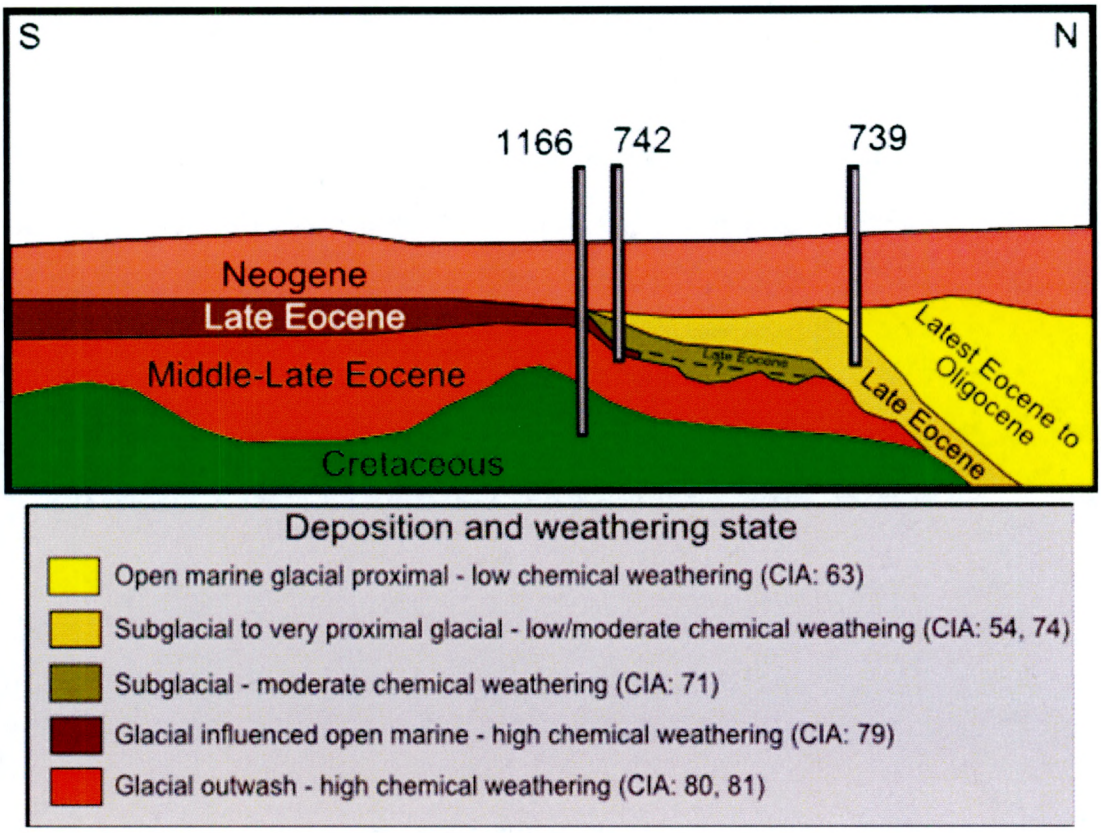

Figure 15. System diagram of stratigraphic units seen in a north-south profile through the study area. The type of deposition and weathering is determined by lithological, grain size, and geochemical analyses performed by this study. Solid black lines denote divisions between units based on seismic and lithological data. Dashed lines represent possible divisions seen in the seismic data that are not corroborated with lithological information.

Re-mapping of sediment interval thickness for this investigation also corroborates the results of previous investigation and offers additional insight into middle-late Eocene deposition. Isopachs produced from seismic data indicate offshore migration of depocenters in the Eocene-Oligocene Transition consistent with ice sheet advance. Furthermore, the middle-late Eocene (pre-EOT) interval mapped across the study area reveals infilling of a valley eroded into Cretaceous sediment.

Additionally, the inferred sequence of depositional events is possibly consistent with modeling by Stocchi et al. (2013) in terms of ordering. The outward migration of a forebulge as proposed by modeling corroborates the visual/grain size analysis results of

this investigation, particularly for Site 1166. However, this investigation is not sufficient to verify or refute the timing of the model events. Future higher resolution sampling and additional analyses will be necessary to achieve coherent chronostratigraphic correlations.

6. REFERENCES

Baldauf, J. G. & Barron, J. A. (1991). Diatom biostratigraphy: Kerguelen Plateau and Prydz Bay regions of the Southern Ocean. In *Proceedings of the Ocean Drilling Program, Scientific Results.* (Vol. 119, pp. 547-598).

Bann, K. L., Fielding, C. R., MacEachern, J. A., and Tye, S. C. (2006). Sedimentology and ichnology of mixed wave- and storm-dominated deltaic deposits: examples from the Permian of Australia. *In* Hampson, G.J., Dalrymple, R. and Burgess, P. (eds.). Advances in Shelf and Shoreline Stratigraphy, SEPM Spec. Publ.

Barron, J. A., Baldauf, J. G., & Larsen, B. (1991). Evidence for late Eocene to early Oligocene Antarctic glaciation and observations on late Neogene glacial history of Antarctica: results from Leg 119. *In*
Barron, J., Larsen, B., et al., Proc. ODP, Sci. Results, 119: College Station, TX (Ocean Drilling Program), 869-891.

Barron, J. A., Larsen, B. et al. (1989). *Proceedings of the Ocean Drilling Program, v. 119A. Initial Reports. College Station, Texas, Ocean Drilling Program.*

Benn, D. I., Kirkbride, M. P., Owen, L. A., & Brazier, V. (2003). Glaciated Valley Landsystems. *Glacial Landsystems*, 372-406. Routledge, Taylor & Francis Group.

Blott, S.J. & Pye, K. 2001. GRADISTAT: A Grain Size Distribution and Statistics Package for the Analysis of Unconsolidated Sediments. *Earth Surface Processes and Landforms* (26), 1237-1248.

Burton, J. H., & Price, T. D. (1990). The ratio of barium to strontium as a paleodietary indicator of consumption of marine resources. *Journal of Archaeological Science*, *17*(5), 547-557.

Cande, S. C., & Stock, J. M. (2004). Cenozoic reconstructions of the Australia-New Zealand–South Pacific sector of Antarctica. *The Cenozoic Southern Ocean: tectonics, sedimentation, and climate change between Australia and Antarctica*, 5-17.

Cantrill, D. J., & Poole, I. (2012). *The vegetation of Antarctica through geological time.* Cambridge University Press.

Cooper, A., Stagg, H., & Geist, E. (1991). Seismic stratigraphy and structure of Prydz Bay, Antarctica: implications from Leg 119 drilling. In *Proc. ODP, Sci. Results* (Vol. 119, pp. 5-26).

Cooper, A., & Webb, P. *Editors*. (1990). International Workshop on Antarctic Offshore Stratigraphy (ANTOSTRAT): Overview and Extended Abstracts. U.S. Geol. Surv. Open-File Rep., 90-309: 290 pp.

Coxall, H.K., Wilson, P.A., Pälike, H., Lear, C.H., and Backman, J. (2005). Rapid stepwise onset of Antarctic glaciation and deeper calcite compensation in the Pacific Ocean. *Nature* (433), 53-57.

DeConto, R. M., Pollard, D., Wilson, P. A., Pälike, H., Lear, C. H., & Pagani, M. (2008). Thresholds for Cenozoic bipolar glaciation. *Nature*, *455*(7213), 652-656.

Erohina, T., Cooper, A., Handwerger, D., and Dunbar, R., (2004). Seismic stratigraphic correlations between ODP Sites 742 and 1166: implications for depositional paleoenvironments in Prydz Bay, Antarctica. In Cooper, A.K., O'Brien, P.E., and Richter, C. (Eds.), Proc. ODP, Sci. Results, 188

Florindo, F., Bohaty, S. M., Erwin, P. S., Richter, C., Roberts, A. P., Whalen, P. A., & Whitehead, J. M. (2003). Magnetobiostratigraphic chronology and palaeoenvironmental history of Cenozoic sequences from ODP sites 1165 and 1166, Prydz Bay, Antarctica. *Palaeogeography, Palaeoclimatology, Palaeoecology*, *198*(1), 69-100.

Folk, R.L. 1974. Grain Size Nomenclature for (Clastic) Sediment. In *Petrology of Sedimentary Rocks*. Univ of Texas.

Force, E. R. (1991). Geology of titanium-mineral deposits (special paper 259). *Geological Society of America*.

Gustavson, T. C., & Boothroyd, J. C. (1987). A depositional model for outwash, sediment sources, and hydrologic characteristics, Malaspina Glacier, Alaska: a modern analog of the southeastern margin of the Laurentide Ice Sheet. *Geological Society of America Bulletin*, *99*(2), 187-200.

Hambrey, M. J., Ehrmann, W., & Larsen, B. (1991). Cenozoic glacial record of the Prydz Bay continental shelf, East Antarctica. *In: Barron, J; Larsen, B, et al.(eds.), Proc. ODP, Sci. Results, College Station, TX.(Ocean Drilling Program), 119, 77-132*, *119*, 77-132.

Hambrey, M. J. & McKelvey, B. (2000). Neogene sedimentation on the western margin of the Lambert Graben, East Antarctica. *Sedimentology, 47:5*,77–607.

Hammer, Ø., Harper, D. A. T., Ryan, P. D. (2001). PAST: Paleontological statistics software package for education and data analysis. *Palaeontologia Electronica* 4(1): 9pp. http://palaeo-electronica.org/2001_1/past/issue1_01.htm

Hansen, M. A. (2011). Determining Middle Miocene Trough Pliocene Changes in Provenance and Basal Ice Conditions Through Sedimentological Analyses of Subglacial Diamictites in AND-2A, Ross Sea, Antarctica. (Master's Thesis) Montclair State University, Montclair, NJ.

Harrowfield, M., Holdgate, G. R., Wilson, C. J., & McLoughlin, S. (2005). Tectonic significance of the Lambert Graben, East Antarctica: reconstructing the Gondwanan rift. *Geology*, *33*(3), 197-200.

Helland, P. E., Huang, P. H., & Diffendal Jr, R. F. (1997). SEM analysis of quartz sand grain surface textures indicates alluvial/colluvial origin of the Quaternary "glacial" boulder clays at Huangshan (Yellow Mountain), East-Central China. Quaternary Research, 48(2), 177-186.

Holdgate, G. R., McLoughlin, S., Drinnan, A. N., Finkelman, R. B., Willett, J. C., & Chiehowsky, L. A. (2005). Inorganic chemistry, petrography and palaeobotany of Permian coals in the Prince Charles Mountains, East Antarctica. *International Journal of Coal Geology*, *63*(1), 156-177.

Houben, A. J., Bijl, P. K., Pross, J., Bohaty, S. M., Passchier, S., Stickley, C. E., ... & Brinkhuis, H. (2013). Reorganization of Southern Ocean plankton ecosystem at the onset of Antarctic glaciation. *Science*, *340*(6130), 341-344.

Houben, A. J., Bijl, P. K., Guerstein, G. R., Sluijs, A., & Brinkhuis, H. (2011). *Malvinia escutiana*, a new biostratigraphically important Oligocene dinoflagellate cyst from the Southern Ocean. *Review of Palaeobotany and Palynology*, *165*(3), 175-182.

Kennett, J. P. (1977). Cenozoic evolution of Antarctic glaciation, the circum - Antarctic Ocean, and their impact on global paleoceanography. *Journal of geophysical research*, *82*(27), 3843-3860.

Konert, M., & Vandenberghe, J. E. F. (1997). Comparison of laser grain size analysis with pipette and sieve analysis: a solution for the underestimation of the clay fraction. *Sedimentology*, *44*(3), 523-535.

Krinsley, D. H., & Doornkamp, J. C. (1973). Atlas of quartz sand surface textures. Cambridge University Press.

LeMasurier. W. E. (1970). Volcanic Evidence for Early Tertiary Glaciation in Marie Byrd Land. *Antarctic Journal of the United States*, 5(5), 154

Macphail, M. K., & Truswell, E. M. (2004). Palynology of Site 1166, Prydz Bay, East Antarctica. In *Proceedings of the Ocean Drilling Program, Scientific Results* (Vol. 188, pp. 1-43).

Mahaney, W. C., Claridge, G., & Campbell, I. (1996). Microtextures on quartz grains in tills from Antarctica. Palaeogeography, Palaeoclimatology, Palaeoecology, 121(1), 89-103.

Mazzullo, J. & Graham, A. G. (eds.) (1988). Handbook for Shipboard Sedimentologists. ODP Tech. Note, 8: 45-67. http://www-odp.tamu.edu/publications/tnotes/digital/tnote_08.pdf

McLennan, S. M., Hemming, S., McDaniel, D. K., & Hanson, G. N. (1993). Geochemical approaches to sedimentation, provenance, and tectonics. *Special Papers-Geological Society of America*, 21-21.

Molnia, B. F. (2008). Glaciers of North America -- Glaciers of Alaska. *In* Williams, R. S., Jr., and Ferrigno, J. G., eds., Satellite image atlas of glaciers of the world: U.S. Geological Survey Professional Paper 1386-K, 525 p.

Moncrieff, A. C. M. (1989). Classification of poorly sorted sedimentary rocks. *Sedimentary Geology, 65*, 191-194.

Morad, S., & Aldahan, A. A. (1986). Alteration of detrital Fe-Ti oxides in sedimentary rocks. *Geological Society of America Bulletin*, *97*(5), 567-578.

Nesbitt, H. W., & Young, G. M. (1982). Early Proterozoic climates and plate motions inferred from major element chemistry of lutites. *Nature*, *299*(5885), 715-717.

Newsome, D., & Ladd, P. (1999). The use of quartz grain microtextures in the study of the origin of sand terrains in Western Australia. *Catena, 35(1)*, 1-17.

NOAA. (2012). Comparative Climatic Data for the United States Through 2012. National Climate Data Center, Asheville, NC.

O'Brien, P.E., Cooper, A.K., Richter, C., et al., 2001. *Proc. ODP, Init. Repts., 188: College Station, TX (Ocean Drilling Program).*

Powers, M. C. (1953). A new roundness scale for sedimentary particles. *Journal of Sedimentary Research, 23(2)*, 117-119.

Reed, S. J. B. (2005). Electron microprobe analysis and scanning electron microscopy in Geology. Cambridge: Cambridge University Press.

Ryan, W. B. F., Carbotte S. M... Zemsky R. (2009). Global Multi-Resolution Topography Synthesis, *Geochem. Geophys. Geosyst.*, 10, Q03014.

Shulski, M., & Wendler, G. (2007). *The Climate of Alaska*. University of Alaska Press.

Sperazza, M., Moore, J. N., & Hendrix, M. S. (2004). High-resolution particle size analysis of naturally occurring very fine-grained sediment through laser diffractometry. *Journal of Sedimentary Research*, *74*(5), 736-743.

Stagg, H. M. J. (1985). The structure and origin of Prydz Bay and MacRobertson shelf, East Antarctica. *Tectonophysics*, *114*(1), 315-340.

Stocchi, P., Escutia, C., Houben, A. J., Vermeersen, B. L., Bijl, P. K., Brinkhuis, H., ... & Yamane, M. (2013). Relative sea-level rise around East Antarctica during Oligocene glaciation. *Nature Geoscience*, *6*(5), 380-384.

Strand, K., Passchier, S., & Näsi, J. (2003). Implications of quartz grain microtextures for onset Eocene/Oligocene glaciation in Prydz Bay, ODP Site 1166, Antarctica. *Palaeogeography, Palaeoclimatology, Palaeoecology*, *198*(1), 101-111.

Sun, L. G., Liu, X. D., Yin, X. B., Xie, Z. Q., & Zhao, J. L. (2005). Sediments in palaeo-notches: potential proxy records for palaeoclimatic changes in Antarctica. *Palaeogeography, Palaeoclimatology, Palaeoecology*, *218*(3), 175-193.

Sun, L. G., Xie, Z. Q., Zhao, J. L. (2000). The characteristics of Sr/Ba and B/Ga in lake sediments on the Ardley Peninsula, maritime Antarctica. *Marine Geology & Quaternary Geology* 20, 44-46

Taylor, J., Siegert, M. J., Payne, A. J., Hambrey, M. J., O'Brien, P. E., Cooper, A. K., & Leitchenkov, G. (2004). Topographic controls on post-Oligocene changes in ice-sheet dynamics, Prydz Bay region, East Antarctica. *Geology*, *32*(3), 197-200.

Taylor, S. R., & McLennan, S. M. (1985). The continental crust: its composition and evolution. Malden, Massachusetts, 312.

Terry, R. D., & Chilingar, G. V. (1955). Summary of "Concerning some additional aids in studying sedimentary formations" by M. S. Shvetsov. *J. Sediment. Petrol., 25*, 229-234.

Truswell, E. M. (1991). Data report: palynology of sediments from Leg 119 drill sites in Prydz Bay, East Antarctica. In *Proceedings of the Ocean Drilling Program, Scientific Results* (Vol. 119, pp. 941-945).

Webb, P. N. (1990). The Cenozoic history of Antarctica and its global impact. *Antarctic Science*, *2*(01), 3-21.

Weibel, R. (2003). Alteration of detrital Fe-Ti oxides in Miocene fluvial deposits, central Jutland, Denmark. *Bulletin of the Geological Society of Denmark*, *50*(2), 141-208.

Wilson, D. S., Jamieson, S. S., Barrett, P. J., Leitchenkov, G., Gohl, K., & Larter, R. D. (2012). Antarctic topography at the Eocene–Oligocene boundary. *Palaeogeography, Palaeoclimatology, Palaeoecology*, *335*, 24-34.

Whitehead, J. M., Quilty, P. G., McKelvey, B. C., & O'Brien, P. E. (2006). A review of the Cenozoic stratigraphy and glacial history of the Lambert Graben-Prydz Bay region, East Antarctica. *Antarctic Science*, *18*(01), 83-99.

Yang, S., Jung, H. S., & Li, C. (2004). Two unique weathering regimes in the Changjiang and Huanghe drainage basins: geochemical evidence from river sediments. *Sedimentary Geology*, *164*(1), 19-34.

Yang, S., Li, C., & Cai, J. (2006). Geochemical compositions of core sediments in eastern China: implication for Late Cenozoic palaeoenvironmental changes. *Palaeogeography, Palaeoclimatology, Palaeoecology*, *229*(4), 287-302.

APPENDIX A: GRAIN SIZE ANALYSIS

TABLE OF CONTENTS

FIGURES

TABLES

SAMPLE PREPARATION

Samples of sub-gravel sized sediment recovered from the Prydz Bay cores were analyzed for grain size distribution statistics using a Malvern Mastersizer 2000 integrated laser particle sizing system. The system utilizes Mie scattering to derive a measurement of suspended particle sizes based on volume percentage of material. The range of sizes detectable by the Mastersizer is from 0.02 μm to 2000 μm, or 12.5 ϕ to -1 ϕ. Size classes are programmable, and for this analysis classes were divided into 0.5 ϕ intervals for the entire detectable range.

Analyzed material for each sample amounted to approximately one eighth to one sixteenth of a teaspoon of sediment. The resulting aliquots, which were derived by mashing with a wine cork (to prevent breakage of grains), were strained through a 2 mm sieve to remove the gravel component and transferred to a beaker treated with 10 mL of 30% hydrogen peroxide to remove organic material. After mixing and standing for several hours, the beakers were transferred to hot plates and boiled until visible foaming had subsided. Next, the beakers were allowed to cool somewhat, and the walls of the beaker were rinsed (if necessary) with filtered water to wash all material back down into the remaining solution. Approximately 5 mL of 10% hydrochloric acid was then added to the beakers to dissolve any biologically derived carbonate cement which might skew the grain size analysis.

Beakers were boiled after adding hydrochloric acid. When solution levels became low, water was added to keep the samples from drying out. Once any reactions had subsided, the beakers were boiled until solution levels were significantly below 50 mL. They were then allowed to cool before their contents were transferred to 50 mL

polypropylene tubes. Any sediment clinging to the inside of the beakers was carefully rinsed into the tubes with filtered water to ensure no significant loss of material.

Tubes were leveled off at 50 mL with filtered water as needed. They were then spun in centrifuges at 1800 rpm for 30 minutes to separate the reaction products from non-dissolved aliquot material. Next, the supernatant was decanted, filtered water was added to restore solution levels to 50 mL, and the tubes were spun again at 1800 rpm for 30 minutes.

An additional step was then taken for sediments with some portion of biogenic silica. Tubes were decanted to the 20 mL level, 1 N sodium hydroxide was added to the 25 mL level, and the tubes were vigorously shaken. The sodium hydroxide treated tubes were next placed in a hot water bath between 85-90 degrees C for one hour in order to digest any biogenic silica. Afterwards, tubes were removed from the bath and allowed to cool for fifteen minutes. Solution levels were then brought to 50 mL with the addition of filtered water, and the tubes were spun in a centrifuge at 1800 rpm for 30 minutes.

The resulting solutions from either methodology were decanted, and the non-dissolved aliquot material was rinsed with filtered water into a 200 mL beaker. Beakers were then filled to 50 mL with an addition of filtered water. Beakers were treated with a pinch of sodium pyrophosphate to disaggregate the sample and transferred to hot plates to bring the pyrophosphate into solution.

Before performing grain size analysis with the Mastersizer, multiple 700 mL beakers (as many as were necessary) filled only with filtered water were cycled through the instrument to clean it. This was done until the machine had stabilized at a consistent obscuration value. Again, a fresh beaker of filtered water was cycled through the instrument, but this was used for calibration purposes, to background out any effect of the

filtered water. After running the calibration, the contents of a 200 mL beaker of sample material treated with pyrophosphate was added to the calibration beaker. The 700 mL beaker containing the sample and background calibrated filtered water was then measured in the instrument.

In order to create useful grain size statistics, the average grain sizes derived by the Mastersizer were input to a digital spreadsheet, and results were computed for mean ϕ size, standard deviation, skew, and kurtosis. Calculations used to generate these statistics were derived from Blott and Pye (2001) in their description of GRADISTAT, a grain size statistics calculation package. The particular method utilized for this analysis followed the logarithmic methods of moments, which was updated from Folk (1974).

GRAIN SIZE PROFILES

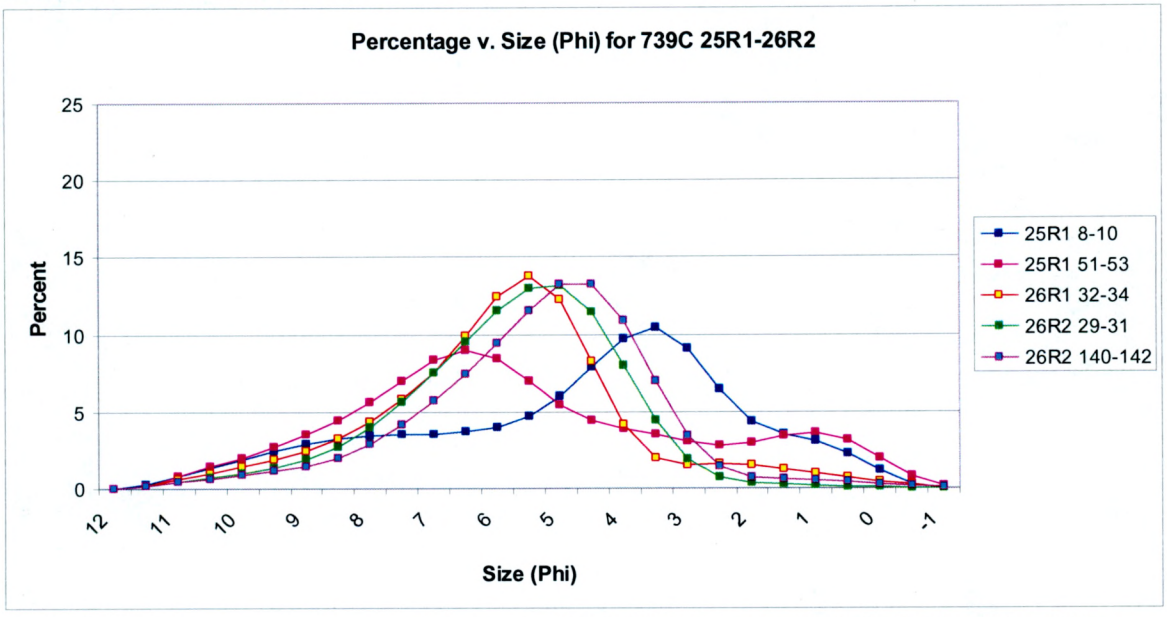

Figure A.1. Percentage of material versus grain size (ϕ) for samples for hole 739C 25R1 to 26R2.

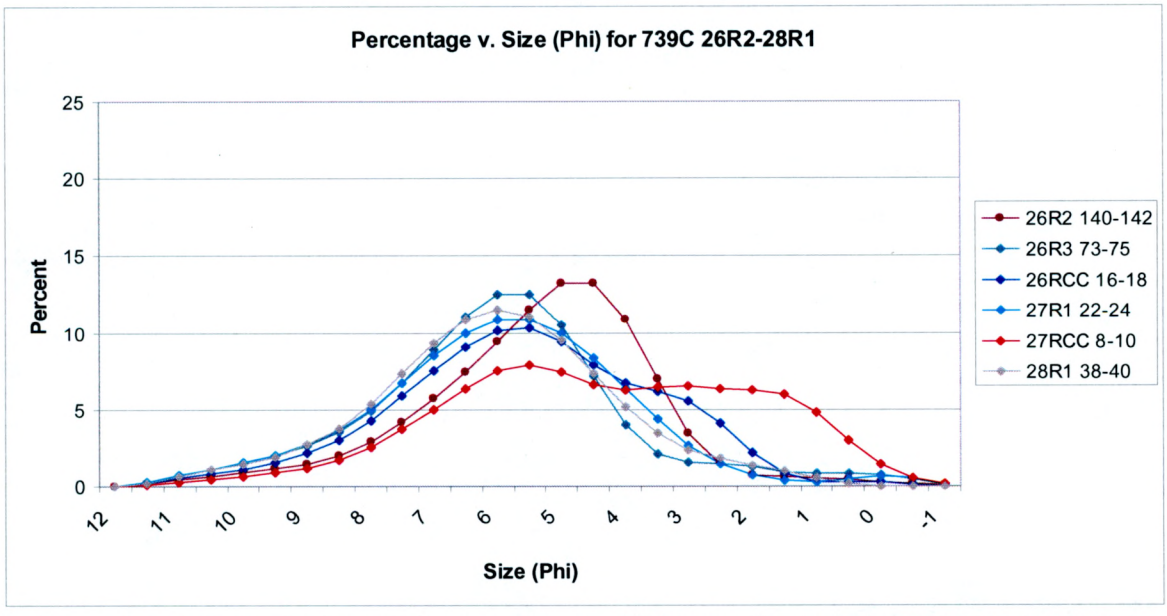

Figure A.2. Percentage of material versus grain size (ϕ) for samples for hole 739C 26R2 to 28R1.

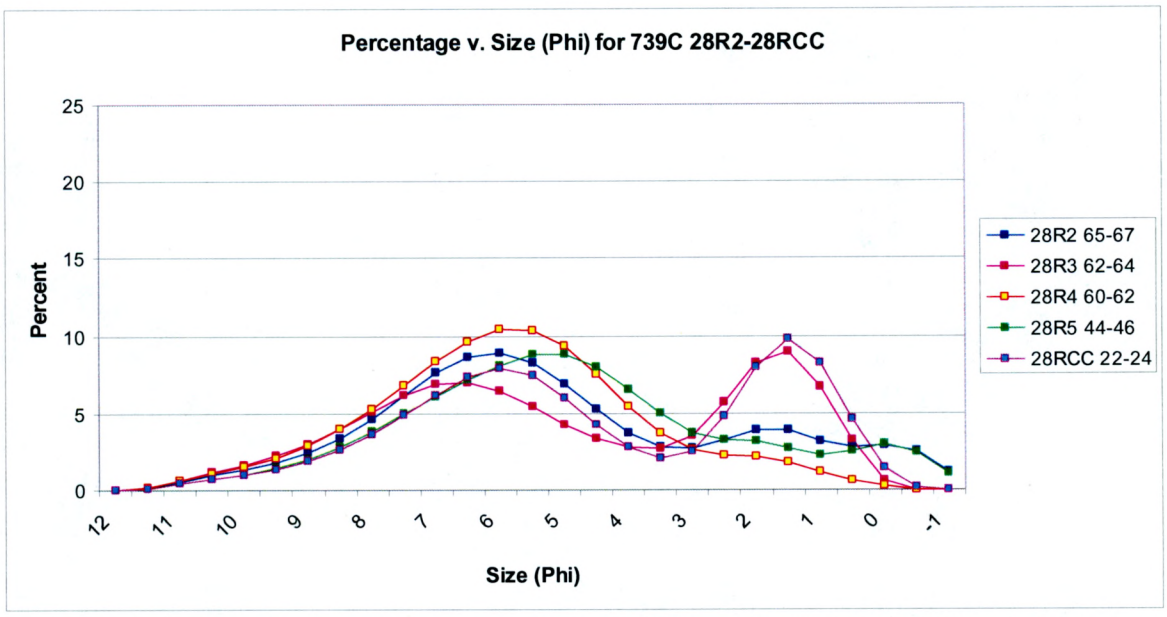

Figure A.3. Percentage of material versus grain size (ϕ) for samples for hole 739C 28R2 to 28RCC.

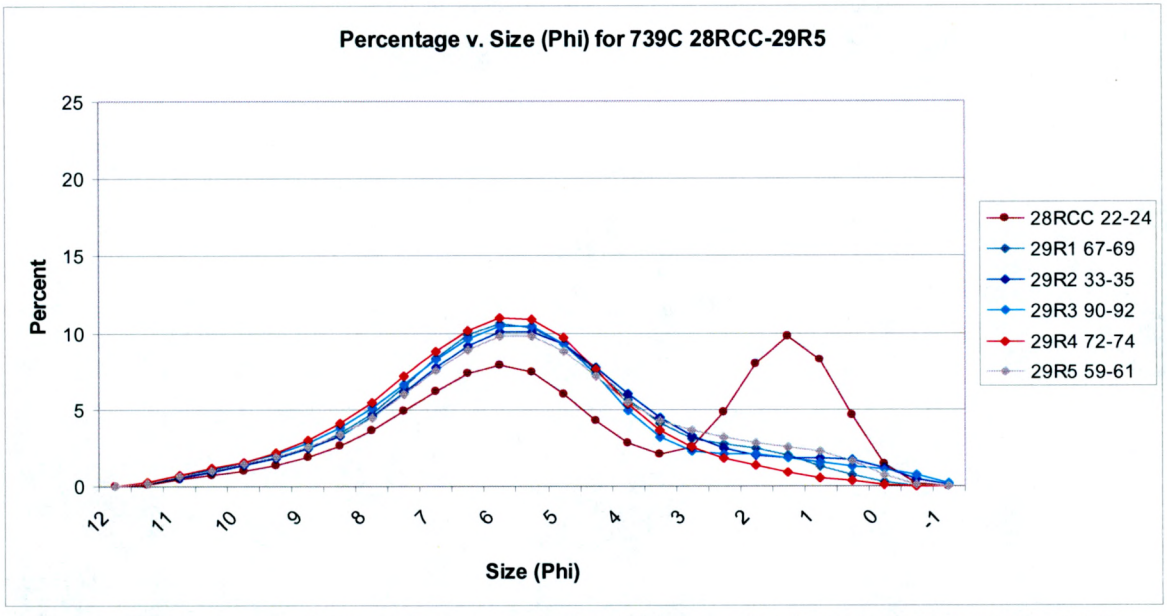

Figure A.4. Percentage of material versus grain size (ϕ) for samples for hole 739C 28RCC to 29R5.

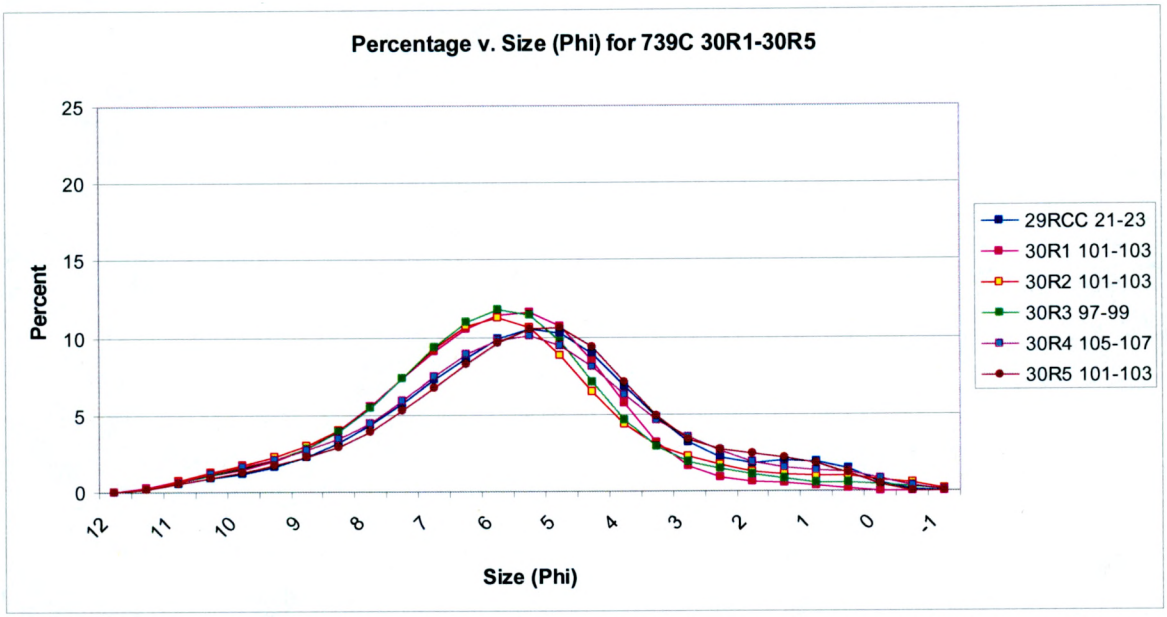

Figure A.5. Percentage of material versus grain size (ϕ) for samples for hole 739C 29RCC to 30R5.

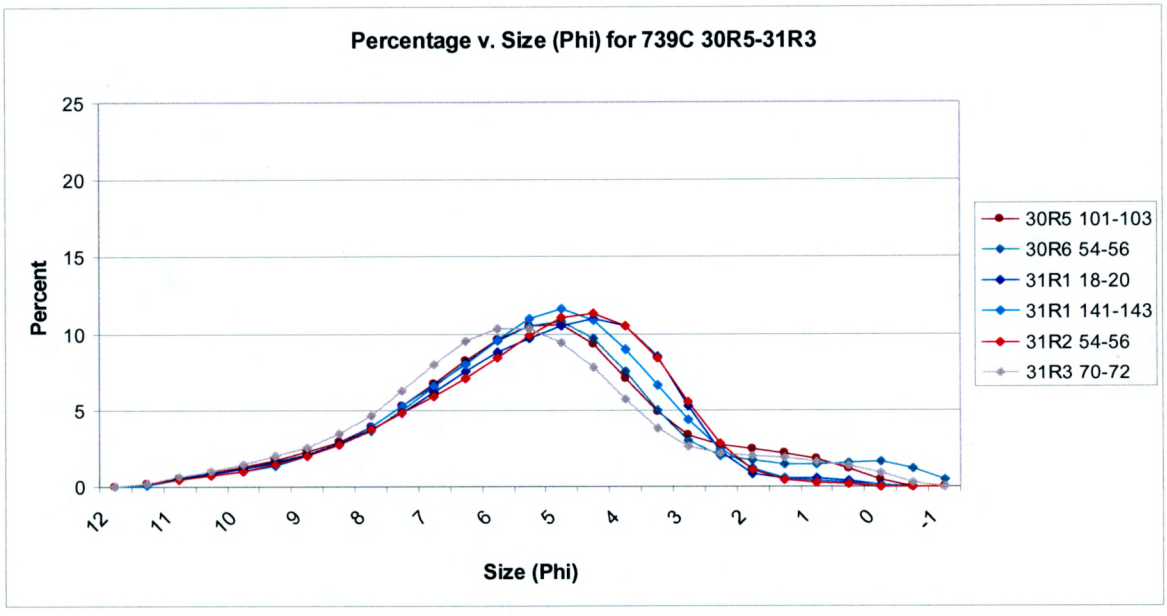

Figure A.6. Percentage of material versus grain size (ϕ) for samples for hole 739C 30R5 to 31R3.

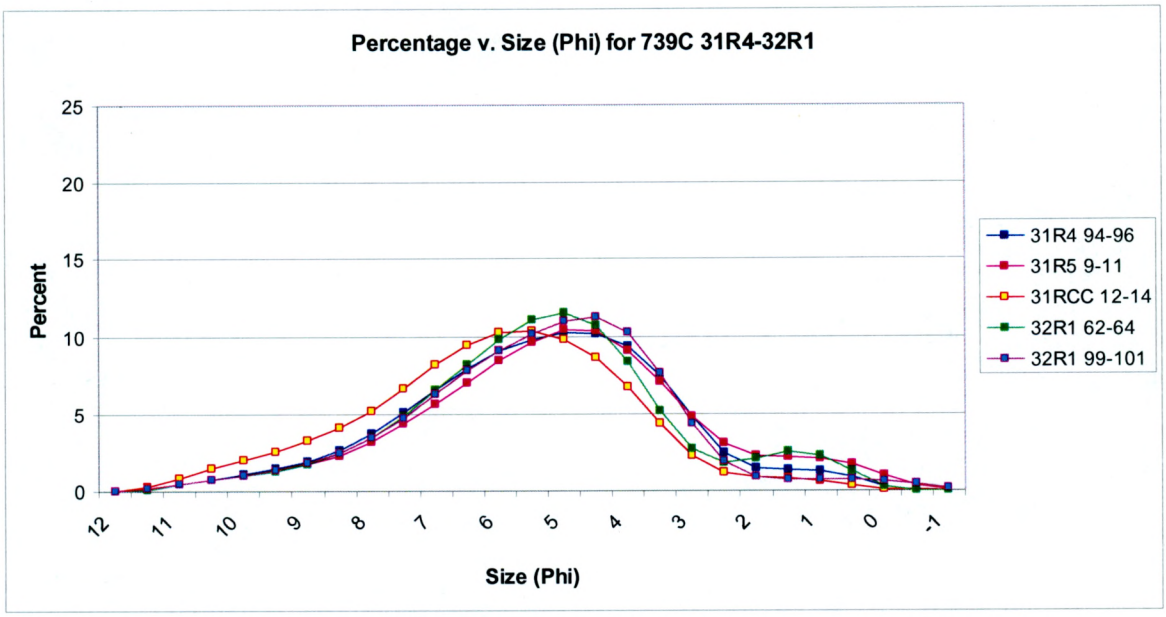

Figure A.7. Percentage of material versus grain size (ϕ) for samples for hole 739C 31R4 to 32R1.

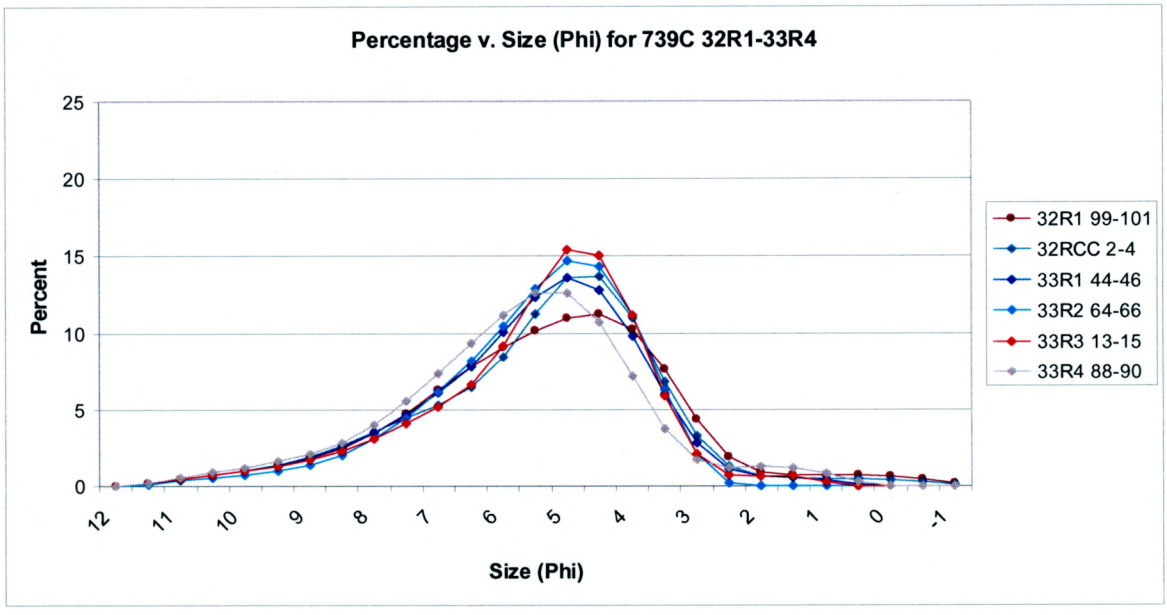

Figure A.8. Percentage of material versus grain size (ϕ) for samples for hole 739C 32R1 to 33R4.

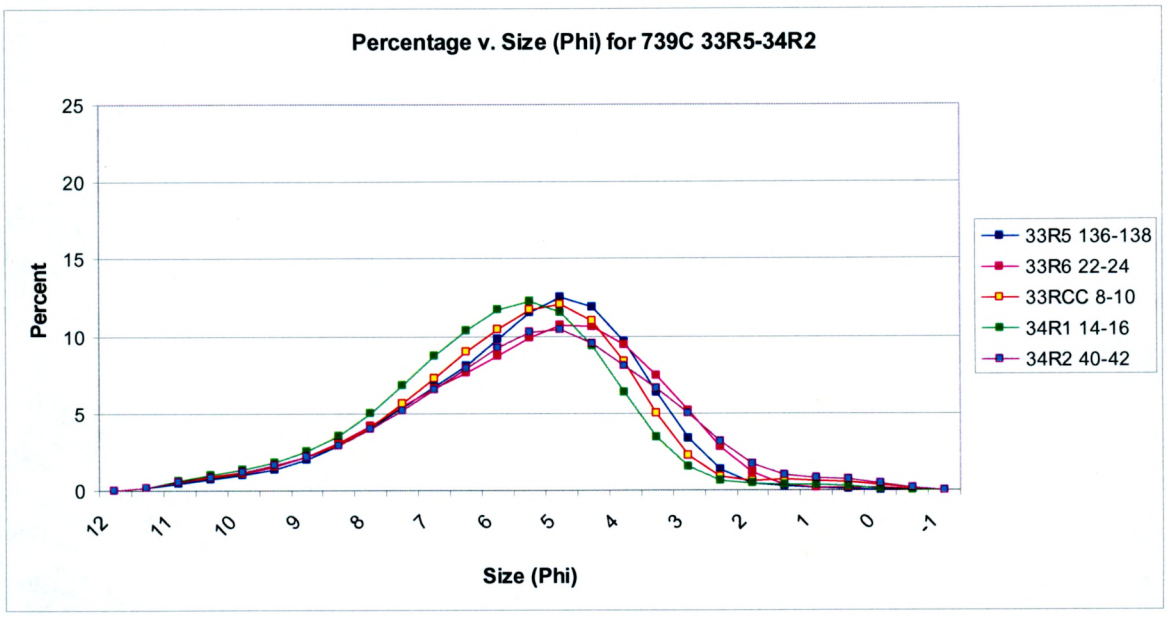

Figure A.9. Percentage of material versus grain size (ϕ) for samples for hole 739C 33R5 to 34R2.

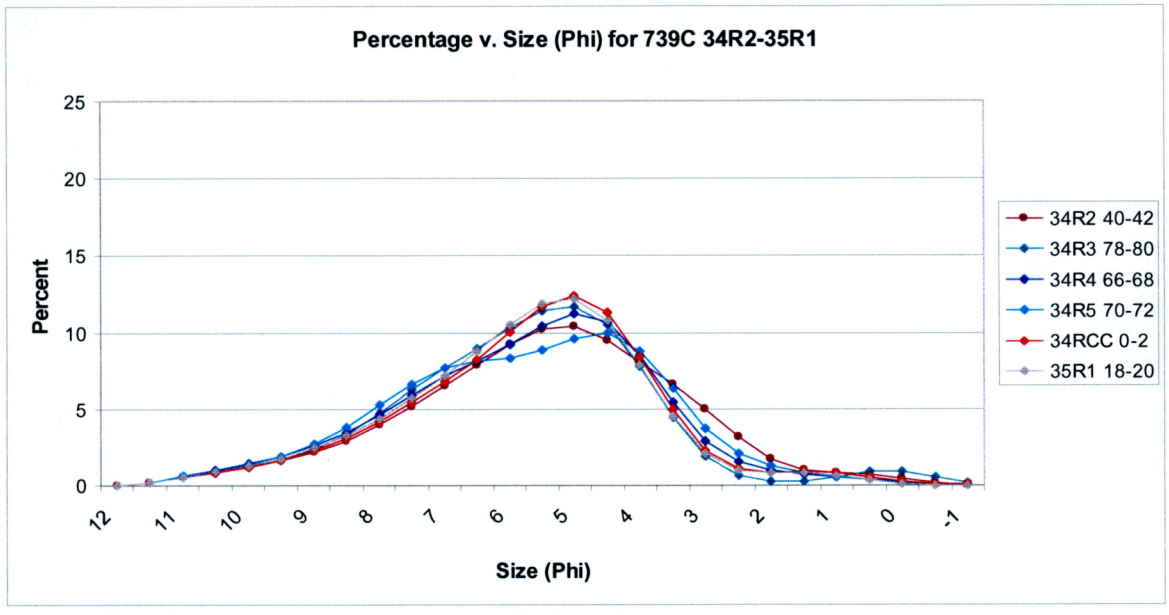

Figure A.10. Percentage of material versus grain size (ϕ) for samples for hole 739C 34R2 to 35R1.

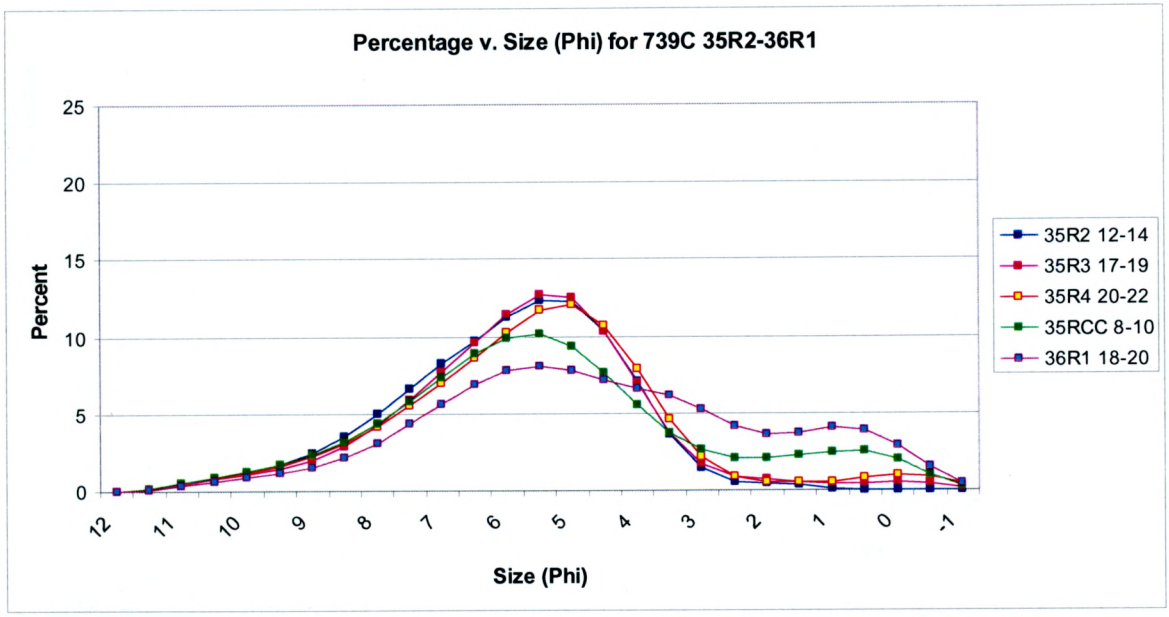

Figure A.11. Percentage of material versus grain size (ϕ) for samples for hole 739C 35R2 to 36R1.

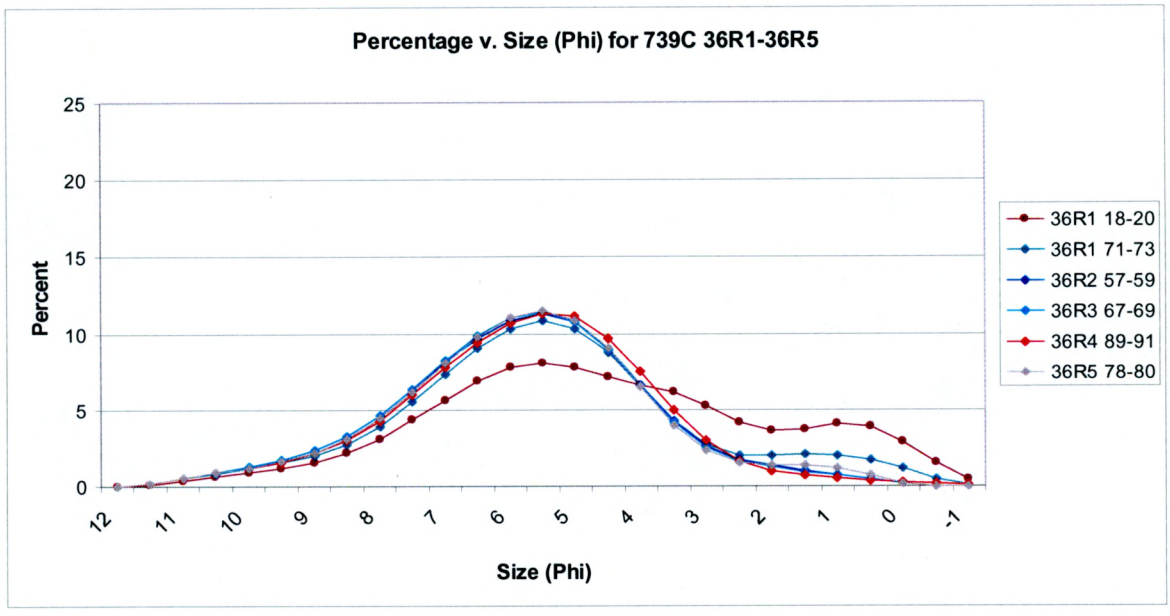

Figure A.12. Percentage of material versus grain size (ϕ) for samples for hole 739C 36R1 to 36R5.

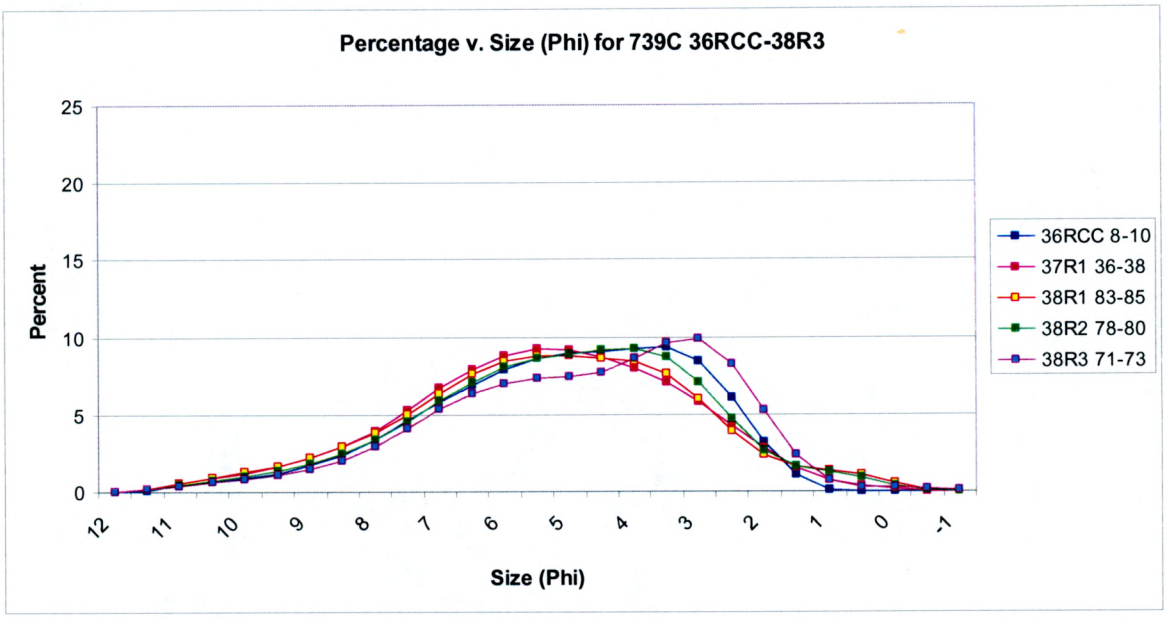

Figure A.13. Percentage of material versus grain size (ϕ) for samples for hole 739C 36RCC to 38R3.

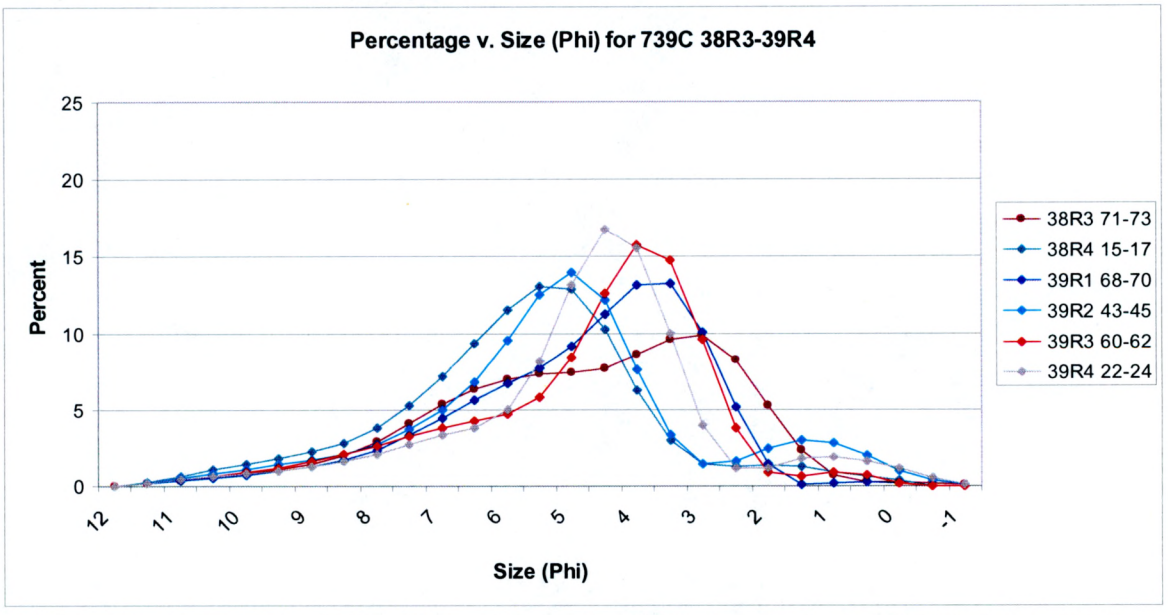

Figure A.14. Percentage of material versus grain size (ϕ) for samples for hole 739C 38R3 to 39R4.

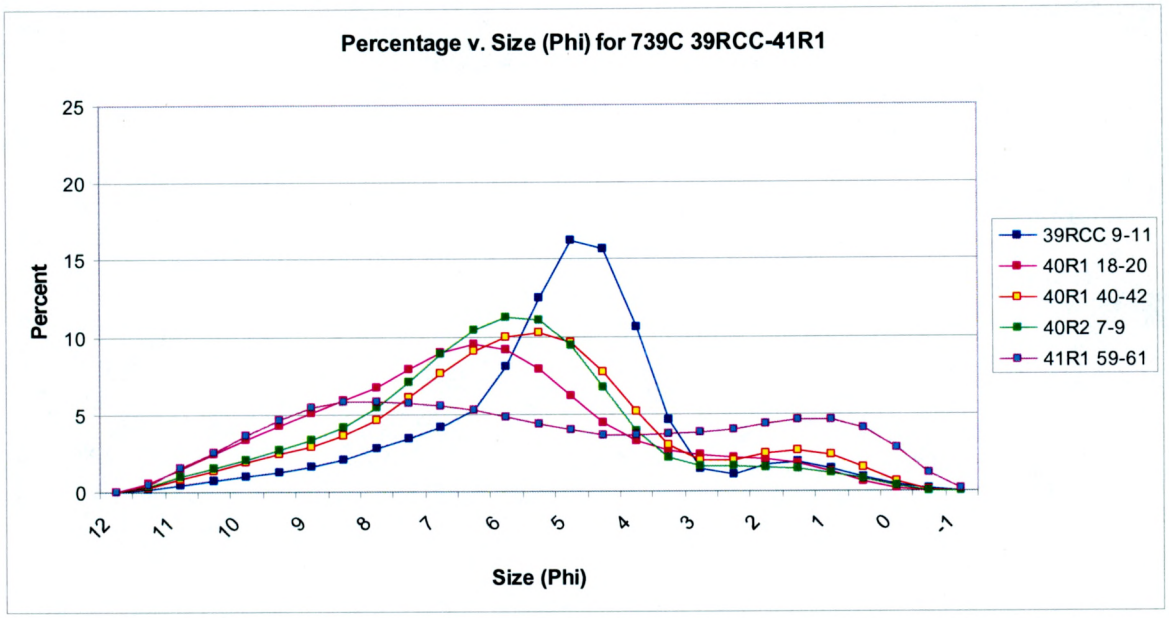

Figure A.15. Percentage of material versus grain size (ϕ) for samples for hole 739C 39RCC to 41R4.

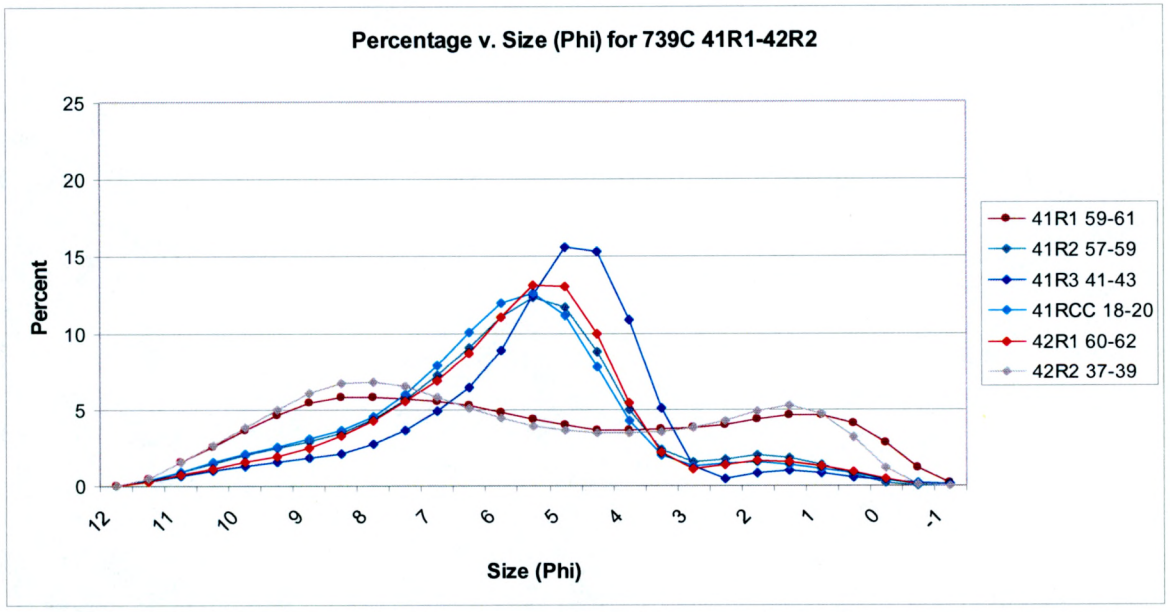

Figure A.16. Percentage of material versus grain size (ϕ) for samples for hole 739C 41R4 to 42R2.

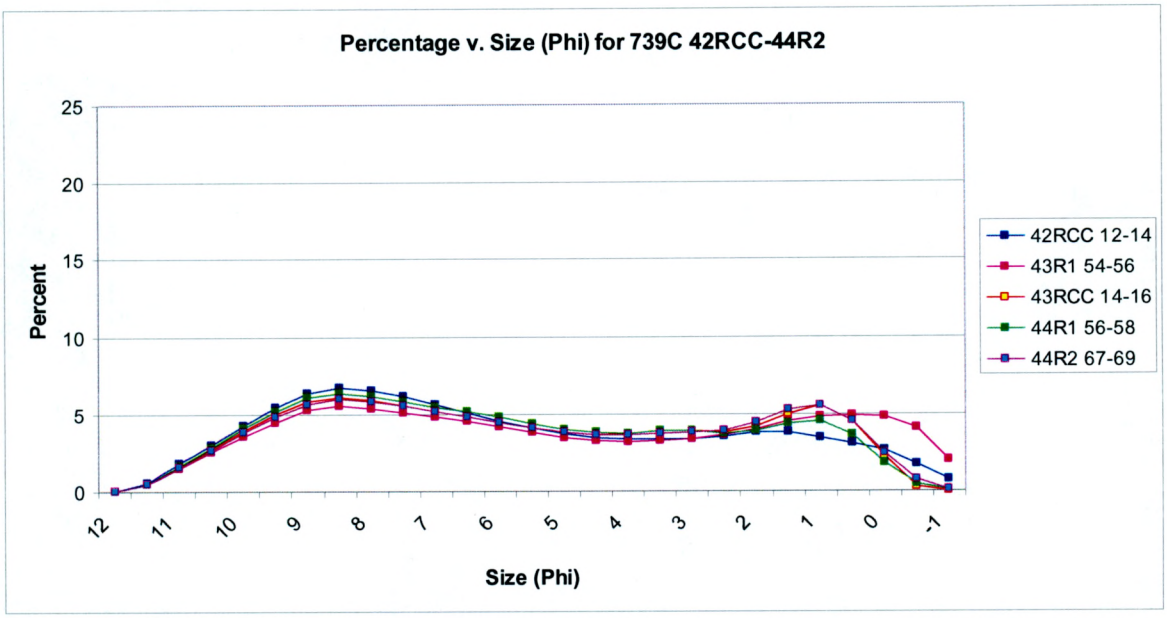

Figure A.17. Percentage of material versus grain size (ϕ) for samples for hole 739C 42RCC to 44R2.

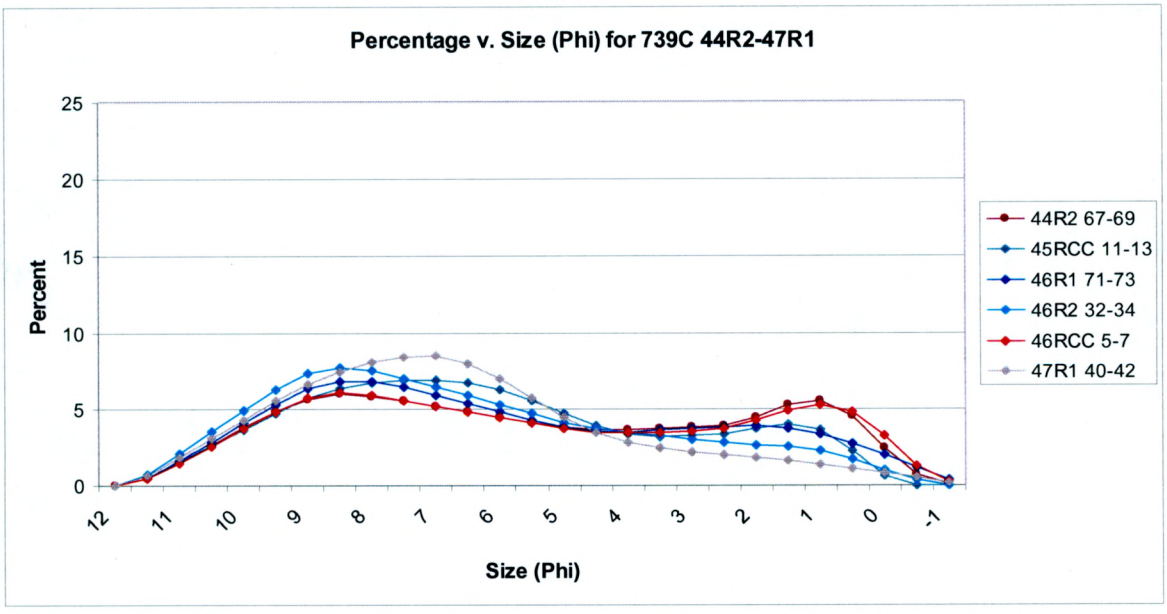

Figure A.18. Percentage of material versus grain size (ϕ) for samples for hole 739C 44R2 to 47R1.

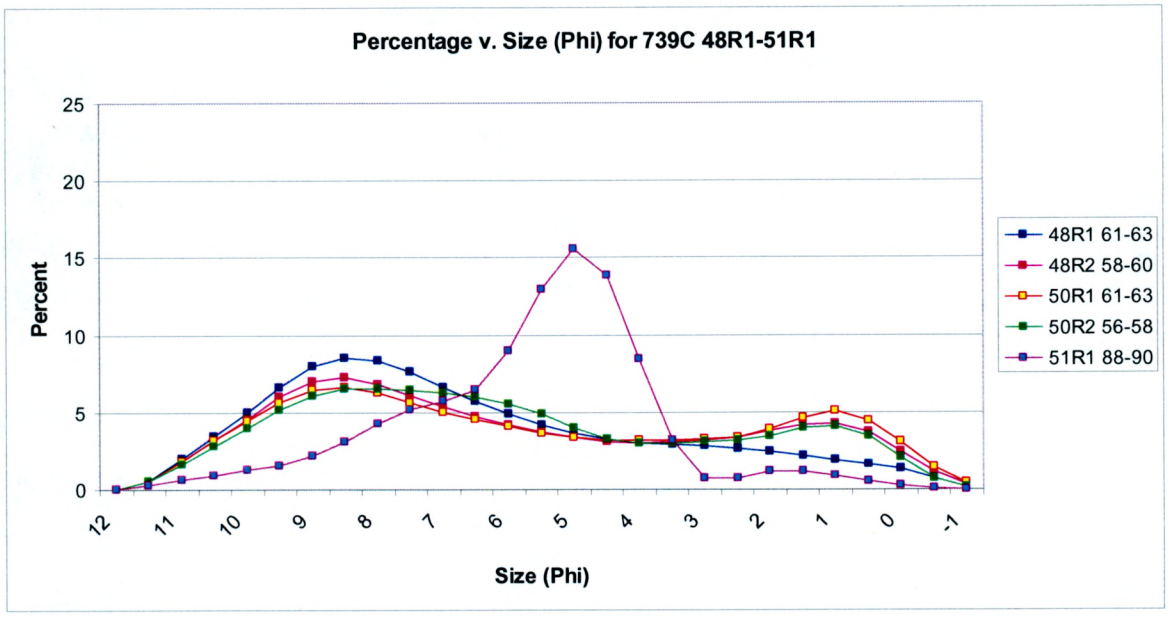

Figure A.19. Percentage of material versus grain size (ϕ) for samples for hole 739C 48R1 to 51R1.

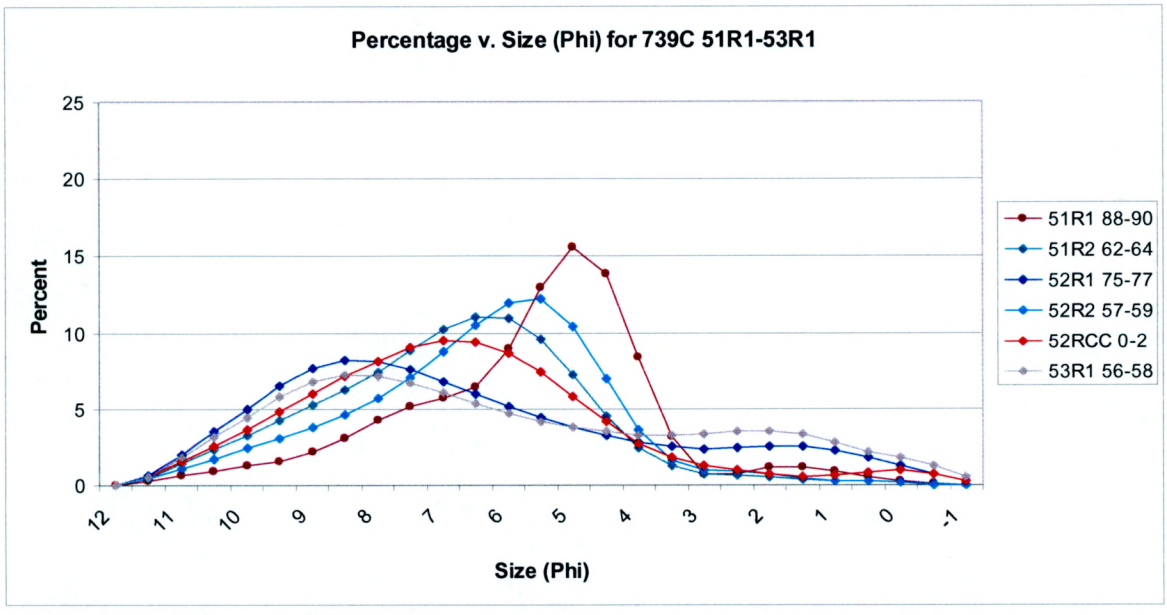

Figure A.20. Percentage of material versus grain size (ϕ) for samples for hole 739C 51R1 to 53R1.

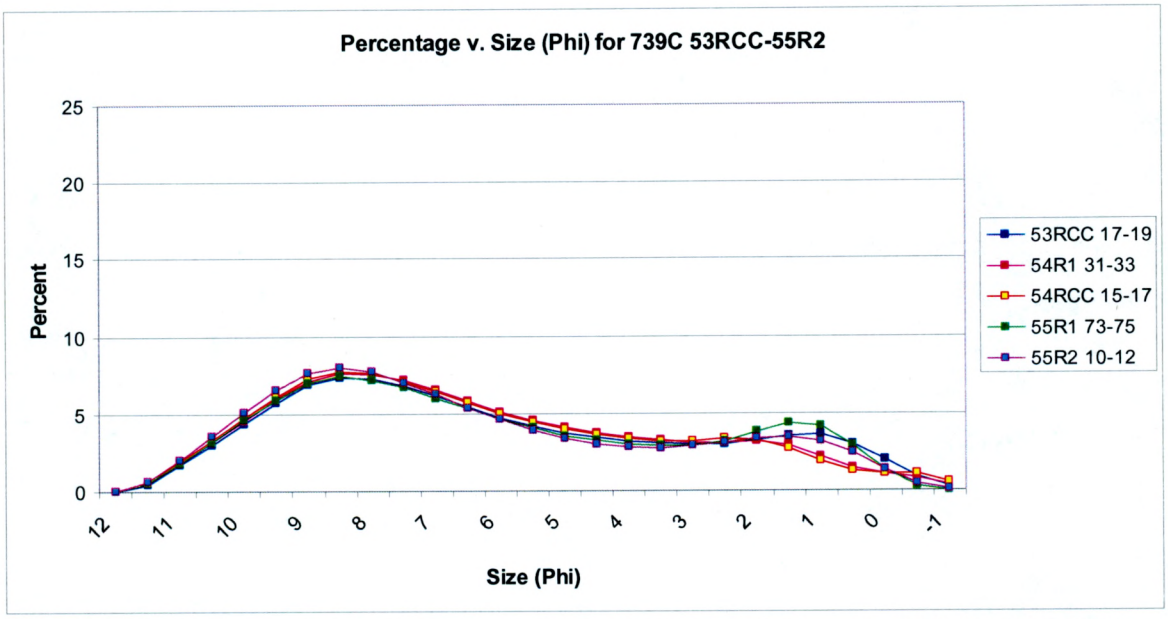

Figure A.21. Percentage of material versus grain size (ϕ) for samples for hole 739C 53RCC to 55R2.

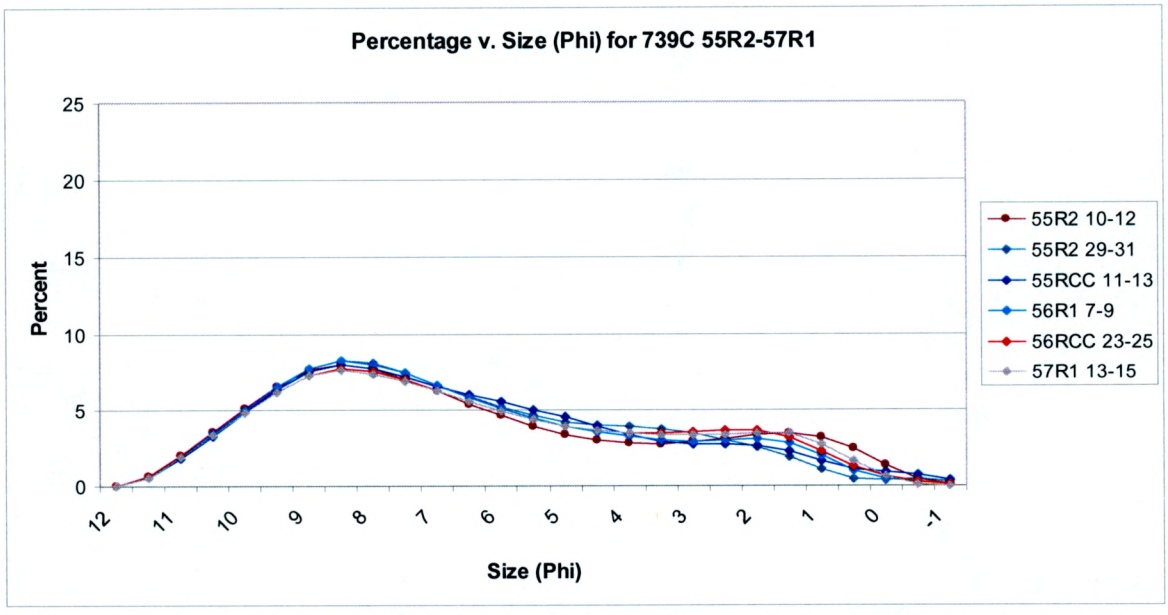

Figure A.22. Percentage of material versus grain size (ϕ) for samples for hole 739C 55R2 to 57R1.

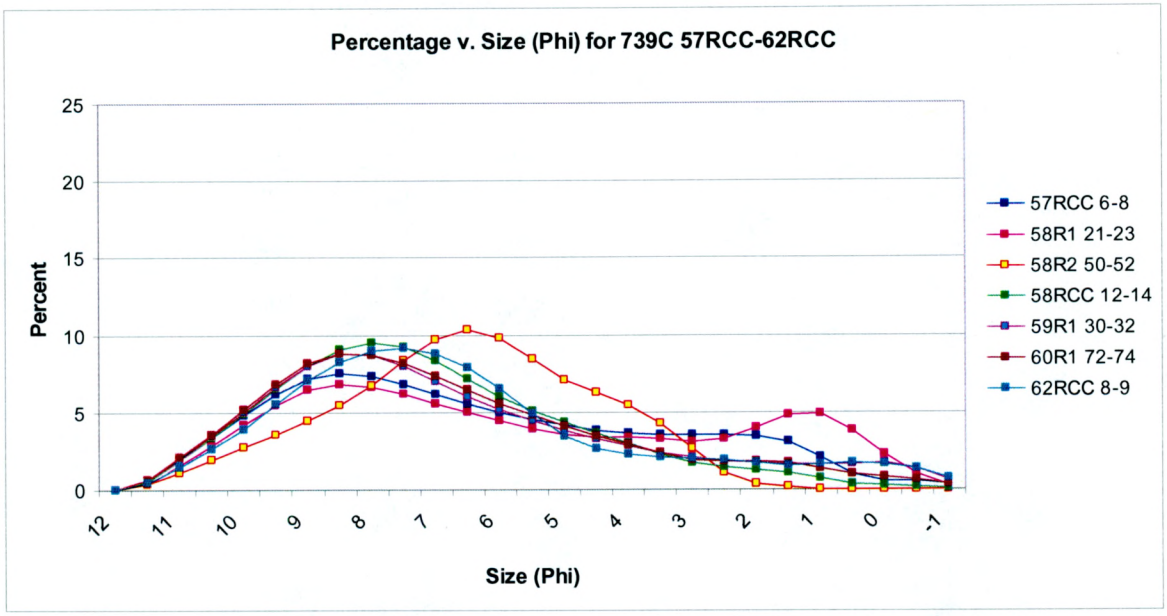

Figure A.23. Percentage of material versus grain size (ϕ) for samples for hole 739C 57RCC to 62RCC.

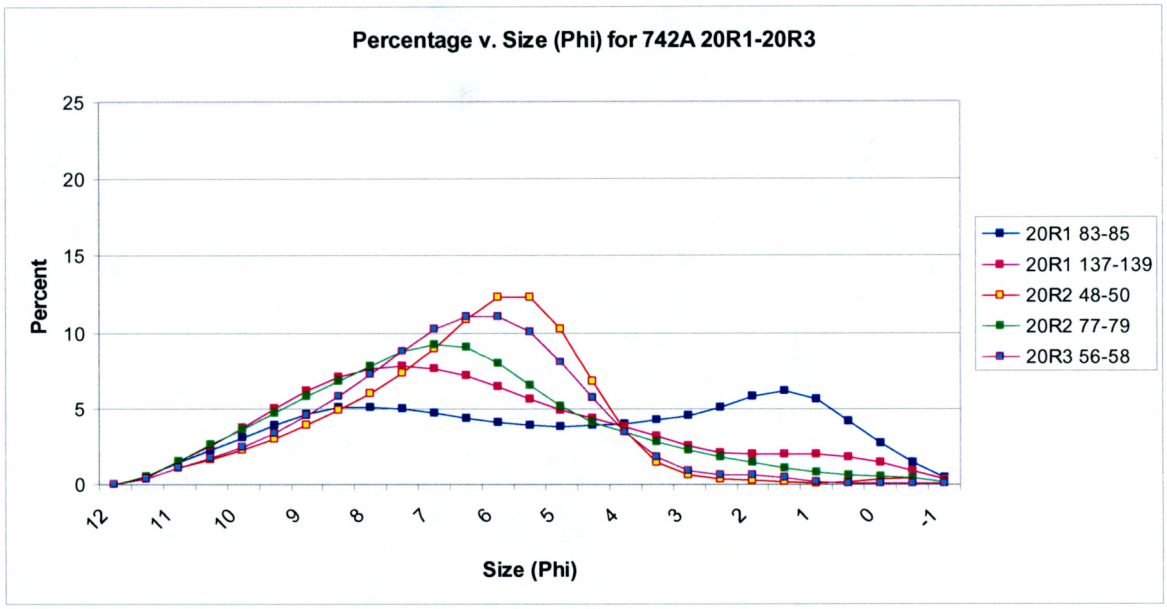

Figure A.24. Percentage of material versus grain size (ϕ) for samples for hole 742A 20R1 to 20R3.

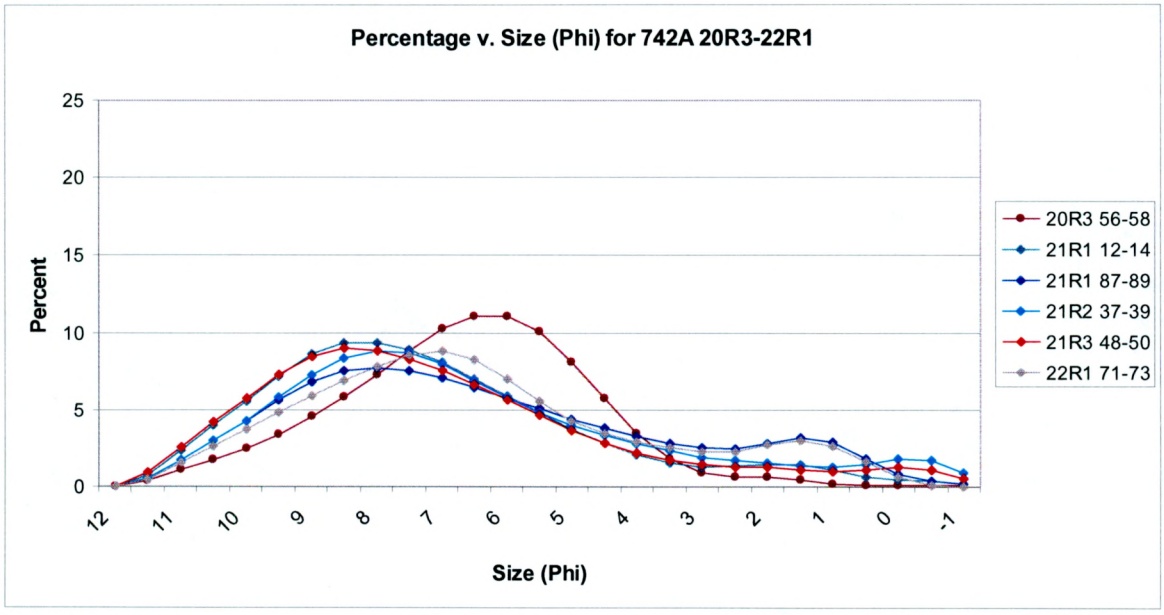

Figure A.25. Percentage of material versus grain size (ϕ) for samples for hole 742A 20R3 to 22R1.

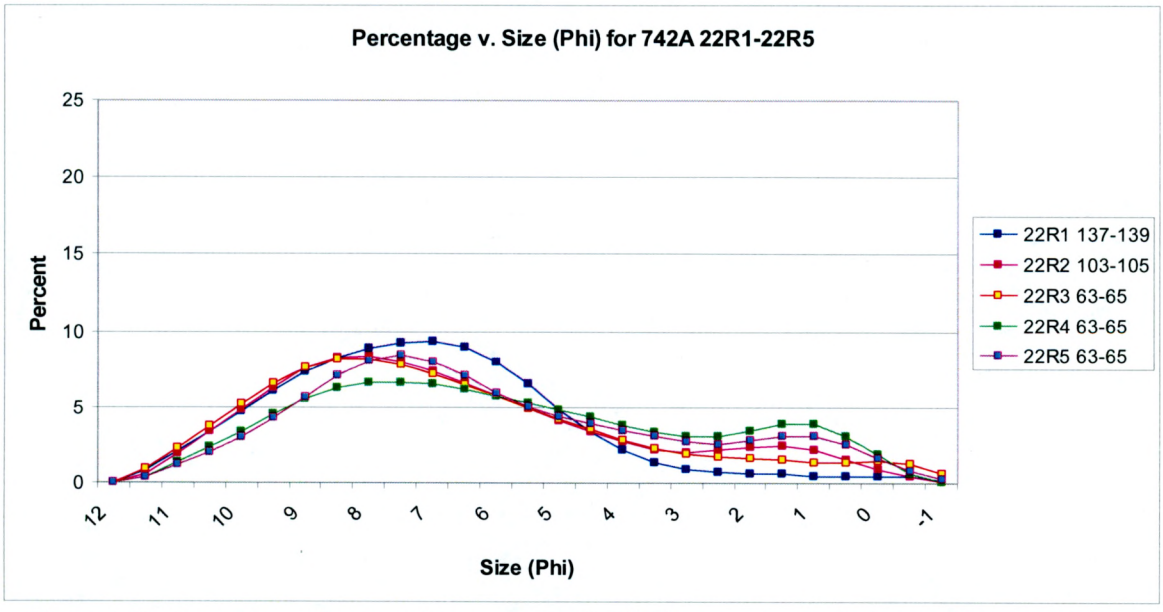

Figure A.26. Percentage of material versus grain size (ϕ) for samples for hole 742A 22R1 to 22R5.

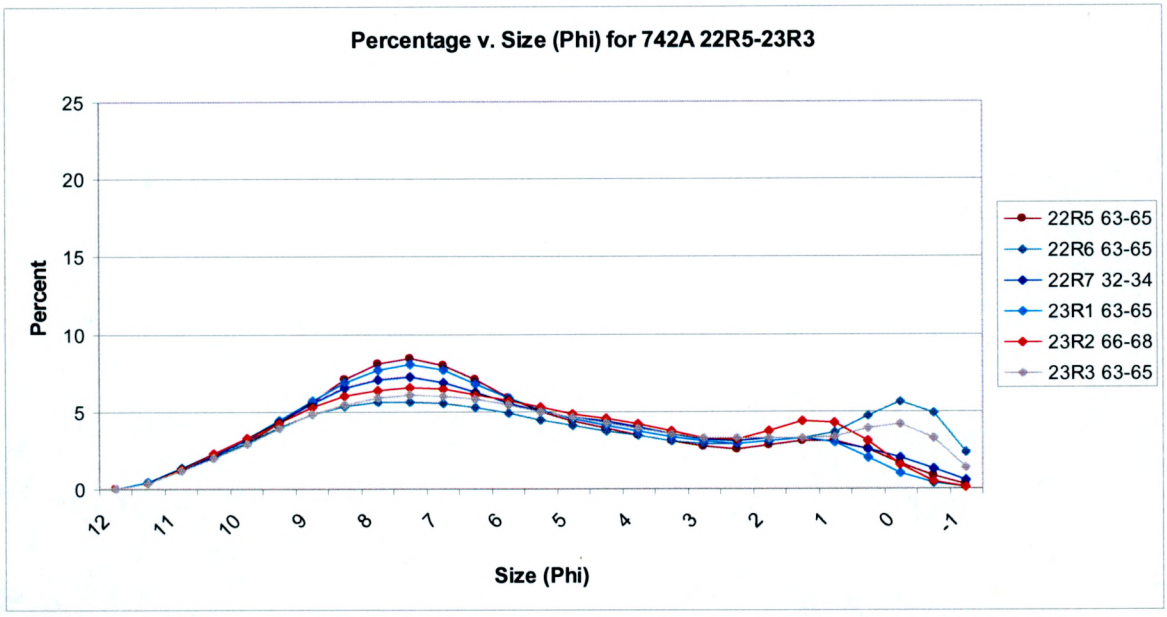

Figure A.27. Percentage of material versus grain size (ϕ) for samples for hole 742A 22R5 to 23R3.

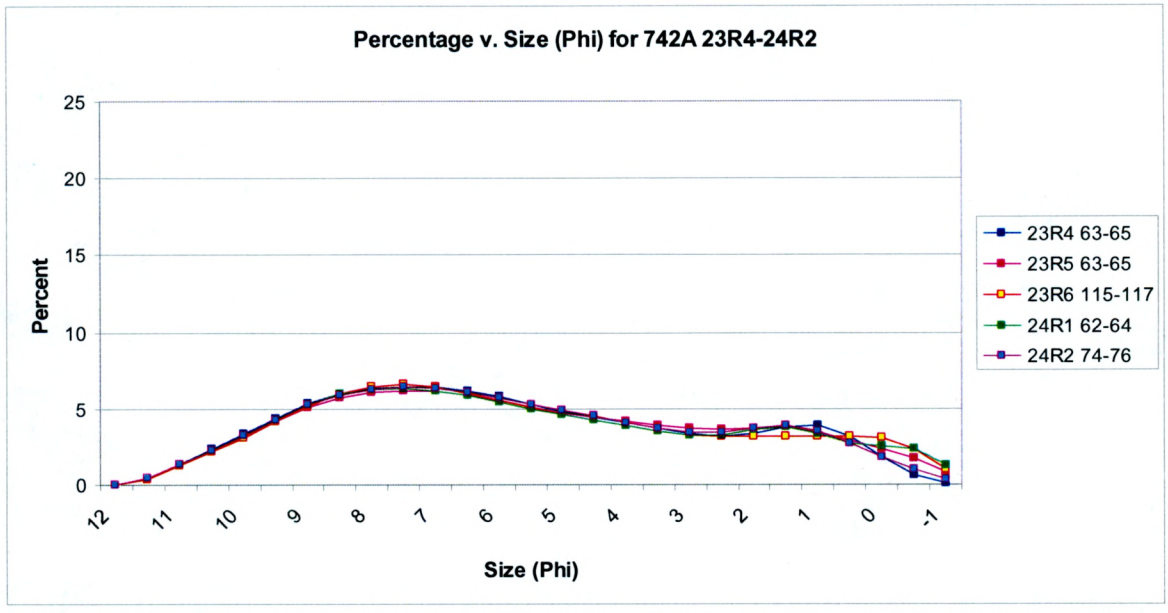

Figure A.28. Percentage of material versus grain size (ϕ) for samples for hole 742A 23R4 to 24R2.

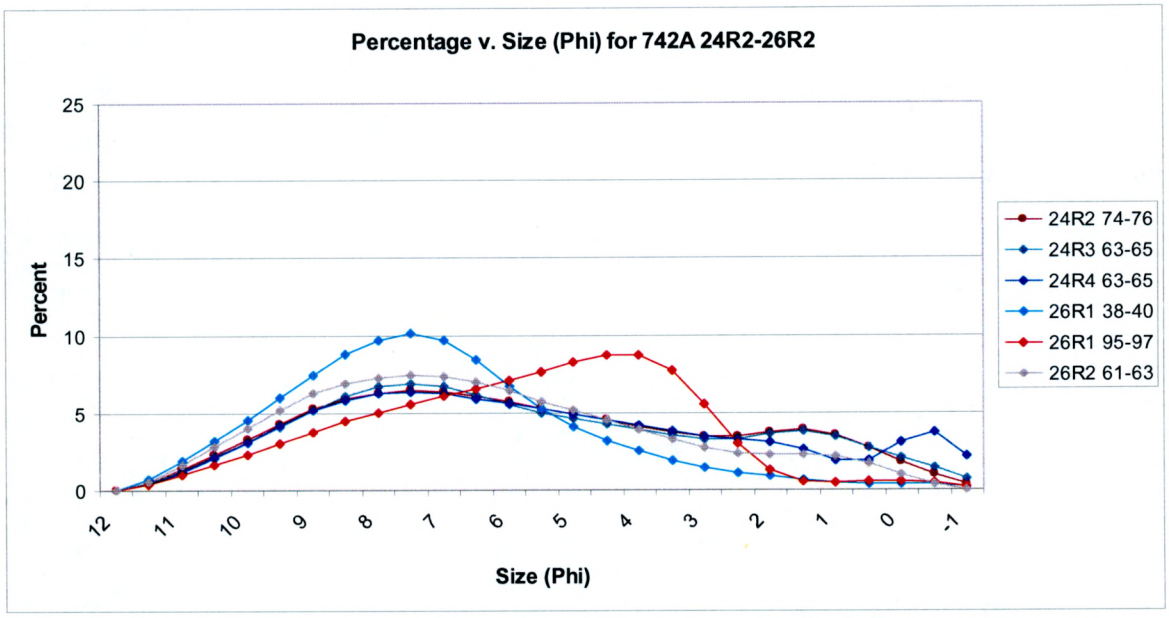

Figure A.29. Percentage of material versus grain size (ϕ) for samples for hole 742A 24R2 to 26R2.

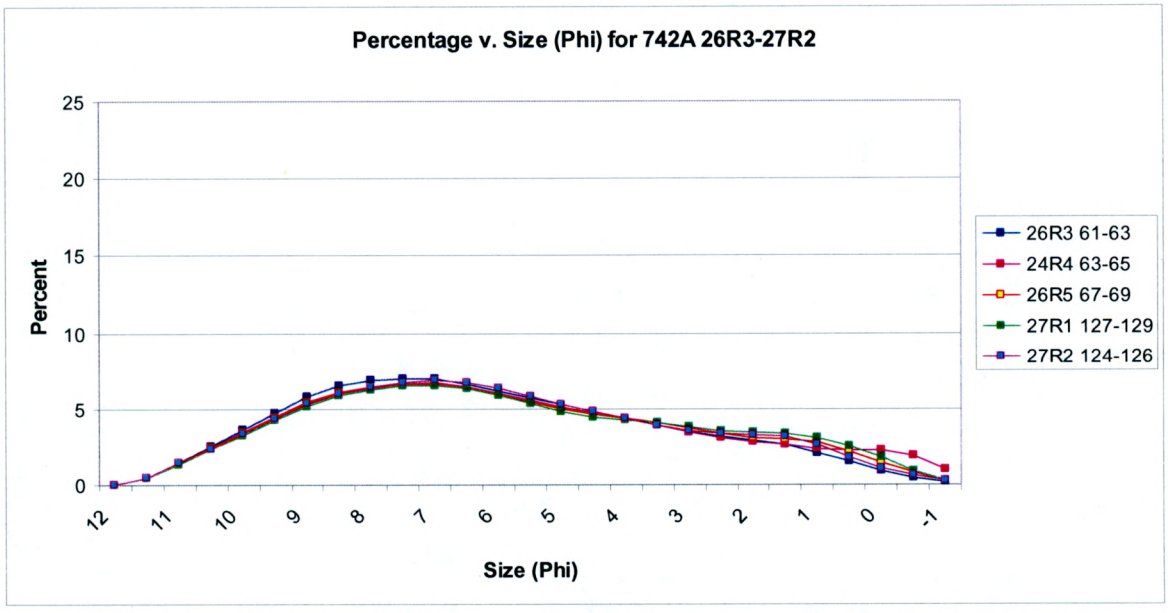

Figure A.30. Percentage of material versus grain size (ϕ) for samples for hole 742A 26R3 to 27R2.

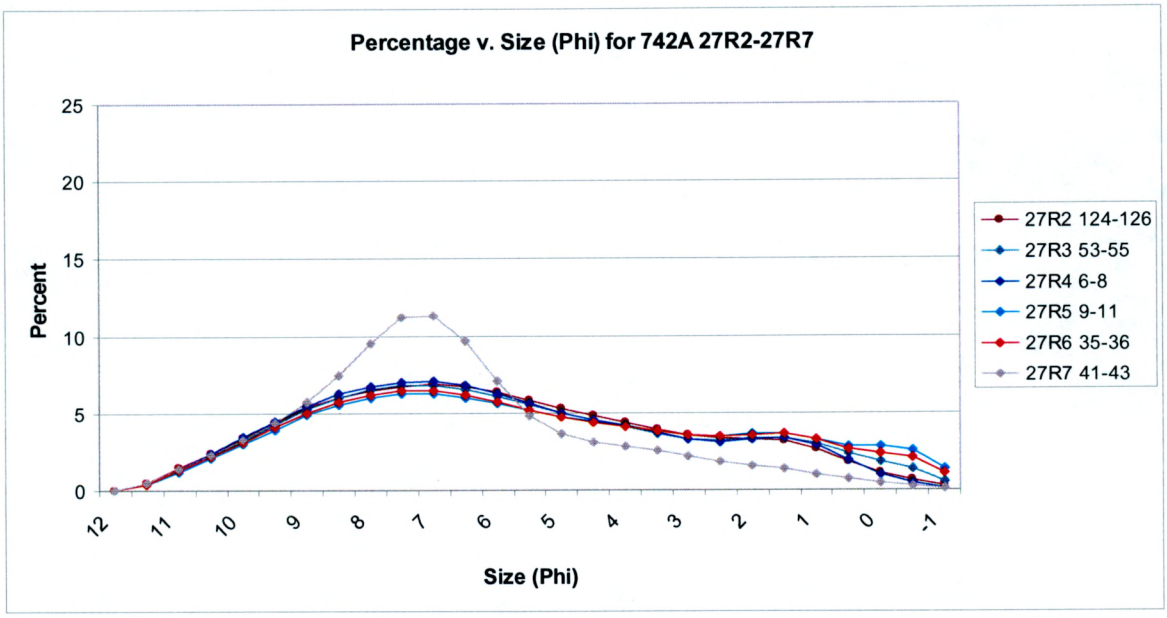

Figure A.31. Percentage of material versus grain size (ϕ) for samples for hole 742A 27R2 to 27R7.

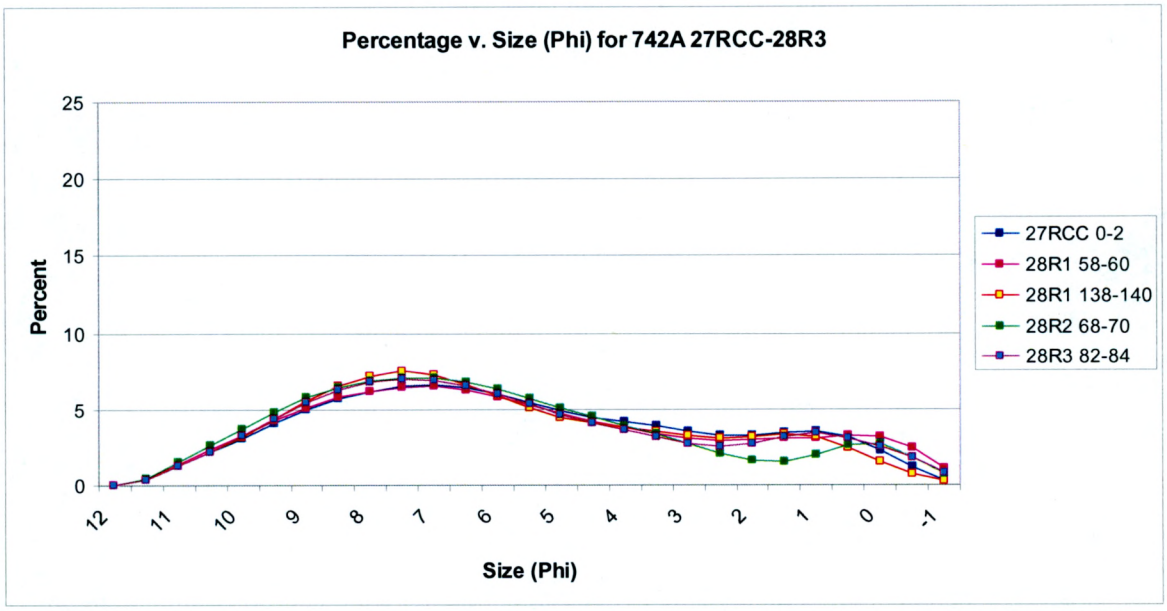

Figure A.32. Percentage of material versus grain size (ϕ) for samples for hole 742A 27RCC to 28R3.

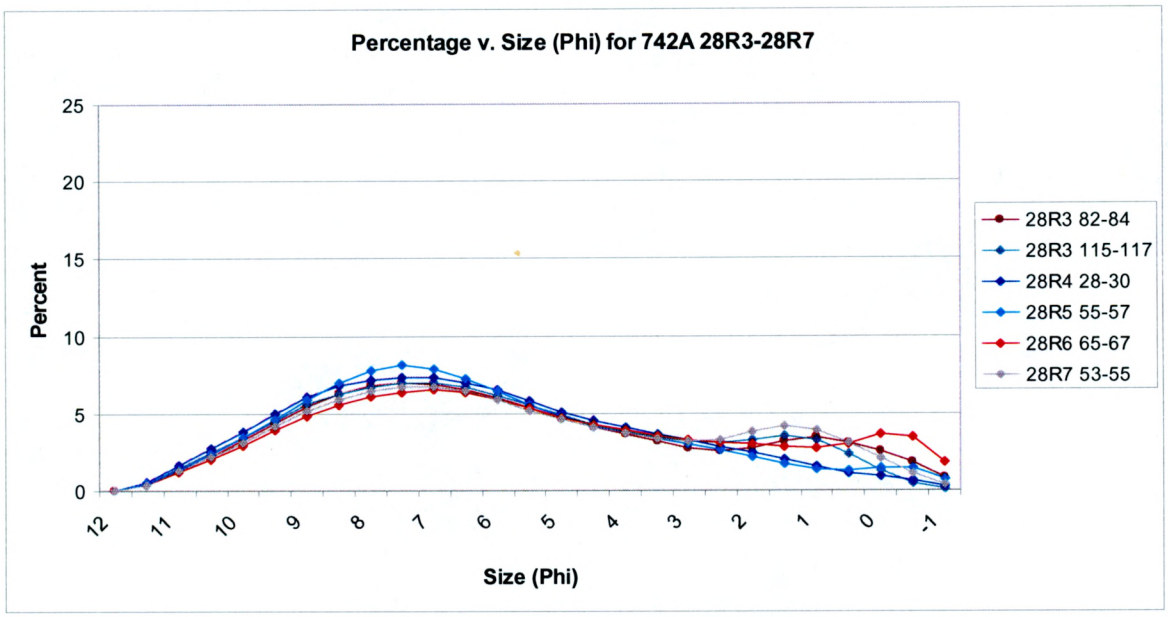

Figure A.33. Percentage of material versus grain size (ϕ) for samples for hole 742A 28R3 to 28R7.

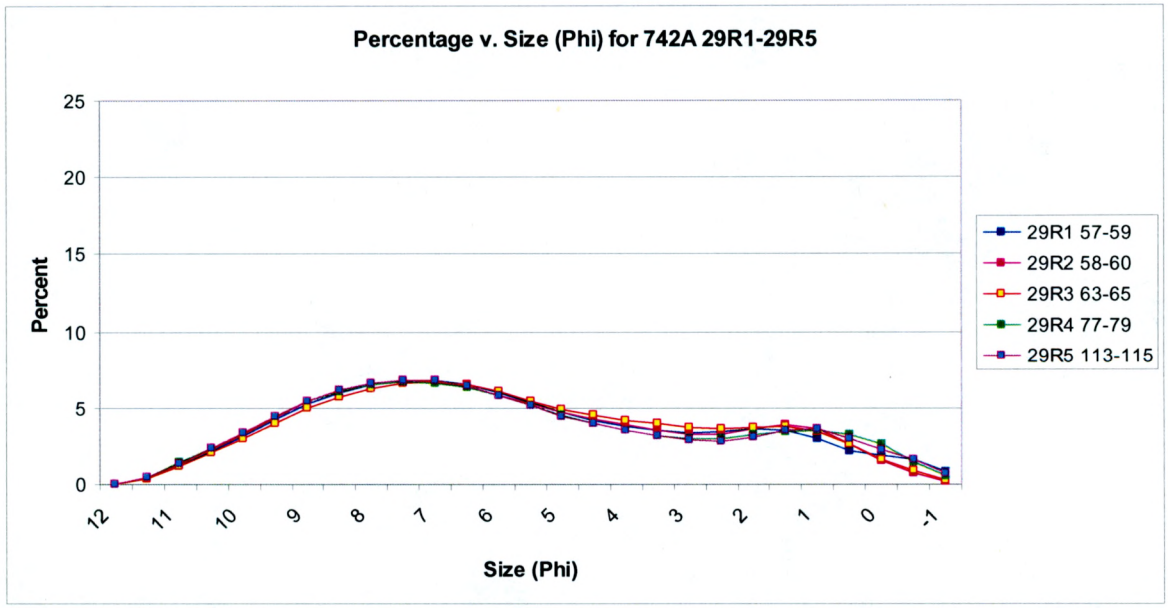

Figure A.34. Percentage of material versus grain size (ϕ) for samples for hole 742A 29R1 to 29R5.

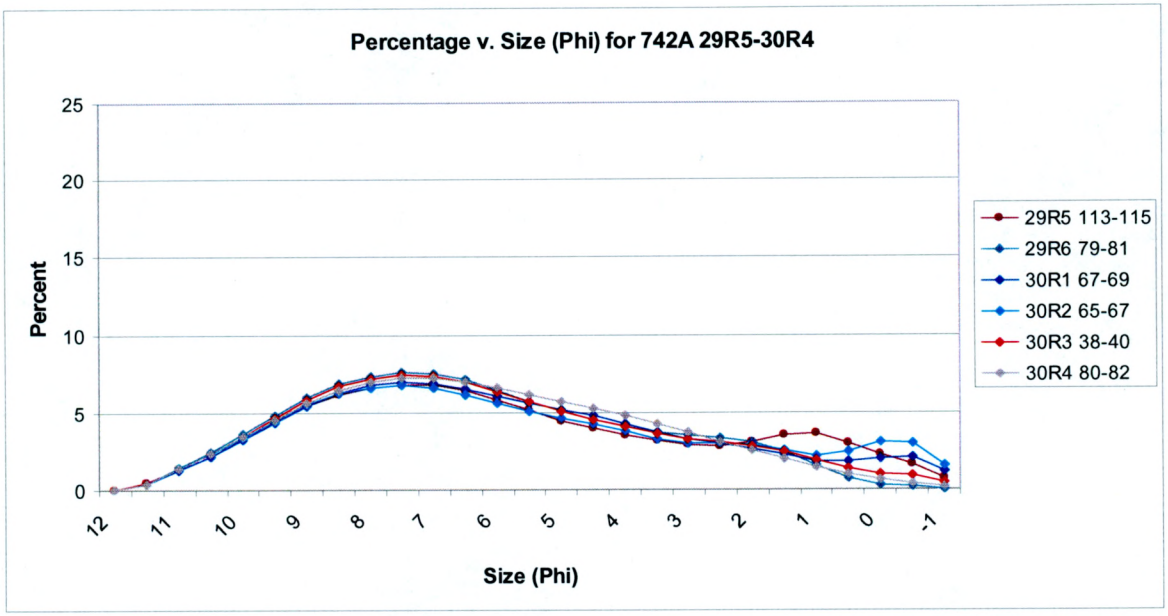

Figure A.35. Percentage of material versus grain size (ϕ) for samples for hole 742A 29R5 to 30R4.

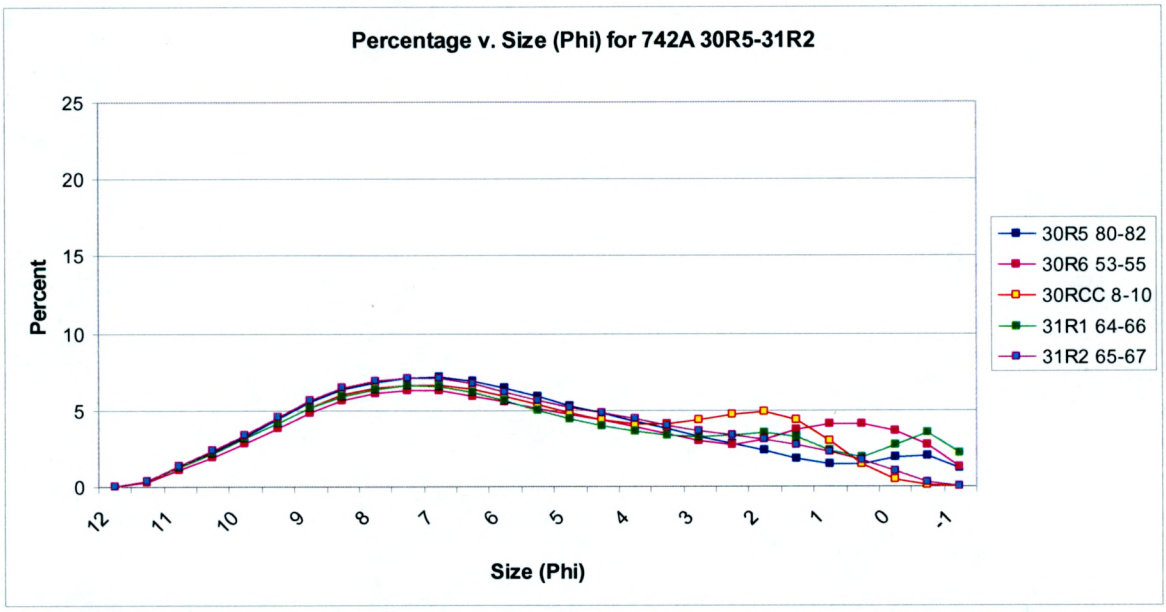

Figure A.36. Percentage of material versus grain size (ϕ) for samples for hole 742A 30R5 to 31R2.

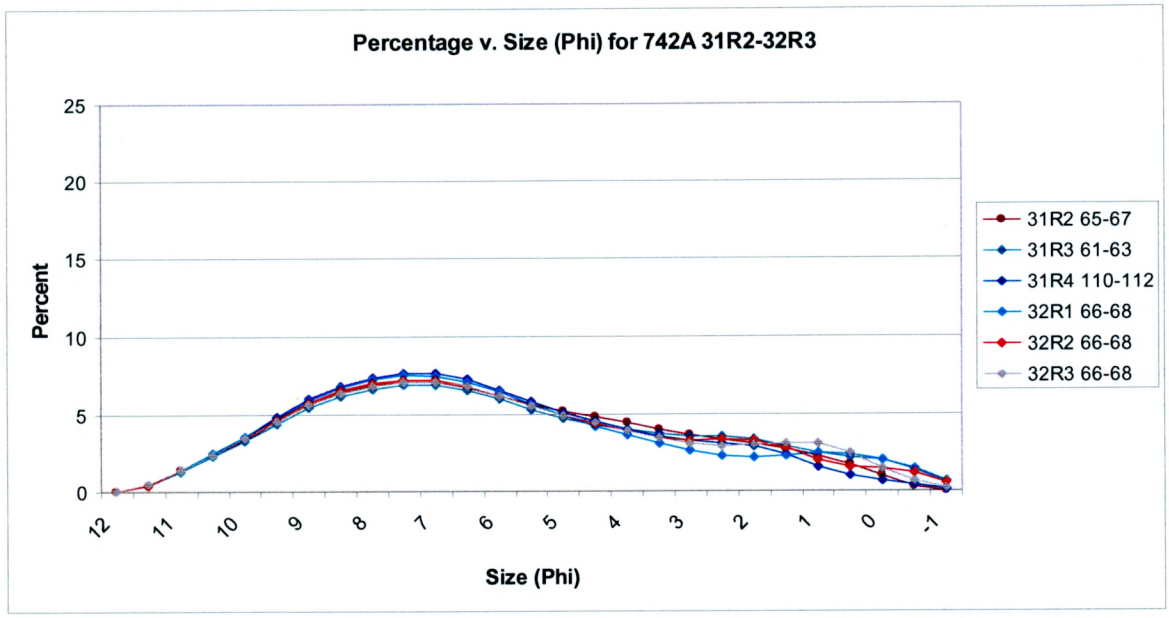

Figure A.37. Percentage of material versus grain size (ϕ) for samples for hole 742A 31R2 to 32R3.

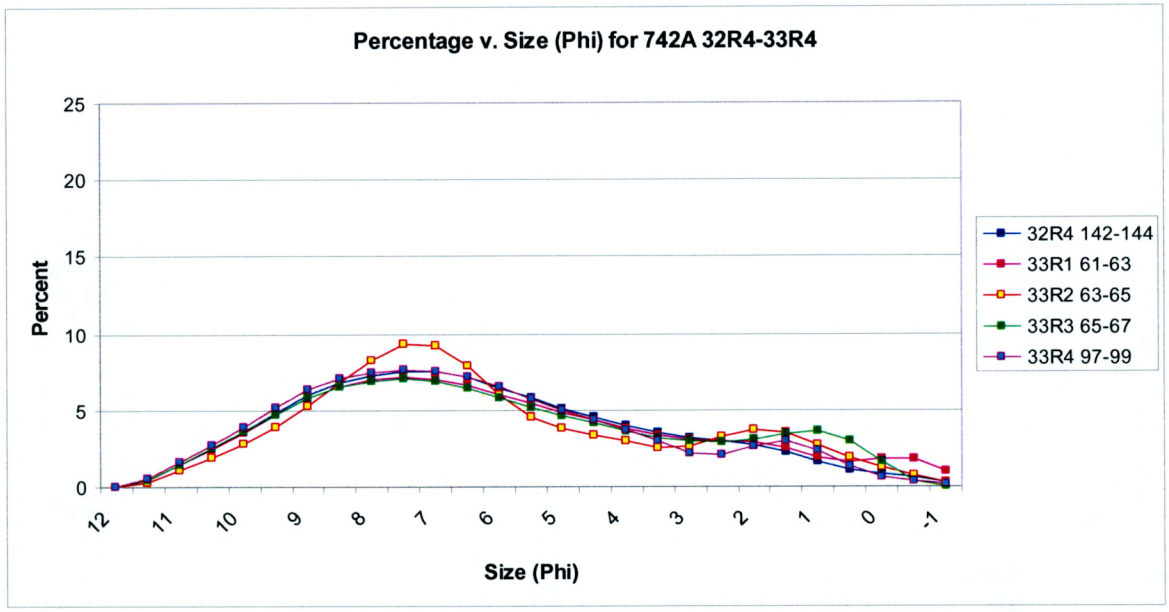

Figure A.38. Percentage of material versus grain size (ϕ) for samples for hole 742A 32R4 to 33R4.

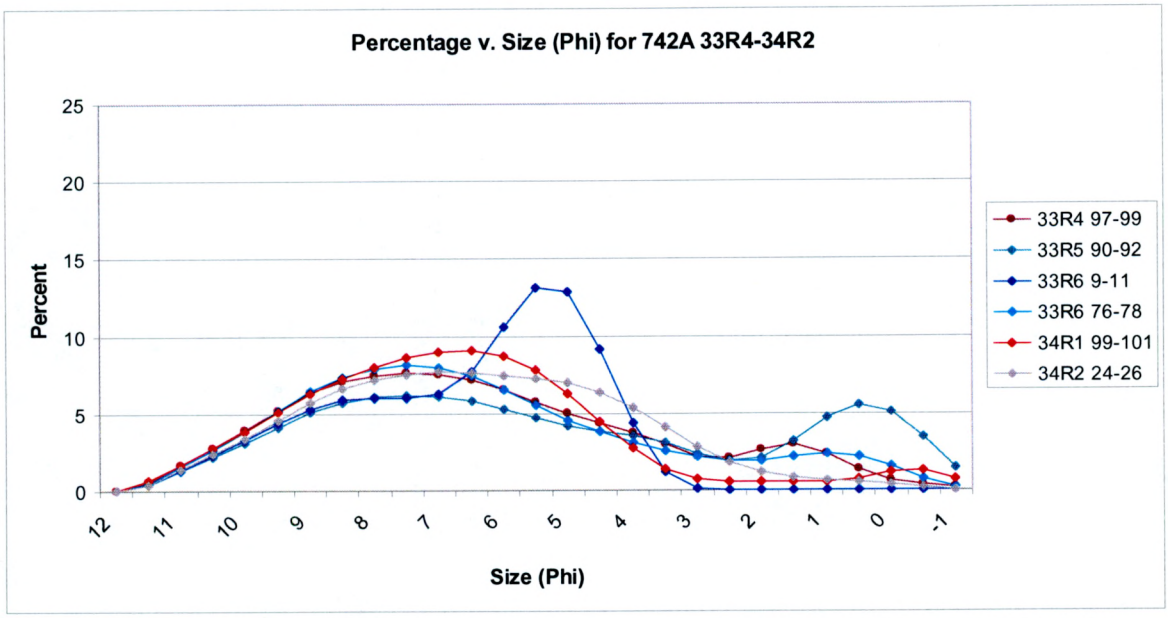

Figure A.39. Percentage of material versus grain size (ϕ) for samples for hole 742A 33R4 to 34R2.

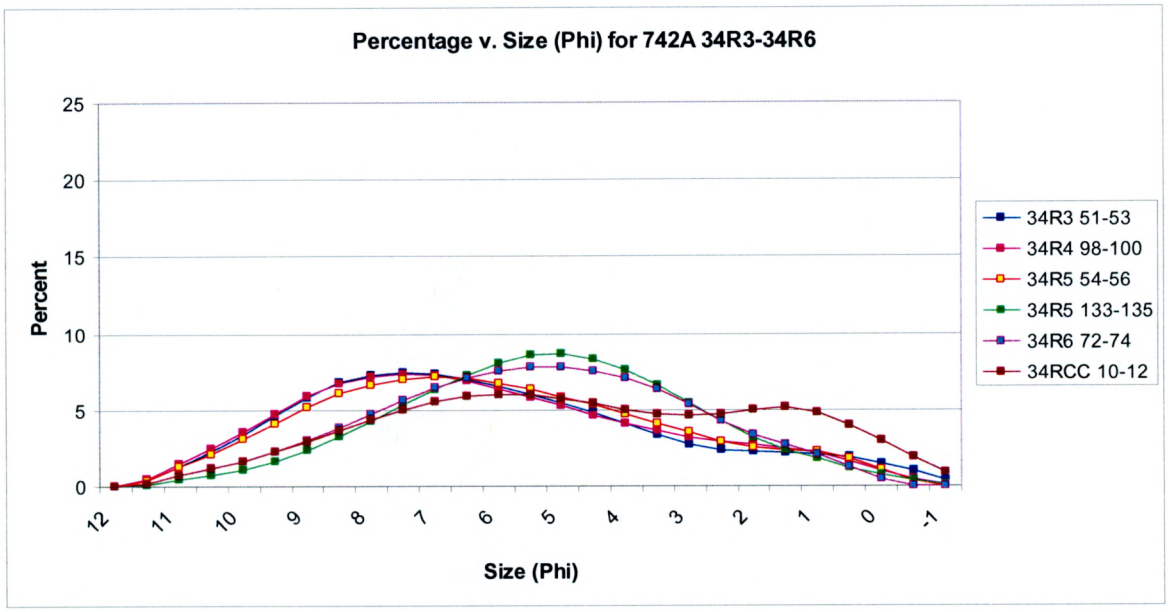

Figure A.40. Percentage of material versus grain size (ϕ) for samples for hole 742A 34R3 to 34RCC.

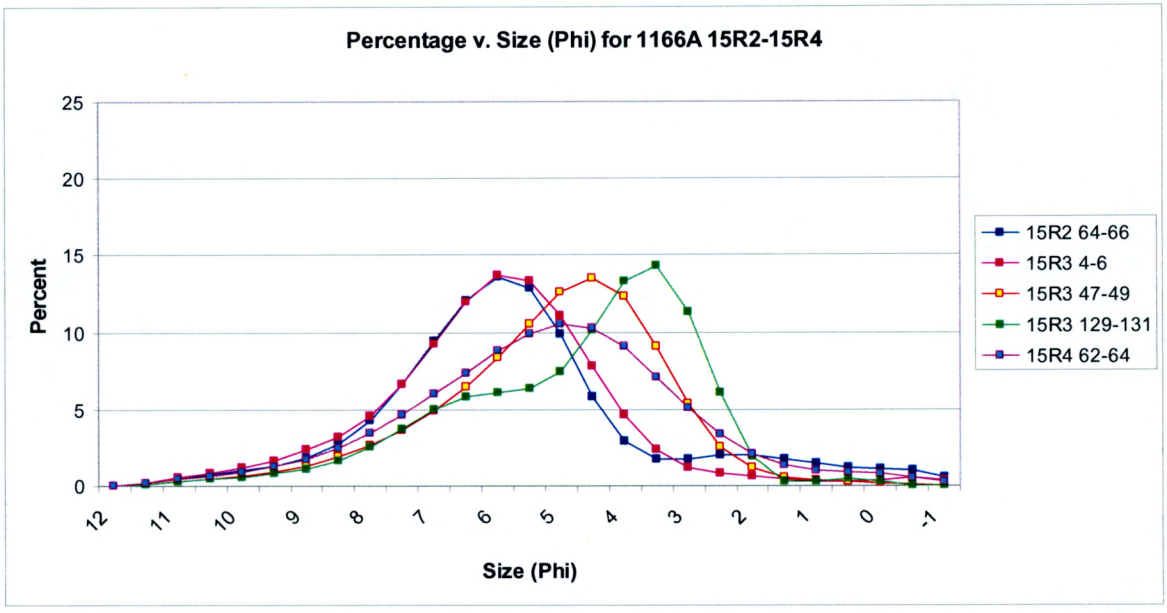

Figure A.41. Percentage of material versus grain size (ϕ) for samples for hole 1166A 15R2 to 15R4.

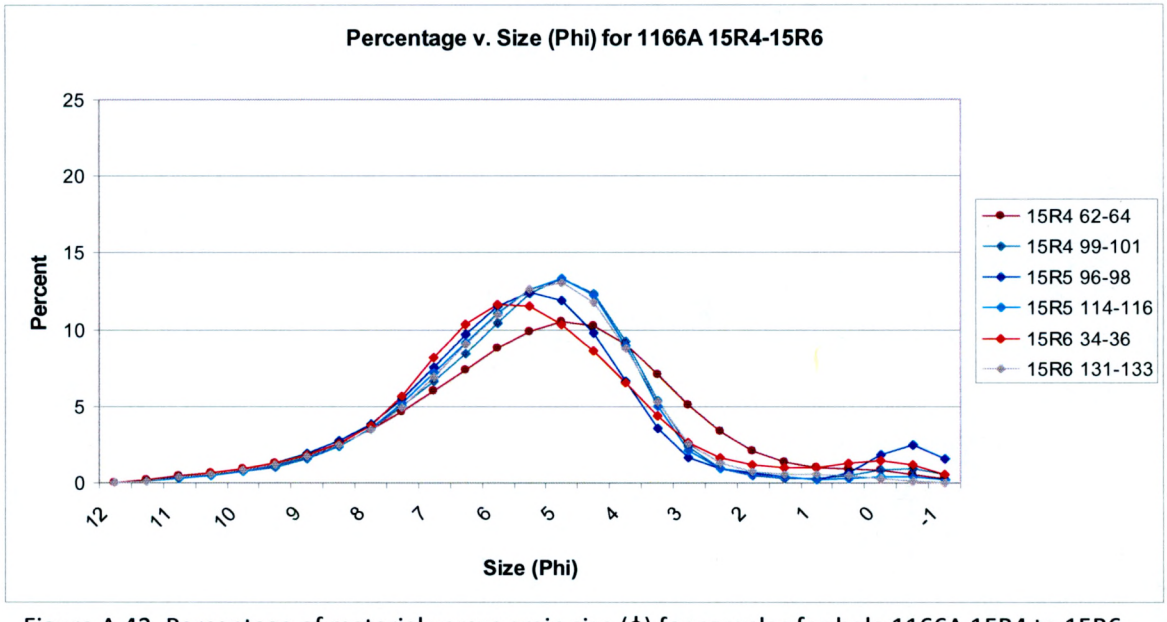

Figure A.42. Percentage of material versus grain size (ϕ) for samples for hole 1166A 15R4 to 15R6.

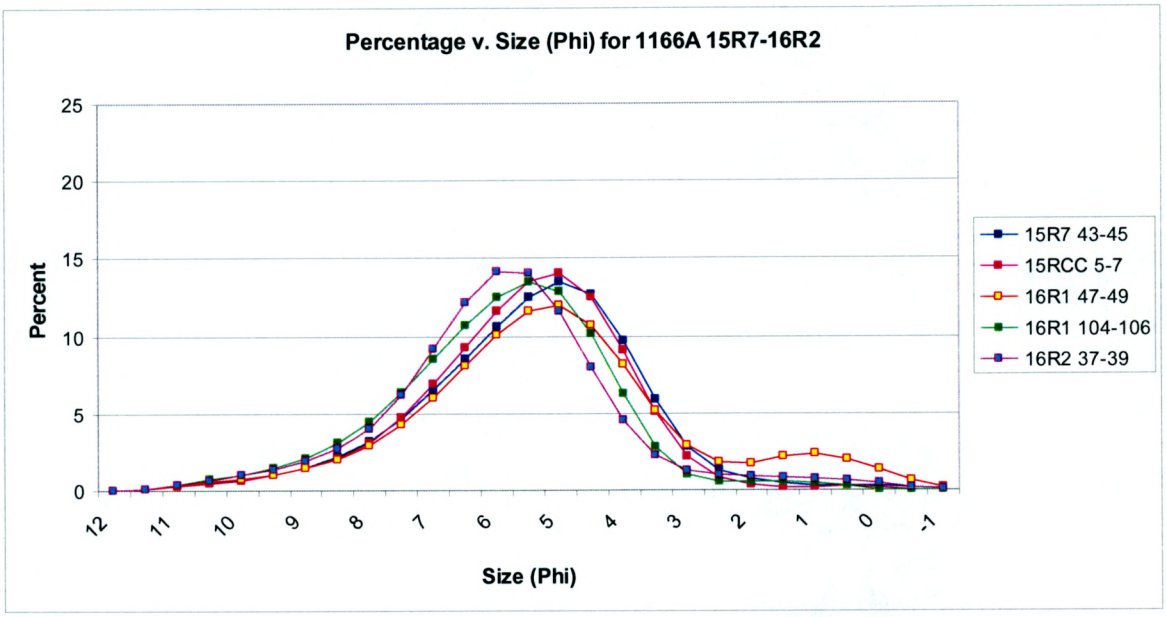

Figure A.43. Percentage of material versus grain size (ϕ) for samples for hole 1166A 15R7 to 16R2.

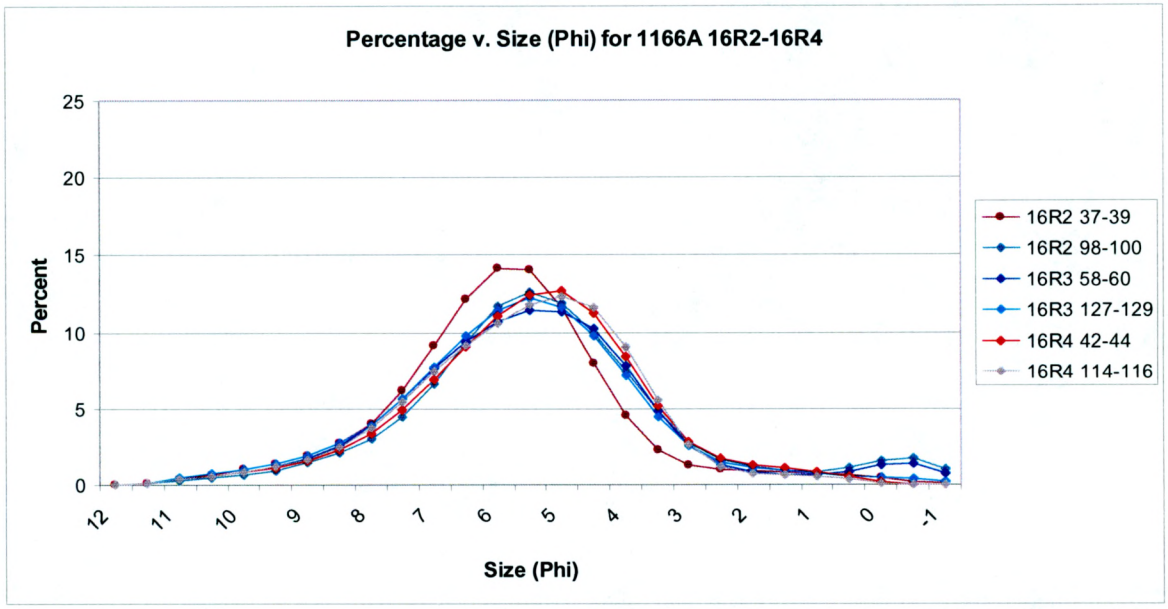

Figure A.44. Percentage of material versus grain size (ϕ) for samples for hole 1166A 16R2 to 16R4.

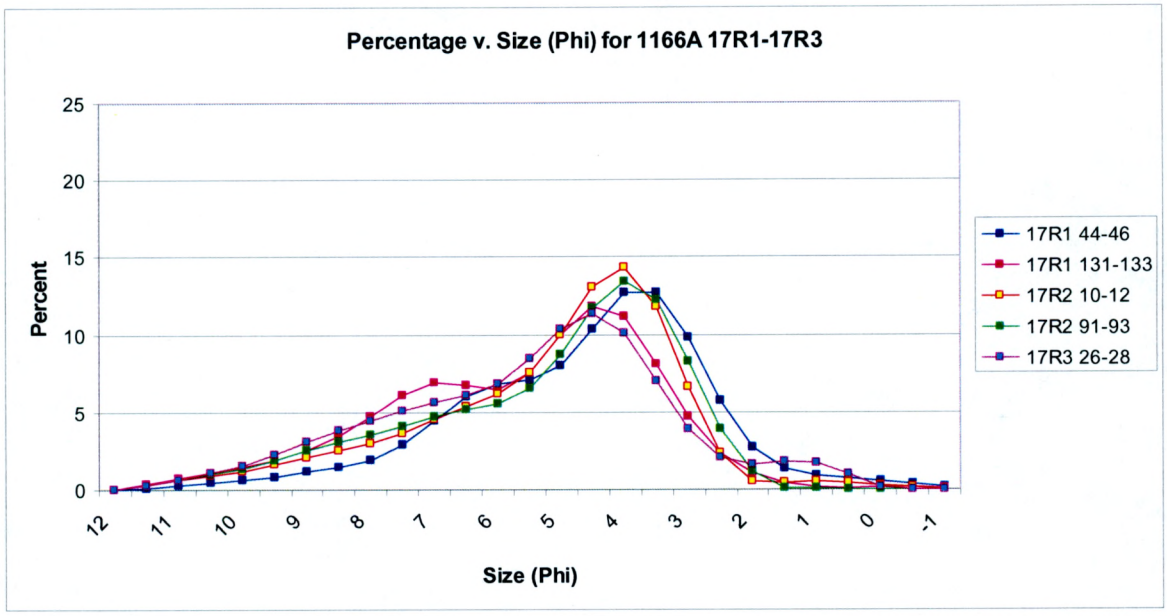

Figure A.45. Percentage of material versus grain size (ϕ) for samples for hole 1166A 17R1 to 17R3.

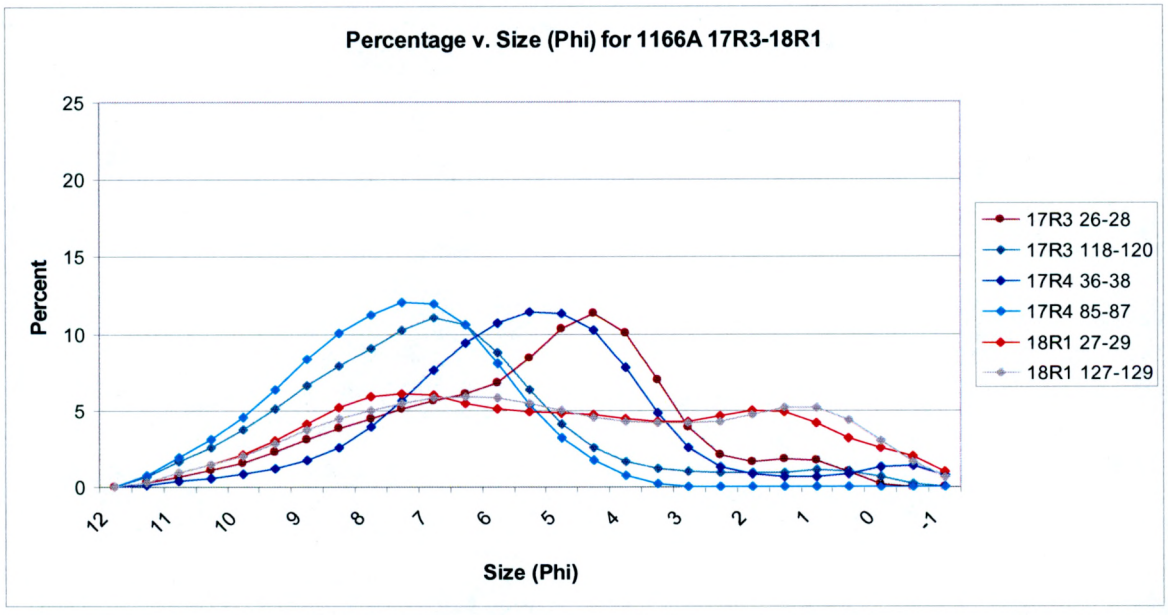

Figure A.46. Percentage of material versus grain size (ϕ) for samples for hole 1166A 17R3 to 18R1.

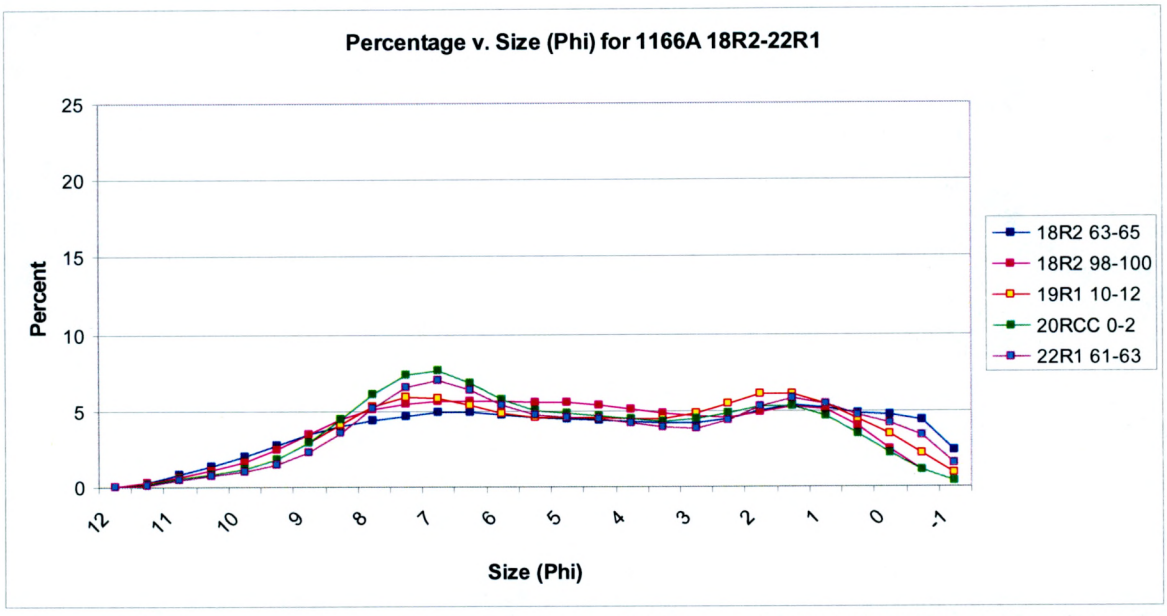

Figure A.47. Percentage of material versus grain size (ϕ) for samples for hole 1166A 18R2 to 22R1.

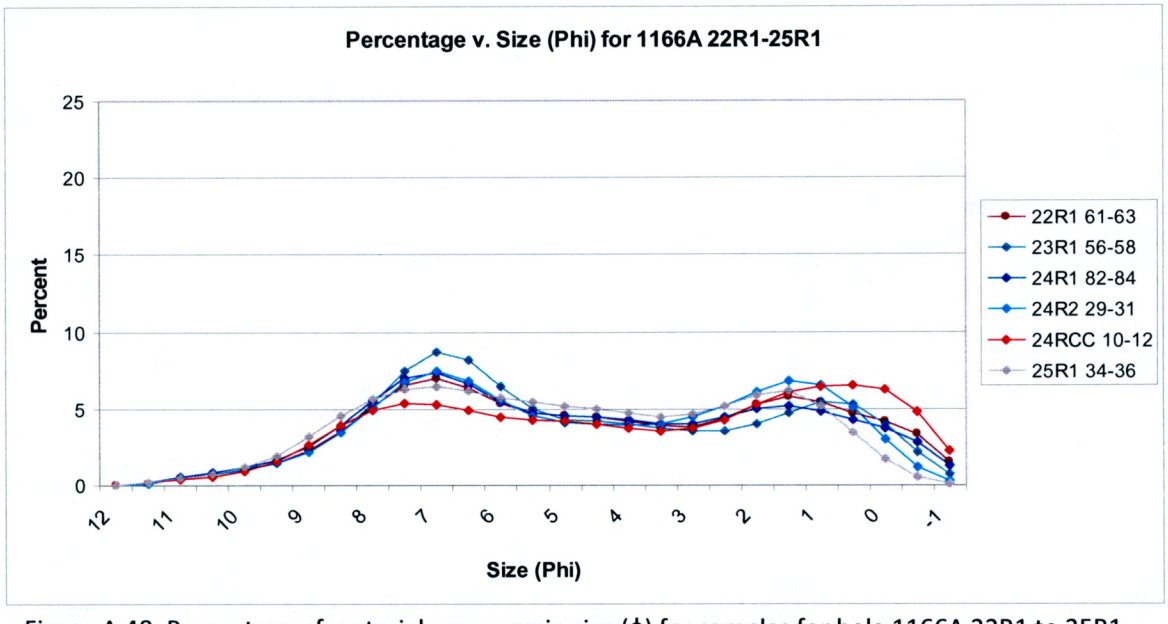

Figure A.48. Percentage of material versus grain size (ϕ) for samples for hole 1166A 22R1 to 25R1.

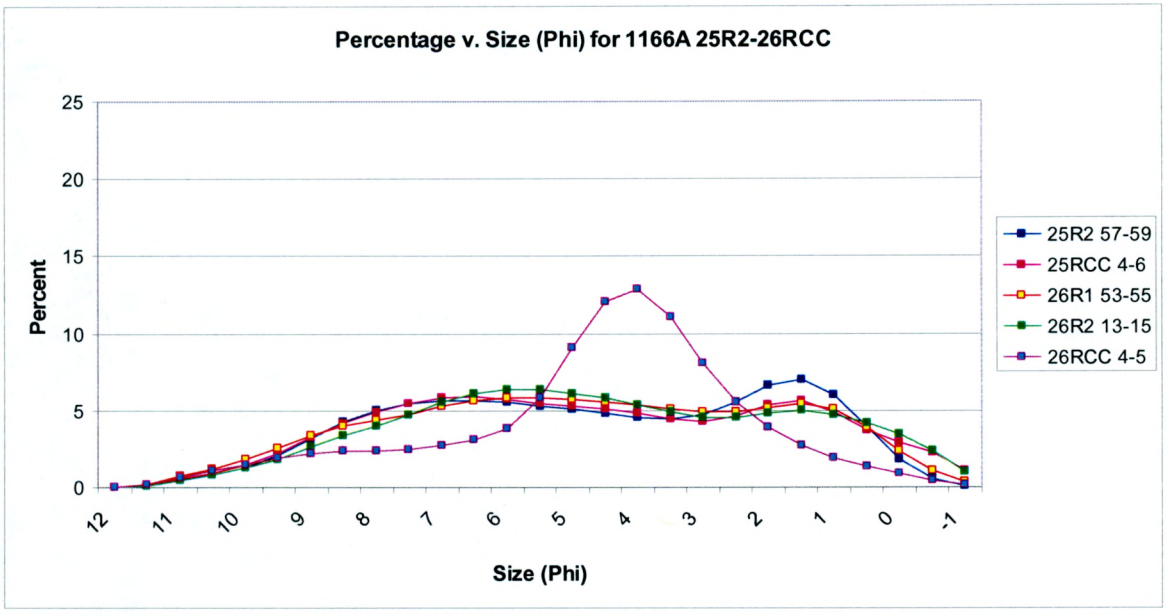

Figure A.49. Percentage of material versus grain size (ϕ) for samples for hole 1166A 25R2 to 26RCC.

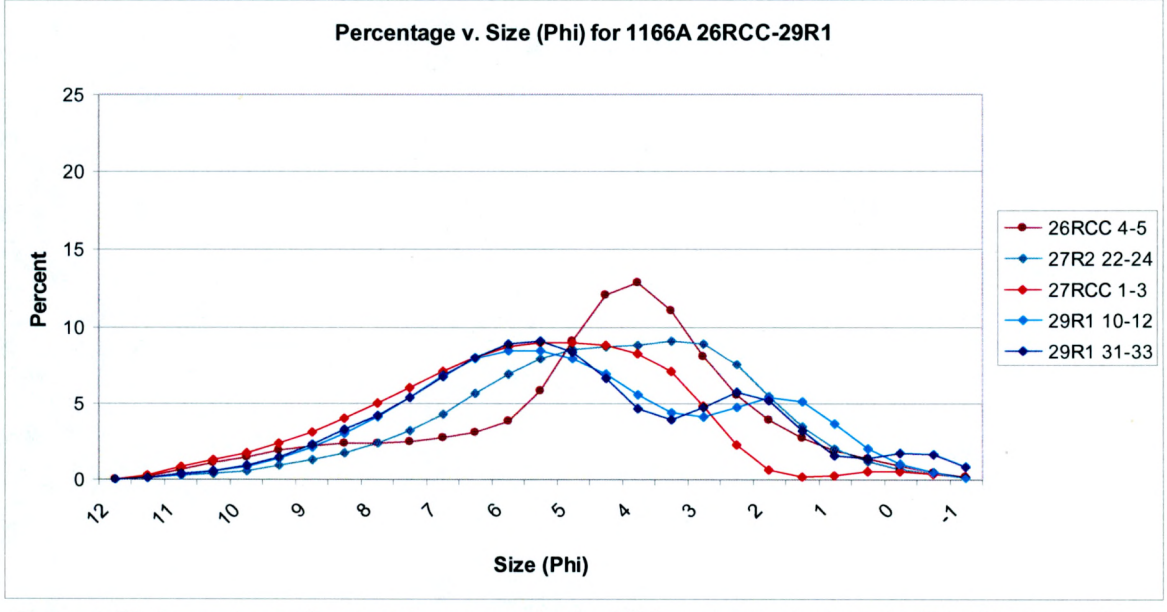

Figure A.50. Percentage of material versus grain size (ϕ) for samples for hole 1166A 26RCC to 29R1.

Table A.1. Statistical Results of Grain Size Analysis

Hole	Section	Obscn	Depth (mbsf)	%Clay	%Silt	%Mud	%Sand	Mean Phi	S. Dev	Skew	Kurt	Interpretation of Statistics (STDEV, SKEW, KURT)		
739C	25R1 8-10	12.94	173.68	16.33	43.05	59.38	40.62	5.016	2.586	0.481	2.544	Very Poorly Sorted	Fine Skew	Platykurtic
739C	25R1 51-53	18.15	174.11	20.68	53.56	74.24	25.76	5.768	2.729	-0.339	2.385	Very Poorly Sorted	Symmetric	Platykurtic
739C	26R1 32-34	20.15	183.52	15.37	74.06	89.43	10.57	6.108	1.991	-0.172	3.774	Poorly Sorted	Symmetric	Leptokurtic
739C	26R2 29-31	27.46	184.99	12.34	79.61	91.95	8.05	6.047	1.686	0.457	3.606	Poorly Sorted	Fine Skew	Mesokurtic
739C	26R2 140-142	23.87	186.10	9.70	75.55	85.25	14.75	5.622	1.804	0.388	3.902	Poorly Sorted	Symmetric	Leptokurtic
739C	26R3 73-75	22.47	186.93	16.62	73.14	89.76	10.24	6.223	2.036	-0.364	3.977	Very Poorly Sorted	Symmetric	Leptokurtic
739C	26RCC 16-18	21.76	187.86	13.61	66.71	80.33	19.67	5.817	2.022	0.120	2.936	Very Poorly Sorted	Symmetric	Mesokurtic
739C	27R1 22-24	34.19	193.12	16.95	71.45	88.40	11.60	6.176	2.015	-0.125	3.649	Very Poorly Sorted	Symmetric	Mesokurtic
739C	27RCC 8-10	18.55	193.78	7.83	50.67	58.50	41.50	4.641	2.382	0.178	2.445	Very Poorly Sorted	Symmetric	Platykurtic
739C	28R1 38-40	23.54	202.88	17.08	72.19	89.27	10.73	6.283	1.913	0.003	3.180	Poorly Sorted	Symmetric	Mesokurtic
739C	28R2 65-67	21.27	204.65	15.34	55.38	70.72	29.28	5.313	2.781	-0.334	2.391	Very Poorly Sorted	Symmetric	Platykurtic
739C	28R3 62-64	19.94	206.12	17.98	42.23	60.21	39.79	5.141	2.861	0.088	1.822	Very Poorly Sorted	Symmetric	Platykurtic
739C	28R4 60-62	21.93	207.60	17.66	67.60	85.26	14.74	6.101	2.114	-0.125	3.003	Very Poorly Sorted	Symmetric	Mesokurtic
739C	28R5 44-46	19.54	208.94	12.41	58.41	70.82	29.18	5.132	2.592	-0.249	2.667	Very Poorly Sorted	Symmetric	Mesokurtic
739C	28RCC 22-24	18.14	209.47	11.75	46.59	58.34	41.66	4.725	2.738	0.126	1.917	Very Poorly Sorted	Symmetric	Platykurtic
739C	29R1 67-69	19.89	212.87	15.48	67.92	83.40	16.60	5.967	2.105	-0.103	2.981	Very Poorly Sorted	Symmetric	Mesokurtic
739C	29R2 33-35	19.60	214.03	15.05	65.84	80.89	19.11	5.785	2.268	-0.248	3.079	Very Poorly Sorted	Symmetric	Mesokurtic
739C	29R3 90-92	24.84	216.10	17.23	66.60	83.83	16.17	5.983	2.282	-0.361	3.263	Very Poorly Sorted	Symmetric	Mesokurtic
739C	29R4 72-74	29.92	217.42	18.36	70.42	88.78	11.22	6.284	1.975	0.003	3.120	Poorly Sorted	Symmetric	Mesokurtic
739C	29R5 59-61	18.66	218.79	15.45	63.31	78.76	21.24	5.752	2.300	-0.151	2.797	Very Poorly Sorted	Symmetric	Mesokurtic
739C	29RCC 21-23	20.33	219.54	14.23	67.80	82.03	17.97	5.775	2.158	-0.104	3.090	Very Poorly Sorted	Symmetric	Mesokurtic
739C	30R1 101-103	26.19	222.81	17.84	74.70	92.54	7.46	6.379	1.820	0.169	3.248	Poorly Sorted	Symmetric	Mesokurtic
739C	30R2 101-103	22.90	224.31	18.66	68.58	87.23	12.77	6.236	2.159	-0.388	3.571	Very Poorly Sorted	Symmetric	Mesokurtic
739C	30R3 97-99	21.79	225.77	17.77	72.17	89.94	10.06	6.309	1.975	-0.230	3.674	Poorly Sorted	Symmetric	Mesokurtic
739C	30R4 105-107	19.27	227.35	16.23	65.75	81.99	18.01	5.884	2.230	-0.132	3.065	Very Poorly Sorted	Symmetric	Mesokurtic
739C	30R5 101-103	18.02	228.81	13.77	67.34	81.11	18.89	5.718	2.146	0.011	3.014	Very Poorly Sorted	Symmetric	Mesokurtic
739C	30R6 54-56	19.94	229.84	12.84	67.65	80.48	19.52	5.570	2.280	-0.259	3.369	Very Poorly Sorted	Symmetric	Mesokurtic
739C	31R1 18-20	20.09	231.58	12.82	68.95	81.77	18.23	5.720	1.931	0.449	3.111	Poorly Sorted	Fine Skew	Mesokurtic
739C	31R1 141-143	23.13	232.81	12.38	71.86	84.24	15.76	5.793	1.865	0.361	3.148	Poorly Sorted	Symmetric	Mesokurtic
739C	31R2 54-56	21.50	233.44	12.35	68.81	81.16	18.84	5.674	1.896	0.532	3.062	Poorly Sorted	Fine Skew	Mesokurtic

739C	31R3 70-72	18.29	235.10	15.89	67.35	83.24	16.76	5.916	2.218	-0.238	3.141	Very Poorly Sorted	Symmetric	Mesokurtic
739C	31R4 94-96	19.40	236.84	12.14	67.92	80.06	19.94	5.631	2.026	0.179	3.113	Very Poorly Sorted	Symmetric	Mesokurtic
739C	31R5 9-11	19.23	237.49	10.61	64.79	75.40	24.60	5.330	2.162	0.047	3.097	Very Poorly Sorted	Symmetric	Mesokurtic
739C	31RCC 12-14	23.75	237.90	19.53	69.86	89.39	10.61	6.307	2.012	0.118	3.025	Very Poorly Sorted	Symmetric	Mesokurtic
739C	32R1 62-64	19.01	241.72	11.05	70.82	81.87	18.13	5.584	2.046	-0.014	3.219	Very Poorly Sorted	Symmetric	Mesokurtic
739C	32R1 99-101	20.09	242.09	11.53	70.29	81.82	18.18	5.621	1.995	0.118	3.562	Poorly Sorted	Symmetric	Mesokurtic
739C	32RCC 2-4	29.99	242.15	11.82	74.11	85.94	14.06	5.680	1.866	0.368	3.773	Poorly Sorted	Symmetric	Leptokurtic
739C	33R1 44-46	20.40	251.14	11.42	77.08	88.50	11.50	5.825	1.740	0.570	3.537	Poorly Sorted	Fine Skew	Mesokurtic
739C	33R2 64-66	19.19	252.84	9.26	82.23	91.49	8.51	5.813	1.546	0.878	3.752	Poorly Sorted	Fine Skew	Leptokurtic
739C	33R3 13-15	22.79	253.83	10.69	79.12	89.81	10.19	5.748	1.692	0.767	3.868	Poorly Sorted	Fine Skew	Leptokurtic
739C	33R4 88-90	17.73	256.08	13.33	76.42	89.76	10.24	6.007	1.843	0.203	3.477	Poorly Sorted	Symmetric	Mesokurtic
739C	33R5 136-138	25.58	258.06	12.73	75.27	88.01	11.99	5.906	1.772	0.530	3.248	Poorly Sorted	Fine Skew	Mesokurtic
739C	33R6 22-24	27.68	258.42	13.58	68.74	82.32	17.68	5.785	1.941	0.369	3.009	Poorly Sorted	Symmetric	Mesokurtic
739C	33RCC 8-10	20.78	259.22	13.63	75.26	88.89	11.11	5.973	1.881	0.158	3.583	Poorly Sorted	Symmetric	Mesokurtic
739C	34R1 14-16	21.26	260.54	16.02	76.82	92.84	7.16	6.288	1.779	0.231	3.443	Poorly Sorted	Symmetric	Mesokurtic
739C	34R2 40-42	20.61	262.30	13.34	67.14	80.48	19.52	5.713	2.055	0.143	3.097	Very Poorly Sorted	Symmetric	Mesokurtic
739C	34R3 78-80	21.28	264.18	15.04	74.49	89.53	10.47	6.030	1.978	-0.166	3.963	Poorly Sorted	Symmetric	Leptokurtic
739C	34R4 66-68	25.41	265.56	15.90	71.20	87.11	12.89	6.008	1.974	0.206	3.171	Poorly Sorted	Symmetric	Mesokurtic
739C	34R5 70-72	26.59	267.10	16.72	67.96	84.68	15.32	5.995	2.023	0.171	2.844	Very Poorly Sorted	Symmetric	Mesokurtic
739C	34RCC 0-2	20.47	267.31	13.86	74.42	88.28	11.72	5.930	1.901	0.166	3.496	Poorly Sorted	Symmetric	Mesokurtic
739C	35R1 18-20	21.15	270.18	14.71	74.95	89.66	10.34	6.045	1.863	0.251	3.346	Poorly Sorted	Symmetric	Mesokurtic
739C	35R2 12-14	22.63	271.62	15.70	77.78	93.48	6.52	6.262	1.722	0.433	3.186	Poorly Sorted	Fine Skew	Mesokurtic
739C	35R3 17-19	22.05	273.17	13.08	77.20	90.29	9.71	6.007	1.873	-0.118	4.167	Poorly Sorted	Symmetric	Leptokurtic
739C	35R4 20-22	23.20	274.70	13.94	73.70	87.63	12.37	5.884	2.051	-0.239	4.043	Very Poorly Sorted	Symmetric	Leptokurtic
739C	35RCC 8-10	22.94	275.33	14.38	64.56	78.94	21.06	5.609	2.426	-0.362	2.987	Very Poorly Sorted	Symmetric	Mesokurtic
739C	36R1 18-20	23.76	279.88	9.87	54.31	64.19	35.81	4.840	2.539	-0.052	2.473	Very Poorly Sorted	Symmetric	Platykurtic
739C	36R1 71-73	21.08	280.41	12.84	68.76	81.59	18.41	5.681	2.205	-0.248	3.240	Very Poorly Sorted	Symmetric	Mesokurtic
739C	36R2 57-59	22.18	281.77	14.85	72.81	87.66	12.34	6.059	1.933	0.058	3.261	Poorly Sorted	Symmetric	Mesokurtic
739C	36R3 67-69	22.33	283.37	15.05	73.14	88.19	11.81	6.091	1.919	0.070	3.275	Poorly Sorted	Symmetric	Mesokurtic
739C	36R4 89-91	28.76	285.09	13.78	73.45	87.23	12.77	5.979	1.919	0.081	3.493	Poorly Sorted	Symmetric	Mesokurtic
739C	36R5 78-80	22.48	286.48	14.19	73.08	87.27	12.73	6.004	1.959	-0.023	3.340	Poorly Sorted	Symmetric	Mesokurtic
739C	36RCC 8-10	23.08	287.19	10.75	61.13	71.88	28.12	5.392	1.987	0.494	2.773	Poorly Sorted	Fine Skew	Mesokurtic

739C	37R1 36-38	26.60	289.66	13.44	63.80	77.23	22.77	5.657	2.097	0.244	2.798	Very Poorly Sorted	Symmetric	Mesokurtic
739C	38R1 83-85	28.89	299.73	13.36	62.00	75.36	24.64	5.554	2.184	0.168	2.843	Very Poorly Sorted	Symmetric	Mesokurtic
739C	38R2 78-80	24.60	301.18	11.21	61.43	72.64	27.36	5.379	2.108	0.290	2.911	Very Poorly Sorted	Symmetric	Mesokurtic
739C	38R3 71-73	31.44	302.61	9.40	53.76	63.15	36.85	5.048	2.126	0.460	2.824	Very Poorly Sorted	Fine Skew	Mesokurtic
739C	38R4 15-17	30.34	303.55	14.06	75.71	89.77	10.23	6.027	1.930	0.083	3.666	Poorly Sorted	Symmetric	Mesokurtic
739C	39R1 68-70	28.09	309.28	8.17	61.30	69.47	30.53	5.148	1.845	0.810	3.568	Poorly Sorted	Fine Skew	Mesokurtic
739C	39R2 43-45	31.88	310.53	10.72	71.15	81.87	18.13	5.429	2.177	-0.081	3.431	Very Poorly Sorted	Symmetric	Mesokurtic
739C	39R3 60-62	35.66	312.20	9.74	58.62	68.36	31.64	5.077	1.946	0.853	3.684	Poorly Sorted	Fine Skew	Mesokurtic
739C	39R4 22-24	30.88	313.32	8.03	68.48	76.51	23.49	5.018	1.979	0.337	4.160	Poorly Sorted	Symmetric	Leptokurtic
739C	39RCC 9-11	28.19	313.51	10.26	75.86	86.13	13.87	5.493	1.920	0.265	4.008	Poorly Sorted	Symmetric	Leptokurtic
739C	40R1 18-20	37.51	318.38	29.70	57.14	86.84	13.16	6.714	2.341	-0.319	2.787	Very Poorly Sorted	Symmetric	Mesokurtic
739C	40R1 40-42	31.93	318.60	17.85	65.43	83.27	16.73	5.972	2.316	-0.195	2.953	Very Poorly Sorted	Symmetric	Mesokurtic
739C	40R2 7-9	39.81	319.77	20.55	68.72	89.27	10.73	6.386	2.118	-0.198	3.314	Very Poorly Sorted	Symmetric	Mesokurtic
739C	41R1 59-61	25.60	328.39	29.76	36.85	66.61	33.39	5.729	3.188	-0.154	1.854	Very Poorly Sorted	Symmetric	Platykurtic
739C	41R2 57-59	29.76	329.87	17.72	70.62	88.34	11.66	6.146	2.105	-0.012	3.250	Very Poorly Sorted	Symmetric	Mesokurtic
739C	41R3 41-43	30.58	331.21	11.27	78.20	89.47	10.53	5.708	1.860	0.433	4.213	Poorly Sorted	Fine Skew	Leptokurtic
739C	41RCC 18-20	32.71	332.48	18.59	71.60	90.19	9.81	6.290	2.067	-0.079	3.459	Very Poorly Sorted	Symmetric	Mesokurtic
739C	42R1 60-62	30.00	338.10	15.49	73.86	89.35	10.65	6.036	2.033	-0.066	3.606	Very Poorly Sorted	Symmetric	Mesokurtic
739C	42R2 37-39	28.88	339.37	32.92	36.19	69.11	30.89	6.018	3.074	-0.203	1.824	Very Poorly Sorted	Symmetric	Platykurtic
739C	42RCC 12-14	34.41	340.42	34.64	35.93	70.57	29.43	6.061	3.224	-0.329	1.974	Very Poorly Sorted	Symmetric	Platykurtic
739C	43R1 54-56	25.09	347.64	28.44	32.19	60.63	39.37	5.262	3.494	-0.085	1.725	Very Poorly Sorted	Symmetric	Platykurtic
739C	43RCC 14-16	23.43	348.74	31.32	35.33	66.65	33.35	5.801	3.187	-0.133	1.787	Very Poorly Sorted	Symmetric	Platykurtic
739C	44R1 56-58	26.50	357.36	32.77	37.09	69.86	30.14	6.008	3.110	-0.216	1.888	Very Poorly Sorted	Symmetric	Platykurtic
739C	44R2 67-69	25.40	358.97	30.63	35.01	65.64	34.36	5.716	3.215	-0.118	1.779	Very Poorly Sorted	Symmetric	Platykurtic
739C	45RCC 11-13	28.02	366.61	31.64	44.21	75.85	24.15	6.275	2.839	-0.305	2.127	Very Poorly Sorted	Symmetric	Platykurtic
739C	46R1 71-73	27.43	376.91	34.25	37.52	71.77	28.23	6.139	3.099	-0.331	2.017	Very Poorly Sorted	Symmetric	Platykurtic
739C	46R2 32-34	32.04	378.02	39.95	40.55	80.50	19.50	6.761	2.835	-0.498	2.361	Very Poorly Sorted	Coarse Skew	Platykurtic
739C	46RCC 5-7	24.79	378.30	30.63	34.61	65.24	34.76	5.662	3.274	-0.146	1.779	Very Poorly Sorted	Symmetric	Platykurtic
739C	47R1 40-42	37.16	386.30	37.50	48.32	85.82	14.18	6.926	2.575	-0.624	2.974	Very Poorly Sorted	Coarse Skew	Mesokurtic
739C	48R1 61-63	29.42	396.21	42.34	38.86	81.20	18.80	6.853	2.849	-0.641	2.564	Very Poorly Sorted	Coarse Skew	Mesokurtic
739C	48R2 58-60	30.86	397.68	37.02	33.43	70.46	29.54	6.145	3.249	-0.346	1.896	Very Poorly Sorted	Symmetric	Platykurtic
739C	50R1 61-63	27.01	415.51	34.80	32.49	67.29	32.71	5.902	3.344	-0.242	1.788	Very Poorly Sorted	Symmetric	Platykurtic

739C	50R2 56-58	29.21	416.96	33.32	39.35	72.67	27.33	6.139	3.091	-0.345	2.036	Very Poorly Sorted	Symmetric	Platykurtic
739C	51R1 88-90	28.07	425.38	14.04	77.06	91.10	8.90	5.907	1.899	0.248	3.743	Poorly Sorted	Symmetric	Leptokurtic
739C	51R2 62-64	34.63	426.62	30.67	64.96	95.64	4.36	7.086	1.935	-0.169	3.405	Poorly Sorted	Symmetric	Mesokurtic
739C	52R1 75-77	32.51	434.95	41.70	39.70	81.40	18.60	6.834	2.873	-0.645	2.575	Very Poorly Sorted	Coarse Skew	Mesokurtic
739C	52R2 57-59	38.30	436.27	22.98	71.54	94.52	5.48	6.669	1.915	0.103	3.317	Poorly Sorted	Symmetric	Mesokurtic
739C	52RCC 0-2	33.20	436.46	34.40	56.80	91.20	8.80	6.999	2.319	-0.716	3.861	Very Poorly Sorted	Coarse Skew	Leptokurtic
739C	53R1 56-58	31.03	439.76	36.91	37.56	74.48	25.52	6.349	3.081	-0.429	2.144	Very Poorly Sorted	Symmetric	Platykurtic
739C	53RCC 17-19	26.52	440.66	36.83	37.54	74.36	25.64	6.323	3.088	-0.432	2.096	Very Poorly Sorted	Coarse Skew	Platykurtic
739C	54R1 31-33	26.21	444.21	38.32	40.32	78.64	21.36	6.602	2.895	-0.498	2.345	Very Poorly Sorted	Coarse Skew	Platykurtic
739C	54RCC 15-17	30.01	445.55	38.88	39.62	78.50	21.50	6.615	2.916	-0.516	2.371	Very Poorly Sorted	Coarse Skew	Platykurtic
739C	55R1 73-75	28.40	449.63	37.67	36.51	74.18	25.82	6.382	3.064	-0.390	1.997	Very Poorly Sorted	Symmetric	Platykurtic
739C	55R2 10-12	28.83	450.50	40.89	36.23	77.11	22.89	6.636	3.010	-0.516	2.192	Very Poorly Sorted	Coarse Skew	Platykurtic
739C	55R2 29-31	15.74	450.69	41.18	41.75	82.93	17.07	6.925	2.653	-0.498	2.463	Very Poorly Sorted	Coarse Skew	Platykurtic
739C	55RCC 11-13	26.14	450.99	40.08	41.92	82.00	18.00	6.793	2.782	-0.570	2.561	Very Poorly Sorted	Coarse Skew	Mesokurtic
739C	56R1 7-9	22.51	453.57	41.45	39.88	81.33	18.67	6.863	2.760	-0.526	2.365	Very Poorly Sorted	Coarse Skew	Platykurtic
739C	56RCC 23-25	22.23	454.38	39.21	38.99	78.20	21.80	6.660	2.847	-0.423	2.173	Very Poorly Sorted	Symmetric	Platykurtic
739C	57R1 13-15	24.60	458.63	39.01	38.96	77.98	22.02	6.634	2.873	-0.413	2.139	Very Poorly Sorted	Symmetric	Platykurtic
739C	57RCC 6-8	22.71	459.28	38.84	39.51	78.36	21.64	6.638	2.864	-0.430	2.238	Very Poorly Sorted	Symmetric	Platykurtic
739C	58R1 21-23	19.64	463.41	34.17	35.27	69.44	30.56	5.991	3.210	-0.283	1.865	Very Poorly Sorted	Symmetric	Platykurtic
739C	58R2 50-52	25.21	465.20	26.08	65.40	91.48	8.52	6.752	1.964	0.121	2.525	Poorly Sorted	Symmetric	Platykurtic
739C	58RCC 12-14	29.48	466.21	43.83	46.69	90.52	9.48	7.333	2.324	-0.667	3.171	Very Poorly Sorted	Coarse Skew	Mesokurtic
739C	59R1 30-32	32.11	468.50	42.93	40.41	83.34	16.66	6.912	2.866	-0.791	2.932	Very Poorly Sorted	Coarse Skew	Mesokurtic
739C	60R1 72-74	31.81	473.62	43.75	42.54	86.29	13.71	7.115	2.648	-0.753	3.046	Very Poorly Sorted	Coarse Skew	Mesokurtic
739C	62RCC 8-9	31.19	482.68	38.09	45.62	83.70	16.30	6.798	2.757	-0.849	3.169	Very Poorly Sorted	Coarse Skew	Mesokurtic
742A	20R1 83-85	29.73	172.13	26.12	33.67	59.79	40.21	5.305	3.230	0.069	1.798	Very Poorly Sorted	Symmetric	Platykurtic
742A	20R1 137-139	24.67	172.67	34.13	47.59	81.72	18.28	6.549	2.747	-0.552	2.675	Very Poorly Sorted	Coarse Skew	Mesokurtic
742A	20R2 48-50	35.78	173.28	23.18	72.60	95.78	4.22	6.703	1.904	-0.120	4.168	Poorly Sorted	Symmetric	Leptokurtic
742A	20R2 77-79	37.00	173.57	33.53	54.27	87.81	12.19	6.875	2.384	-0.538	3.159	Very Poorly Sorted	Coarse Skew	Mesokurtic
742A	20R3 56-58	26.67	174.86	26.65	68.43	95.08	4.92	6.880	1.884	-0.087	3.380	Poorly Sorted	Symmetric	Mesokurtic
742A	21R1 12-14	30.10	181.12	46.97	43.27	90.24	9.76	7.439	2.441	-0.853	3.529	Very Poorly Sorted	Coarse Skew	Mesokurtic
742A	21R1 87-89	24.31	181.87	37.06	43.12	80.18	19.82	6.618	2.819	-0.508	2.401	Very Poorly Sorted	Coarse Skew	Platykurtic
742A	21R2 37-39	37.21	182.87	39.69	44.22	83.91	16.09	6.818	2.827	-0.826	3.124	Very Poorly Sorted	Coarse Skew	Mesokurtic

742A	21R3 48-50	37.50	184.48	46.74	41.35	88.09	11.91	7.304	2.689	-0.937	3.554	Very Poorly Sorted	Coarse Skew	Mesokurtic
742A	22R1 71-73	38.94	191.41	33.59	48.73	82.32	17.68	6.649	2.644	-0.526	2.596	Very Poorly Sorted	Coarse Skew	Mesokurtic
742A	22R1 137-139	31.93	192.07	41.36	52.30	93.66	6.34	7.392	2.217	-0.714	3.954	Very Poorly Sorted	Coarse Skew	Leptokurtic
742A	22R2 103-105	24.11	193.23	41.02	42.61	83.63	16.37	6.915	2.733	-0.654	2.698	Very Poorly Sorted	Coarse Skew	Mesokurtic
742A	22R3 63-65	37.13	194.55	42.47	42.53	85.00	15.00	6.997	2.806	-0.762	3.037	Very Poorly Sorted	Coarse Skew	Mesokurtic
742A	22R4 63-65	27.68	195.83	30.41	43.15	73.56	26.44	6.054	2.963	-0.302	2.094	Very Poorly Sorted	Symmetric	Platykurtic
742A	22R5 63-65	32.41	197.33	31.49	46.05	77.54	22.46	6.280	2.837	-0.504	2.396	Very Poorly Sorted	Coarse Skew	Platykurtic
742A	22R6 63-65	31.67	198.83	26.46	37.09	63.55	36.45	5.261	3.440	-0.175	1.814	Very Poorly Sorted	Symmetric	Platykurtic
742A	22R7 32-34	31.37	200.02	30.52	43.96	74.48	25.52	6.086	2.954	-0.382	2.229	Very Poorly Sorted	Symmetric	Platykurtic
742A	23R1 63-65	34.04	200.93	32.04	45.83	77.87	22.13	6.351	2.777	-0.420	2.316	Very Poorly Sorted	Symmetric	Platykurtic
742A	23R2 66-68	26.50	202.46	29.04	43.41	72.45	27.55	5.966	2.941	-0.239	2.047	Very Poorly Sorted	Symmetric	Platykurtic
742A	23R3 63-65	21.92	203.93	26.39	40.96	67.35	32.65	5.515	3.221	-0.245	1.986	Very Poorly Sorted	Symmetric	Platykurtic
742A	23R4 63-65	32.46	205.43	29.49	43.45	72.94	27.06	6.001	2.962	-0.266	2.091	Very Poorly Sorted	Symmetric	Platykurtic
742A	23R5 63-65	32.37	206.93	28.03	42.02	70.05	29.95	5.790	3.062	-0.245	2.074	Very Poorly Sorted	Symmetric	Platykurtic
742A	23R6 115-117	31.56	208.98	28.62	42.33	70.95	29.05	5.805	3.120	-0.330	2.113	Very Poorly Sorted	Symmetric	Platykurtic
742A	24R1 62-64	32.10	210.52	28.92	41.56	70.48	29.52	5.806	3.126	-0.304	2.090	Very Poorly Sorted	Symmetric	Platykurtic
742A	24R2 74-76	29.77	212.14	29.01	43.24	72.26	27.74	5.950	2.972	-0.258	2.101	Very Poorly Sorted	Symmetric	Platykurtic
742A	24R3 63-65	36.18	213.53	28.92	43.12	72.03	27.97	5.920	3.014	-0.317	2.134	Very Poorly Sorted	Symmetric	Platykurtic
742A	24R4 63-65	27.54	215.03	28.01	42.92	70.93	29.07	5.739	3.157	-0.364	2.197	Very Poorly Sorted	Symmetric	Platykurtic
742A	26R1 38-40	38.26	229.58	42.33	49.88	92.21	7.79	7.385	2.236	-0.746	3.768	Very Poorly Sorted	Coarse Skew	Leptokurtic
742A	26R1 95-97	36.22	230.15	21.41	58.41	79.83	20.17	5.997	2.328	0.133	2.674	Very Poorly Sorted	Symmetric	Mesokurtic
742A	26R2 61-63	32.10	231.31	34.51	47.38	81.89	18.11	6.600	2.696	-0.450	2.504	Very Poorly Sorted	Coarse Skew	Platykurtic
742A	26R3 61-63	24.87	232.81	31.87	46.86	78.72	21.28	6.374	2.739	-0.347	2.353	Very Poorly Sorted	Symmetric	Platykurtic
742A	24R4 63-65	27.98	234.33	29.30	44.96	74.26	25.74	6.011	2.986	-0.370	2.304	Very Poorly Sorted	Symmetric	Platykurtic
742A	26R5 67-69	29.42	235.87	30.19	45.04	75.23	24.77	6.152	2.874	-0.306	2.236	Very Poorly Sorted	Symmetric	Platykurtic
742A	27R1 127-129	27.03	240.07	29.00	44.08	73.08	26.92	6.008	2.929	-0.268	2.154	Very Poorly Sorted	Symmetric	Platykurtic
742A	27R2 124-126	30.41	241.54	29.63	46.72	76.35	23.65	6.189	2.802	-0.293	2.271	Very Poorly Sorted	Symmetric	Platykurtic
742A	27R3 53-55	21.66	242.33	29.00	45.18	74.18	25.82	6.024	2.930	-0.339	2.237	Very Poorly Sorted	Symmetric	Platykurtic
742A	27R4 6-8	27.79	243.36	30.49	46.46	76.95	23.05	6.252	2.791	-0.324	2.260	Very Poorly Sorted	Symmetric	Platykurtic
742A	27R5 9-11	18.68	244.89	26.90	42.38	69.28	30.72	5.674	3.115	-0.270	2.088	Very Poorly Sorted	Symmetric	Platykurtic
742A	27R6 35-36	20.94	246.65	27.80	42.92	70.72	29.28	5.801	3.062	-0.290	2.129	Very Poorly Sorted	Symmetric	Platykurtic
742A	27R7 41-43	39.04	248.21	34.45	53.59	88.03	11.97	6.988	2.311	-0.703	3.391	Very Poorly Sorted	Coarse Skew	Mesokurtic

742A	27RCC 0-2	26.05	248.43	27.88	44.34	72.22	27.78	5.902	2.972	-0.276	2.136	Very Poorly Sorted	Symmetric	Platykurtic
742A	28R1 58-60	35.51	249.08	28.74	42.89	71.64	28.36	5.841	3.134	-0.344	2.142	Very Poorly Sorted	Symmetric	Platykurtic
742A	28R1 138-140	37.31	249.88	30.68	44.66	75.34	24.66	6.173	2.882	-0.381	2.242	Very Poorly Sorted	Symmetric	Platykurtic
742A	28R2 68-70	32.67	250.68	32.16	46.59	78.75	21.25	6.291	2.946	-0.528	2.547	Very Poorly Sorted	Coarse Skew	Platykurtic
742A	28R3 82-84	35.34	252.32	29.90	44.14	74.05	25.95	6.002	3.038	-0.416	2.230	Very Poorly Sorted	Symmetric	Platykurtic
742A	28R3 115-117	27.54	252.65	30.96	45.23	76.18	23.82	6.227	2.855	-0.338	2.219	Very Poorly Sorted	Symmetric	Platykurtic
742A	28R4 28-30	39.27	253.28	33.72	47.55	81.27	18.73	6.563	2.689	-0.430	2.549	Very Poorly Sorted	Coarse Skew	Platykurtic
742A	28R5 55-57	35.24	255.05	32.87	48.03	80.90	19.10	6.476	2.756	-0.584	2.769	Very Poorly Sorted	Coarse Skew	Mesokurtic
742A	28R6 65-67	27.08	256.65	26.60	43.21	69.81	30.19	5.643	3.171	-0.334	2.123	Very Poorly Sorted	Symmetric	Platykurtic
742A	28R7 53-55	24.19	258.03	28.43	43.30	71.74	28.26	5.901	2.999	-0.288	2.083	Very Poorly Sorted	Symmetric	Platykurtic
742A	29R1 57-59	30.49	258.67	28.99	44.17	73.16	26.84	5.982	2.978	-0.347	2.215	Very Poorly Sorted	Symmetric	Platykurtic
742A	29R2 58-60	26.13	260.18	29.87	43.85	73.71	26.29	6.060	2.924	-0.303	2.127	Very Poorly Sorted	Symmetric	Platykurtic
742A	29R3 63-65	23.64	261.73	27.50	44.85	72.34	27.66	5.916	2.907	-0.255	2.137	Very Poorly Sorted	Symmetric	Platykurtic
742A	29R4 77-79	35.16	263.37	30.06	42.66	72.73	27.27	5.979	3.064	-0.350	2.133	Very Poorly Sorted	Symmetric	Platykurtic
742A	29R5 113-115	31.95	265.23	30.33	42.97	73.30	26.70	6.011	3.058	-0.379	2.172	Very Poorly Sorted	Symmetric	Platykurtic
742A	29R6 79-81	22.63	266.39	32.92	48.15	81.07	18.93	6.564	2.579	-0.324	2.327	Very Poorly Sorted	Symmetric	Platykurtic
742A	30R1 67-69	16.77	268.47	29.86	46.40	76.26	23.74	6.107	2.926	-0.450	2.450	Very Poorly Sorted	Coarse Skew	Platykurtic
742A	30R2 65-67	27.05	269.95	30.20	42.76	72.96	27.04	5.931	3.138	-0.425	2.233	Very Poorly Sorted	Symmetric	Platykurtic
742A	30R3 38-40	24.25	271.18	31.88	47.42	79.30	20.70	6.388	2.744	-0.435	2.494	Very Poorly Sorted	Coarse Skew	Platykurtic
742A	30R4 80-82	20.12	273.10	31.07	49.90	80.96	19.04	6.451	2.589	-0.311	2.446	Very Poorly Sorted	Symmetric	Platykurtic
742A	30R5 80-82	27.33	274.60	30.32	47.74	78.06	21.94	6.215	2.872	-0.492	2.593	Very Poorly Sorted	Coarse Skew	Mesokurtic
742A	30R6 53-55	17.36	275.83	26.46	41.88	68.34	31.66	5.562	3.184	-0.265	1.997	Very Poorly Sorted	Symmetric	Platykurtic
742A	30RCC 8-10	20.48	276.62	28.68	43.98	72.66	27.34	6.062	2.787	-0.153	2.005	Very Poorly Sorted	Symmetric	Platykurtic
742A	31R1 64-66	23.34	278.04	28.52	42.00	70.53	29.47	5.767	3.181	-0.374	2.158	Very Poorly Sorted	Symmetric	Platykurtic
742A	31R2 65-67	22.29	279.55	30.81	47.17	77.98	22.02	6.314	2.715	-0.310	2.281	Very Poorly Sorted	Symmetric	Platykurtic
742A	31R3 61-63	24.08	281.01	29.85	44.52	74.36	25.64	6.077	2.935	-0.369	2.267	Very Poorly Sorted	Symmetric	Platykurtic
742A	31R4 110-112	22.35	283.00	32.69	48.47	81.16	18.84	6.535	2.616	-0.393	2.463	Very Poorly Sorted	Symmetric	Platykurtic
742A	32R1 66-68	22.30	287.76	32.25	46.77	79.02	20.98	6.338	2.871	-0.533	2.537	Very Poorly Sorted	Coarse Skew	Platykurtic
742A	32R2 66-68	25.39	289.26	31.28	45.87	77.15	22.85	6.266	2.837	-0.416	2.389	Very Poorly Sorted	Symmetric	Platykurtic
742A	32R3 66-68	28.38	290.76	30.83	45.81	76.65	23.35	6.225	2.853	-0.372	2.282	Very Poorly Sorted	Symmetric	Platykurtic
742A	32R4 142-144	27.71	293.02	32.90	47.98	80.89	19.11	6.516	2.677	-0.430	2.530	Very Poorly Sorted	Symmetric	Platykurtic
742A	33R1 61-63	27.99	297.31	31.90	45.08	76.98	23.02	6.243	2.934	-0.475	2.447	Very Poorly Sorted	Coarse Skew	Platykurtic

742A	33R2 63-65	30.07	298.83	30.26	47.11	77.37	22.63	6.298	2.782	-0.524	2.417	Very Poorly Sorted	Coarse Skew	Platykurtic
742A	33R3 65-67	32.48	300.35	31.96	43.81	75.77	24.23	6.230	2.913	-0.361	2.178	Very Poorly Sorted	Symmetric	Platykurtic
742A	33R4 97-99	33.22	302.17	34.80	47.51	82.32	17.68	6.628	2.689	-0.473	2.530	Very Poorly Sorted	Coarse Skew	Platykurtic
742A	33R5 90-92	29.67	303.60	27.77	39.49	67.27	32.73	5.497	3.355	-0.267	1.881	Very Poorly Sorted	Symmetric	Platykurtic
742A	33R6 9-11	31.77	304.29	28.74	70.04	98.78	1.22	6.887	1.864	0.541	2.326	Poorly Sorted	Fine Skew	Platykurtic
742A	33R6 76-78	28.06	304.96	35.24	47.04	82.28	17.72	6.624	2.755	-0.620	2.727	Very Poorly Sorted	Coarse Skew	Mesokurtic
742A	34R1 99-101	38.64	307.29	35.42	56.45	91.87	8.13	7.003	2.410	-0.824	4.129	Very Poorly Sorted	Coarse Skew	Leptokurtic
742A	34R2 24-26	23.38	308.04	31.43	56.12	87.56	12.44	6.703	2.320	-0.236	2.659	Very Poorly Sorted	Symmetric	Mesokurtic
742A	34R3 51-53	20.28	309.81	31.77	48.53	80.30	19.70	6.379	2.757	-0.490	2.583	Very Poorly Sorted	Coarse Skew	Mesokurtic
742A	34R4 98-100	31.06	311.78	32.36	47.49	79.85	20.15	6.437	2.708	-0.391	2.414	Very Poorly Sorted	Symmetric	Platykurtic
742A	34R5 54-56	23.65	312.84	28.87	50.12	78.99	21.01	6.263	2.662	-0.303	2.400	Very Poorly Sorted	Symmetric	Platykurtic
742A	34R5 133-135	28.35	313.63	13.74	60.28	74.01	25.99	5.478	2.260	0.016	2.708	Very Poorly Sorted	Symmetric	Mesokurtic
742A	34R6 72-74	16.70	314.52	17.41	56.88	74.29	25.71	5.661	2.376	0.074	2.477	Very Poorly Sorted	Symmetric	Platykurtic
742A	34RCC 10-12	13.64	315.10	16.75	44.54	61.30	38.70	4.972	2.904	0.034	2.101	Very Poorly Sorted	Symmetric	Platykurtic
1166A	15R2 64-66	29.50	134.69	12.42	73.13	85.55	14.45	5.921	2.160	-0.692	4.002	Very Poorly Sorted	Coarse Skew	Leptokurtic
1166A	15R3 4-6	25.93	135.59	14.46	78.42	92.87	7.13	6.261	1.819	-0.301	4.740	Poorly Sorted	Symmetric	Leptokurtic
1166A	15R3 47-49	27.19	136.02	8.10	72.31	80.40	19.60	5.390	1.743	0.502	3.725	Poorly Sorted	Fine Skew	Leptokurtic
1166A	15R3 129-131	28.85	136.84	7.39	57.72	65.10	34.90	5.017	1.863	0.709	3.304	Poorly Sorted	Fine Skew	Mesokurtic
1166A	15R4 62-64	35.96	137.67	11.02	66.46	77.48	22.52	5.451	2.100	0.024	3.305	Very Poorly Sorted	Symmetric	Mesokurtic
1166A	15R4 99-101	20.36	138.04	10.09	77.51	87.60	12.40	5.699	1.874	-0.262	4.527	Poorly Sorted	Symmetric	Leptokurtic
1166A	15R5 96-98	23.93	139.51	11.58	74.85	86.44	13.56	5.701	2.208	-0.760	4.410	Very Poorly Sorted	Coarse Skew	Leptokurtic
1166A	15R5 114-116	20.16	139.69	10.06	79.70	89.76	10.24	5.831	1.720	0.060	4.195	Poorly Sorted	Symmetric	Leptokurtic
1166A	15R6 34-36	20.71	140.39	11.26	72.61	83.87	16.13	5.715	2.128	-0.517	3.857	Very Poorly Sorted	Coarse Skew	Leptokurtic
1166A	15R6 131-133	19.00	141.36	10.42	77.97	88.39	11.61	5.813	1.744	0.191	3.733	Poorly Sorted	Symmetric	Leptokurtic
1166A	15R7 43-45	16.10	141.98	9.28	78.58	87.86	12.14	5.723	1.704	0.236	3.941	Poorly Sorted	Symmetric	Leptokurtic
1166A	15RCC 5-7	21.27	142.35	9.11	81.47	90.58	9.42	5.833	1.602	0.387	3.880	Poorly Sorted	Symmetric	Leptokurtic
1166A	16R1 47-49	9.74	142.67	9.00	70.67	79.68	20.32	5.360	2.121	-0.275	3.417	Very Poorly Sorted	Symmetric	Mesokurtic
1166A	16R1 104-106	13.67	143.24	13.28	80.69	93.97	6.03	6.188	1.659	0.222	3.680	Poorly Sorted	Symmetric	Mesokurtic
1166A	16R2 37-39	13.66	144.07	11.98	79.73	91.71	8.29	6.120	1.783	-0.332	4.485	Poorly Sorted	Symmetric	Leptokurtic
1166A	16R2 98-100	17.75	144.68	8.75	73.90	82.65	17.35	5.478	2.106	-0.596	4.106	Very Poorly Sorted	Coarse Skew	Leptokurtic
1166A	16R3 58-60	15.27	145.78	11.14	74.05	85.19	14.81	5.703	2.069	-0.493	4.122	Very Poorly Sorted	Coarse Skew	Leptokurtic
1166A	16R3 127-129	13.94	146.47	11.99	75.29	87.28	12.72	5.883	1.905	-0.145	3.842	Poorly Sorted	Symmetric	Leptokurtic

1166A	16R4 42-44	14.77	147.12	9.86	76.57	86.44	13.56	5.739	1.791	0.116	3.592	Poorly Sorted	Symmetric	Mesokurtic
1166A	16R4 114-116	15.04	147.84	10.79	77.41	88.20	11.80	5.844	1.746	0.219	3.480	Poorly Sorted	Symmetric	Mesokurtic
1166A	17R1 44-46	44.04	151.84	6.76	58.07	64.83	35.17	4.901	1.949	0.464	3.514	Poorly Sorted	Fine Skew	Mesokurtic
1166A	17R1 131-133	22.42	152.71	16.18	66.42	82.60	17.40	5.859	2.056	0.408	2.885	Very Poorly Sorted	Symmetric	Mesokurtic
1166A	17R2 10-12	41.71	153.00	12.28	64.54	76.81	23.19	5.441	2.004	0.700	3.469	Very Poorly Sorted	Fine Skew	Mesokurtic
1166A	17R2 91-93	37.93	153.81	14.23	60.00	74.23	25.77	5.507	2.043	0.797	2.937	Very Poorly Sorted	Fine Skew	Mesokurtic
1166A	17R3 26-28	46.06	154.66	17.15	63.60	80.75	19.25	5.748	2.200	0.227	2.783	Very Poorly Sorted	Symmetric	Mesokurtic
1166A	17R3 118-120	28.57	155.58	37.19	55.13	92.31	7.69	7.238	2.196	-0.781	4.038	Very Poorly Sorted	Coarse Skew	Leptokurtic
1166A	17R4 36-38	41.64	156.26	11.14	74.05	85.19	14.81	5.703	2.069	-0.493	4.122	Very Poorly Sorted	Coarse Skew	Leptokurtic
1166A	17R4 85-87	14.97	156.75	46.20	53.60	99.80	0.20	7.904	1.572	0.105	2.581	Poorly Sorted	Symmetric	Mesokurtic
1166A	18R1 27-29	35.00	161.27	22.71	41.34	64.05	35.95	5.321	3.028	-0.092	1.981	Very Poorly Sorted	Symmetric	Platykurtic
1166A	18R1 127-129	29.17	162.27	20.50	42.27	62.77	37.23	5.184	3.019	-0.025	1.978	Very Poorly Sorted	Symmetric	Platykurtic
1166A	18R2 63-65	31.69	163.13	19.02	36.69	55.70	44.30	4.694	3.238	0.100	1.898	Very Poorly Sorted	Symmetric	Platykurtic
1166A	18R2 98-100	29.26	163.48	19.04	43.87	62.91	37.09	5.146	2.881	0.012	2.029	Very Poorly Sorted	Symmetric	Platykurtic
1166A	19R1 10-12	31.03	170.70	16.90	39.86	56.77	43.23	4.794	2.971	0.082	1.938	Very Poorly Sorted	Symmetric	Platykurtic
1166A	20RCC 0-2	25.98	180.30	17.95	46.43	64.38	35.62	5.247	2.813	-0.116	2.008	Very Poorly Sorted	Symmetric	Platykurtic
1166A	22R1 61-63	21.95	200.11	14.55	42.99	57.54	42.46	4.687	2.996	-0.027	1.886	Very Poorly Sorted	Symmetric	Platykurtic
1166A	23R1 56-58	34.19	209.66	15.04	48.01	63.06	36.94	5.025	2.935	-0.176	1.956	Very Poorly Sorted	Symmetric	Platykurtic
1166A	24R1 82-84	31.06	219.52	16.34	44.35	60.69	39.31	4.932	2.980	-0.097	1.946	Very Poorly Sorted	Symmetric	Platykurtic
1166A	24R2 29-31	27.52	220.49	14.63	42.96	57.58	42.42	4.830	2.879	0.043	1.871	Very Poorly Sorted	Symmetric	Platykurtic
1166A	24RCC 10-12	21.15	220.69	14.89	36.16	51.05	48.95	4.277	3.149	0.160	1.806	Very Poorly Sorted	Symmetric	Platykurtic
1166A	25R1 34-36	19.47	228.64	17.79	44.93	62.72	37.28	5.156	2.773	0.001	1.964	Very Poorly Sorted	Symmetric	Platykurtic
1166A	25R2 57-59	24.64	229.87	17.34	41.93	59.28	40.72	4.981	2.828	0.118	1.942	Very Poorly Sorted	Symmetric	Platykurtic
1166A	25RCC 4-6	22.06	229.99	17.47	43.39	60.86	39.14	4.961	2.933	-0.017	2.005	Very Poorly Sorted	Symmetric	Platykurtic
1166A	26R1 53-55	31.75	238.43	18.21	43.61	61.82	38.18	5.080	2.865	0.084	2.076	Very Poorly Sorted	Symmetric	Platykurtic
1166A	26R2 13-15	15.44	239.53	14.35	46.24	60.58	39.42	4.813	2.840	0.008	2.127	Very Poorly Sorted	Symmetric	Platykurtic
1166A	26RCC 4-5	18.75	240.30	12.15	51.84	63.99	36.01	4.907	2.295	0.637	3.322	Very Poorly Sorted	Fine Skew	Mesokurtic
1166A	27R2 22-24	24.54	249.32	7.57	53.74	61.31	38.69	4.790	2.120	0.339	2.917	Very Poorly Sorted	Symmetric	Mesokurtic
1166A	27RCC 1-3	15.600	249.38	18.52	64.67	83.19	16.81	6.035	2.147	0.101	3.013	Very Poorly Sorted	Symmetric	Mesokurtic
1166A	29R1 10-12	17.14	266.90	12.12	57.14	69.26	30.74	5.216	2.419	-0.091	2.359	Very Poorly Sorted	Symmetric	Platykurtic
1166A	29R1 31-33	18.25	267.11	13.02	57.42	70.44	29.56	5.282	2.475	-0.239	2.600	Very Poorly Sorted	Symmetric	Mesokurtic

APPENDIX B: CORE LOGS

LOGS

FIGURES

Figure B.1. Visual core logs of site 1166 (Hole A), site 742 (Hole A), and site 739 (Hole C). Visual logs indicate observed grain size using scale at top of each borehole diagram (C-clay, Si-silt, Sa-sand, G-gravel), with depth in meters below seafloor (mbsf) along left side. Interval colors are based on description in logs and are not related to grain size. Vertical resolution is 2 pixels per meter.

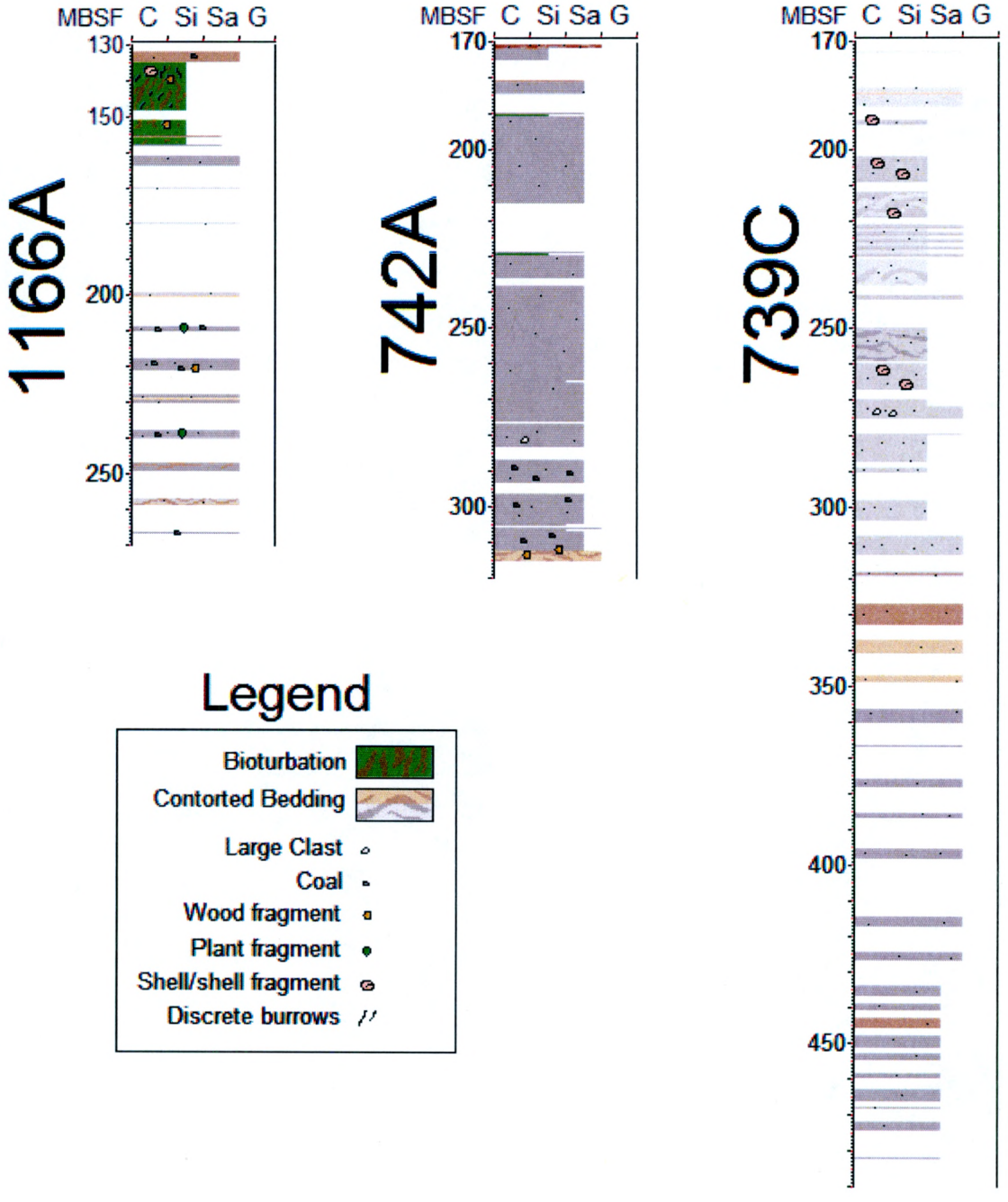

LOGS

Format

Core logging followed a standard nomenclature and described the following features:

- Volume percent gravel, per Terry & Chilingar (1955)
- Matrix grain size, (with respect to gravel per Moncrieff [1989]), based on estimation of clay-silt-sand per Mazullo & Graham (1988)
- Degree of bioturbation, per Bann et al. (2006)
- Fossil abundance
- Color
- Sedimentary structures
- Contacts/deformation

The structure of the log summaries is outlined below:

Core Number, Core Sections [R1,2,3…CC], (total cored interval in mbsf)
*Section 1
Depth of interval in section: Description
Depth of interval in section: Description
*Section 2
Depth of interval in section: Description
>>Depth of object in interval of section: Description of object
Depth of interval in section: Description
>>Depth of object in interval of section: Description of object
>>Depth of object in interval of section: Description of object
*Section CC ("CC" is core capture section, which is final/deepest section of core)
Depth of interval in section: Description

Note: Total cored interval in mbsf may be somewhat different than total logged interval due to incomplete recovery and expansion/contraction of cored material.

Site 1166, Hole A

15 R1,2,3,4,5,6,7,CC (132.6 to 142.2 mbsf)
*Section 1
0-150 cm: Dark brownish gray clast poor sandy diamictite (~3-5% clasts)
*Section 2
0-150 cm: Dark brownish gray clast poor sandy diamictite (~3-5% clasts)
>>19 cm: Coal clast
>>38 cm: Coal clast
*Section 3
0-6 cm: Dark brownish gray clast poor sandy diamictite (~3-5% clasts)
6-119 cm: Olive green claystone, sparsely bioturbated; very few dispersed sand grains e.g. 16-17 and 44-45 cm
119-133 cm: Olive gray interlaminated sandstone and siltstone with dispersed clasts; laminae are ~0.5 cm thick and are disrupted by bioturbation. Some reddish brown clasts of irregular shape are present (bog iron?)
>>21 cm: Discrete burrow, 1 mm in diameter
>>32 cm: Discrete burrow, 1 mm in diameter
>>68 cm: Discrete burrow, 1 mm in diameter
>>70 cm: Discrete burrow, 1 mm in diameter
>>133 cm: Coal clast
133-150 cm: Olive gray silty claystone w/ dispersed clasts; moderately bioturbated
*Section 4
0-150 cm: Olive gray silty claystone w/ dispersed clasts; moderately bioturbated
>>5-10 cm: ~0.5 cm thick sand and mud laminae disrupted by bioturbation
>>8 cm: Shell fragment
>>10 cm: Coal clast
>>23 cm: Shell fragment
>>31-36 cm: ~0.5 cm thick sand and mud laminae disrupted by bioturbation
>>57-61 cm: ~0.5 cm thick sand and mud laminae disrupted by bioturbation
>>89-92 cm: ~0.5 cm thick sand and mud laminae disrupted by bioturbation
>>147-148 cm: ~0.5 cm thick sand and mud laminae disrupted by bioturbation
*Section 5
0-70 cm: Olive gray silty claystone w/ dispersed clasts; moderately bioturbated
>>30-53 cm: Possible flaser bedding grading down into lenticular bedding; discrete 1-3 cm long brown mud lenses and gray very fine sand lenses oriented horizontally
>>53-58 cm: ~0.5 cm thick sand and mud laminae disrupted by bioturbation
>>68-74 cm: ~0.5 cm thick sand and mud laminae disrupted by bioturbation
70-150 cm: Olive gray diatom bearing silty claystone w/dispersed clasts; moderately bioturbated
>>74-76 cm: Syneresis crack or mud crack
>>81-86 cm: ~0.5 cm thick sand and mud laminae disrupted by bioturbation
>>98-101 cm: ~0.5 cm thick sand and mud laminae disrupted by bioturbation
>>100 cm: Wood fragment (lignitized)
>>127-133 cm: ~0.5 cm thick sand and mud laminae disrupted by bioturbation
>>138-142 cm: ~0.5 cm thick sand and mud laminae disrupted by bioturbation
>>140 cm: Wood fragment (lignitized)

*Section 6
0-150 cm: Olive gray diatom bearing silty claystone w/dispersed clasts; moderately bioturbated
>>6-10 cm: ~0.5 cm thick sand and mud laminae disrupted by bioturbation
>>24-26 cm: Coal clast
>>25-38 cm: ~0.5 cm thick sand and mud laminae disrupted by bioturbation
>>81 cm: Wood fragment (soft)
*Section 7
0-75 cm: Olive gray diatom bearing silty claystone w/dispersed clasts; moderately bioturbated. Silt fraction increased relative to overlying material in section 5 and 6; few sand grains and granules. Some mm-scale horizontal burrows present.
>>11 cm: Coal clast
*Section CC
0-15 cm: Olive gray diatom bearing silty claystone w/dispersed clasts; moderately bioturbated. Silt fraction increased relative to overlying material in section 5 and 6; few sand grains and granules. Some mm-scale horizontal burrows present.
15-20 cm: Missing

16 R1,2,3,4 (142.2 to 148.4 mbsf)
*Section 1
0-150 cm: Olive gray diatom bearing silty claystone w/ dispersed clasts; moderate to common bioturbation
>>40-47 cm: Bioturbated sand bed
>>48-49 cm: Mud lenses
>>66 cm: Possible Serpulid worm tube
>>110-115 cm: Bioturbated sand bed
>>126-136 cm: Bioturbated sand bed (sharp lower contact)

*Section 2
0-150 cm: Olive gray diatom bearing silty claystone w/ dispersed clasts; moderate to common bioturbation
>>30-45 cm: Bioturbated sand bed (sharp lower contact)
>>50-55 cm: mm scale burrows (*Chondrites*?); horizontal orientation
>>60-65 cm: Bioturbated sand bed
>>73-82 cm: mm scale burrows (*Chondrites*?)
>>95-97 cm: mm scale burrows (*Chondrites*?)
>>103-105 cm: mm scale burrows (*Chondrites*?)
>>105-120 cm: Bioturbated sand bed
>>133-136 cm: Bioturbated sand bed
*Section 3
0-150 cm: Olive gray diatom bearing silty claystone w/ dispersed clasts; variable bioturbation
>>0-36 cm: Abundant bioturbation
>>12-16 cm: Bioturbated sand bed
>>29-34 cm: Bioturbated sand bed
>>36-68 cm: Common bioturbation
>>66-87 cm: Moderate bioturbation

>>68-72 cm: Bioturbated sand bed
>>87-118: Uncommon bioturbation
>>107-113 cm: Pyrite cement
>>118-126 cm: Sparse bioturbation
>>122 cm: Possible Serpulid worm tube
>>126-138 cm: Uncommon bioturbation
>>130-136 cm: Bioturbated sand bed
>>138-150 cm: Moderate bioturbation
>>139-145 cm: Bioturbated sand bed
*Section 4
0-150 cm: Olive gray diatom bearing silty claystone w/ dispersed clasts; variable bioturbation
>>0-37 cm: Moderate bioturbation
>>8-9 cm: Bioturbated sand bed
>>11-12 cm: Bioturbated sand bed
>>27 cm: Possible Serpulid worm tube
>>32-33 cm: Bioturbated sand bed
>>37-67 cm: Common bioturbation
>>45-46 cm: Bioturbated sand bed
>>67-81 cm: Abundant bioturbation
>>80-81 cm: Bioturbated sand bed
>>81-150 cm: Complete bioturbation
>>109 cm: Possible *Palaeophycus* burrow
>>138 cm: Possible *Palaeophycus* burrow

17 R1,2,3,4 (151.4 to 157.0 mbsf)
*Section 1
0-80 cm: Olive gray silty claystone w/ dispersed clasts
>>0-46 cm: Common bioturbation
>>46-80 cm: Moderate bioturbation
>>48 cm: Indurated sandstone lamina
>>52 cm: Wood fragment
>>82 cm: ~0.5 cm diameter mud intraclast
80-150 cm: Olive gray sandy silty claystone w/ crude stratification disturbed by moderate bioturbation
*Section 2
0-59 cm: Olive gray sandy silty claystone w/ crude stratification disturbed by moderate bioturbation
59-150 cm: Rhythmically laminated light brownish gray sandy siltstone and clayey siltstone w/ dispersed clasts; 0.5-1.5 cm thick embedded gravel clasts depress underlying laminae
>>59-75 cm: Uncommon to sparse bioturbation (75+ cm, bioturbation absent)
*Section 3
0-23 cm: Rhythmically laminated light brownish gray sandy siltstone and clayey siltstone w/ dispersed clasts; 0.5-1.5 cm thick embedded gravel clasts depress underlying laminae
0-130 cm: Brownish gray interlaminated sandy claystone and claystone w/ dispesed clasts; laminae 1 mm to 1 cm thick. Bedding is inclinded. Laminae have sharp boundaries;

numerous sand-sized coal clasts are present. Some claystone laminae have a dark brown color. Bioturbation is sparse to uncommon.
130-150 cm: Light gray interlaminated silty sandstone and siltstone. Laminae have irregular spacing with thicker siltstone beds and thinner sandstone laminae towards the bottom of the interval. Laminae are between 1 mm and 6 cm thick, with mud laminae typically thicker. Laminae are inclined with sharp contact. Dispersed sand grains present, but no gravel.
*Section 4
0-76 cm: Light gray interlaminated silty sandstone and siltstone.
76-94 cm: Massive light gray muddy coarse-gravelly sand; coal clasts present

18 R1,2 (161.0 to 163.6 mbsf)
*Section 1
0-150 cm: Massive light to dark gray muddy coarse sandstone w/ dispersed clasts; darkens down core and appears to increase in mud content. Matrix supported.
*Section 2
0-59 cm: Massive light to dark gray muddy coarse sandstone w/ dispersed clasts; darkens down core and appears to increase in mud content. Matrix supported.
59-70 cm: Dark brownish gray sandy mudstone; crudely stratified
70-105 cm: Massive light gray very fine to coarse sandstone w/ dispersed clasts; coal clasts present throughout
>>100 cm: Organic remains (plant seed?)

19 R1 (170.6 to 171.0 mbsf)
*Section 1
0-31 cm: Massive light gray muddy coarse sandstone w/ dispersed clasts
31-38 cm: Void

20 CC (180.3 to 180.4 mbsf)
*Section CC
0-7 cm: Massive light gray muddy coarse sandstone w/ dispersed clasts
7-10 cm: Void

Core 21 missing.

22 R1 (199.5 to 200.7 mbsf)
*Section 1
0-112 cm: Massive light gray muddy coarse to very coarse sand with dispersed clasts (<1%); matrix supported, sand grains (quartz and coal) subangular to subrounded and pebbles rounded to well-rounded
>>101-112 cm: Indurated, with gray, yellow, and brown banding respectively in down core direction; possible soil profile

23 R1 (209.1 to 210.2 mbsf)
*Section 1
0-98 cm: Massive gray muddy coarse to very coarse sand w/ dispersed clasts (<1%); coal fragments present

>>4 cm: Dark brown possible plant fragment
>>45 cm: Dark brown possible plant fragment

24 R1,2,CC (218.7 to 220.9 mbsf)
*Section 1
0-135 cm: Massive gray muddy coarse to very coarse sand w/ dispersed clasts (<1%); matrix supported. Gravel clast shapes are subrounded to wellrounded up to 4 cm in diameter. Sand grains subangular to subrounded. Coal fragments present.
135-150 cm: Void
*Section 2
0-39 cm: Massive gray muddy coarse to very coarse sand w/ dispersed clasts (<1%); coal fragments present
*Section CC
0-16 cm: Massive gray muddy coarse to very coarse sand w/ dispersed clasts (<1%); coal fragments present.
>>13.5-16 cm: One large wood fragment, with original wood structure preserved, only slightly altered. (2.5 x 2.0 x 1.0 cm)
16-26 cm: Missing (sampled)

25 R1,2,CC (228.3 to 230.1 mbsf)
*Section 1
0-100 cm: Massive gray muddy coarse to very coarse sand w/ dispersed clasts (<1%); matrix supported. Sand and gravel have subangular to subrounded appearance. Some clasts up to 3.5 cm, with irregular shapes.
>>29-39 cm: Clast supported interbed of gray coarse to very coarse sand with crude stratification
>>39-42 cm: Gray-yellowish patch
>>44-45 cm: Gray-yellowish patch
>>53-54 cm: Gray-yellowish patch
>>56 cm: Fibrous fragment (yellowish color)
>>62-66 cm: Gray-yellowish patch
*Section 2
0-65 cm: Massive gray muddy coarse to very coarse sand w/ dispersed clasts (<1%); matrix supported.
>>45-47 cm: Gray-yellowish patch (soil?)
*Section CC
0-5 cm: Light gray sandy silt w/ some coarse sand grains present
5-10 cm: Missing

26 R1,2,CC (237.9 to 240.4 mbsf)
0-45 cm: Gray sandy siltstone w/ dispersed clasts, matrix-supported
45-150 cm: Massive gray muddy coarse to very coarse sand w/ dispersed clasts (<1%); grains subangular to subrounded. Few coal fragments present.
>>53-54 cm: Possible plant debris
>>85 cm: Dark gray horizon (wavy, but semi-horizontal)
87-89 cm: Whitish concretion (85-89 cm, possible soil horizon?)

*Section 2
0-86 cm: Massive gray muddy coarse to very coarse sand w/ dispersed clasts (<1%); grains subangular to subrounded. Few coal fragments present.
>>14-27 cm: Brown horizon
>>27-44 cm: Gray color
>>44-50 cm: Light gray horizon (~2 mm thick, inclined, with darker gray patch below)
>>50-70 cm: Brownish color
>>70-86 cm: Inclined color banding
>>77-78 cm: Possible plant debris
>>77-86 cm: Cemented with calcite
*Section CC
0-5 cm: Gray sandy silt; deformed white laminae and interlamination of sandy silt and silt (all deformed)

27 R1,2,CC (247.6 to 249.4 mbsf)
*Section 1
0-150 cm: Massive gray coarse to very coarse sand with dispersed clasts; clast supported. Core is overgrown with fungus.
>>2 cm: Possible plant fragment
>>83-150 cm: Convoluted and contorted horizons, defined by changes in colors
>>83-87 cm: Yellow horizon; inclined, ~2 cm thick
>>94-100 cm: Contorted whitish and brownish horizons
*Section 2
0-27 cm: Light gray interlaminated silt and fine sand with coarse sand laminae, all contorted (possible glaciotectonic deformation)
*Section CC
0-5 cm: Black carbonaceous clay; gray silt is attached to the piece (3 cm long) in the core catcher

28 R1 (257.2 to 259.0 mbsf)
*Section 1
0-28 cm: Massive light gray medium to coarse silty sand; clast supported, with brown mottling
28-36 cm: Massive light gray coarse to very coarse sand; matrix supported, with inclined and sharp lower contact
36-62 cm: Folded, interlaminated carbonaceous debris and muddy medium-coarse sand (clast supported)
62-84 cm: Dark gray medium to very coarse sand; clast supported, with grain shapes subangular to rounded
84-92 cm: Massive light gray medium to coarse silty sand; clast supported, with brown mottling
92-96 cm: Massive light gray coarse to very coarse sand; matrix supported, with planar stratification
96-117 cm: Dark gray medium to very coarse sand (clast supported), with carbonaceous mud. Interval is contorted.
Note: Interval 36-84 cm appears to be repeated at 84-117 cm (Possible thrust glacio-tectonics?)

117-147 cm: Dark brownish gray medium sand with dispersed clasts. Some coarse sand grains present. Grain shapes are angular to subrounded. Beds are intensely folded with tight fold hinge.
29 R1 (266.8 to 267.2 mbsf)
*Section 1
0-10 cm: Greenish gray siltstone clasts; probably fall in from Upper Eocene sections
10-16 cm: Dark gray muddy medium to coarse sand; matrix supported with sharp lower contact
16-34 cm: Light gray muddy coarse to very coarse sand; matrix supported with sharp lower contact
>>26-31 cm: PAL sample
34-38 cm: Dark gray muddy medium to coarse sand; matrix supported. Some very coarse sand grains present.
>>34 cm: Coal clast (<2 mm diameter)

Site 742, Hole A

20 R1,2,3 (171.3 to 175.0 mbsf)
*Section 1
0-133 cm: Dark brown clast rich sandy diamictite; ~5% clasts
>>120 cm: Deformed lower contact, sheared, with contorted bedding
>>124 cm: Deformed lower contact, sheared, with contorted bedding
>>133-134 cm: Deformed lower contact, sheared, with contorted bedding
133-150 cm: Gray sandy clayey silt with dispersed clasts
*Section 2
0-48 cm: Gray sandy clayey silt with dispersed clasts
48-56 cm: Greenish gray silty claystone
56-115 cm: Gray sandy clayey silt with dispersed clasts (similar to 739 52R, but material here is slightly less sandy)
115-150 cm: Missing (sampled)
*Section 3
0-44 cm: Gray sandy clayey silt with dispersed clasts (similar to 739 52R, but material here is slightly less sandy)
44-67 cm: Green gray silty claystone

21 R1,2,3 (181.0 to 184.8 mbsf)
*Section 1
0-38 cm: Brownish gray sandy mudstone with dispersed clasts (granules); clasts <1%
>>4-14 cm: Soft sediment deformed beds
38-77 cm: Gray clayey silty sandstone with dispersed clasts; sand fraction is moderately sorted (fine-medium sand)
77-91 cm: Gray sandy mudstone with dispersed clasts (<1%)
91-150 cm: Gray clayey silty sandstone with dispersed clasts; sand fraction is moderately sorted (fine-medium sand)
*Section 2
0-146 cm: Gray clayey silty sandstone with dispersed clasts; sand fraction is moderately sorted (fine-medium sand)
146-150 cm: Light gray sandy mudstone with dispersed clasts (<1%); very poorly sorted sand fraction with numerous coarse sand grains
>>146-150 cm: Soft sediment deformation
*Section 3
0-76 cm: Light gray sandy mudstone with dispersed clasts (<1%); very poorly sorted sand fraction with numerous coarse sand grains

22 R1,2,3,4,5,6,7 (190.7 to 200.0 mbsf)
*Section 1
0-42 cm: Gray muddy sandstone with dispersed clasts (<1%); sand fraction is poorly sorted w/ coarse sand component
42-87 cm: Gray muddy sandstone with dispersed clasts (<1%); sand fraction is finer than above and moderately sorted.
>>83-87 cm: Stratification with ~0.5 cm thick sand and mud laminae
87-150 cm: Greenish gray clayey siltstone with dispersed clasts (<1%)

*Section 2
0-16 cm: Greenish gray clayey siltstone with dispersed clasts (<1%)
16-150 cm: Gray sandy mudstone with dispersed clasts (<1%); more sand in matrix than above, and variations of sand% in matrix
*Section 3
0-130 cm: Gray sandy mudstone with dispersed clasts (<1%); more sand in matrix than above, and variations of sand% in matrix
130-150 cm: Gray muddy sandstone with dispersed clasts (~1% clasts); very poorly sorted sand fraction w/ coarse sand component
*Section 4
0-150 cm: Gray muddy sandstone with dispersed clasts (~1% clasts); very poorly sorted sand fraction w/ coarse sand component
*Section 5
0-2 cm: Gray muddy sandstone with dispersed clasts (~1% clasts); very poorly sorted sand fraction w/ coarse sand component
2-20 cm: Gradational change to gray sandy mudstone
20-150 cm: Gray sandy mudstone w/ dispersed clasts
*Section 6
0-150 cm: Gray sandy mudstone w/ dispersed clasts
*Section 7
0-34 cm: Gray sandy mudstone w/ dispersed clasts; sand in matrix becomes more poorly sorted than above, w/ a larger coarse sand fraction. Clasts are angular to subangular.

23 R1,2,3,4,5,6,CC (200.3 to 209.4 mbsf)
*Section 1
0-150 cm: Gray sandy mudstone w/ dispersed clasts (~1% or less). Granule sized clasts are angular to subangular and low sphericity.
*Section 2
0-150 cm: Gray sandy mudstone w/ dispersed clasts (~1% or less). Granule sized clasts are angular to subangular and low sphericity.
>>14-20 cm: Carbonate cemented patch
*Section 3
0-150 cm: Gray sandy mudstone w/ dispersed clasts (~1% or less). Granule sized clasts are angular to subangular and low sphericity.
*Section 4
0-150 cm: Gray sandy mudstone w/ dispersed clasts (~1% or less). Granule sized clasts are angular to subangular and low sphericity.
>>72-105 cm: Carbonate cemented patch
*Section 5
0-153 cm: Gray sandy mudstone w/ dispersed clasts (~1% or less). Granule sized clasts are angular to subangular and low sphericity.
*Section 6
0-154 cm: Gray sandy mudstone w/ dispersed clasts (~1% or less). Granule sized clasts are angular to subangular and low sphericity.

24 R1,2,3,4 (209.9 to 215.7 mbsf)
*Section 1
0-150 cm: Gray sandy mudstone w/ dispersed clasts (~1% or less)
>>89-91 cm: Well-rounded granite clasts
*Section 2
0-150 cm: Gray sandy mudstone w/ dispersed clasts (~1% or less); sand finer in middle of section
*Section 3
0-150 cm: Gray sandy mudstone w/ dispersed clasts (~1% or less)
>>53-54 cm: Silt lamina
*Section 4
0-130 cm: Gray sandy mudstone w/ dispersed clasts (~1% or less)

Core 25 missing.

26 R1,2,3,4,5 (229.2 to 236.6 mbsf)
*Section 1
0-3 cm: Gray sandy mudstone
3-76 cm: Gray clayey siltstone w/ dispersed clasts; <20% sand, <1% clasts
76-98 cm: Greenish gray silty claystone w/ dispersed clasts; <10% sand, <1% clasts
98-150 cm: Gray sandy siltstone w/ dispersed clasts (<1%)
*Section 2
0-150 cm: Gray sandy siltstone w/ dispersed clasts (<1%)
*Section 3
0-150 cm: Gray sandy siltstone w/ dispersed clasts (<1%); sorting poorer than above sections
*Section 4
0-150 cm: Gray sandy siltstone w/ dispersed clasts (<1%)
>>46-47 cm: Band of relatively fine, moderately sorted sand
>>84-89 cm: Clast cluster
*Section 5
0-119 cm: Gray sandy siltstone w/ dispersed clasts (<1%)
>>105-110 cm: Clast cluster

27 R1,2,3,4,5,6,7,CC (238.8 to 248.6 mbsf)
*Section 1
0-150 cm: Gray sandy siltstone w/ dispersed clasts (1% or less)
*Section 2
0-150 cm: Gray sandy siltstone w/ dispersed clasts (1% or less)
>>100-150 cm: Silty sandstone interbed
*Section 3
0-150 cm: Gray sandy siltstone w/ dispersed clasts (1% or less)
>>90-150 cm: Silty sandstone interbed; gradational upper contact
*Section 4
0-115 cm: Gray sandy siltstone w/ dispersed clasts (1% or less)
>>0-10 cm: Silty sandstone interbed; abrupt lower contact
115-150 cm: Missing (sampled)

*Section 5
0-150 cm: Gray sandy siltstone w/ dispersed clasts (1% or less)
>>125-150 cm: Silty sandstone interbed
*Section 6
0-150 cm: Gray sandy siltstone w/ dispersed clasts (1% or less)
>>0-34 cm: Silty sandstone interbed
>>20-26 cm: Carbonate patch
>>34-38 cm: Silt interbed (disturbed by drilling)
*Section 7
0-63 cm: Gray sandy siltstone w/ dispersed clasts (1% or less)
>>0-9 cm: Silt interbed (disturbed by drilling)
*Section CC
0-17 cm: Gray sandy siltstone w/ dispersed clasts (1% or less)
>>7-12 cm: Cemented Patch
>>12-17 cm: Missing

28 R1,2,3,4,5,6,7 (248.6 to 258.4 mbsf)
*Section 1
0-150 cm: Gray sandy siltstone with dispersed clasts (1% or less); some clast clusters
>>0-9 cm: Gray silty sandstone interbed
>>133-150 cm: Gray silty sandstone interbed (transitional boundary from 113 cm)
*Section 2
0-150 cm: Gray sandy siltstone with dispersed clasts (1% or less); some clast clusters
>>0-9 cm: Gray silty sandstone interbed
*Section 3
0-150 cm: Gray sandy siltstone with dispersed clasts (1% or less); some clast clusters
>>82-87 cm: Gray silty sandstone interbed (transitional boundary from 77 cm)
*Section 4
0-150 cm: Gray sandy siltstone with dispersed clasts (1% or less); some clast clusters
>>0-50 Gray silty sandstone interbed with dispersed clasts (1% or less)
*Section 5
0-150 cm: Gray sandy siltstone with dispersed clasts (1% or less); some clast clusters
>>0-5 cm: Siltstone interbed
*Section 6
0-150 cm: Gray sandy siltstone with dispersed clasts (1% or less); some clast clusters
*Section 7
0-80 cm: Gray sandy siltstone with dispersed clasts (1% or less); some clast clusters

29 R1,2,3,4,5,6 (258.4 to 267.1 mbsf)
*Section 1
0-150 cm: Massive gray sandy siltstone with dispersed clasts (1% or less)
*Section 2
0-150 cm: Massive gray sandy siltstone with dispersed clasts (1% or less)
*Section 3
0-150 cm: Massive gray sandy siltstone with dispersed clasts (1% or less)

*Section 4
0-150 cm: Massive gray sandy siltstone with dispersed clasts (1% or less)
*Section 5
0-150 cm: Massive gray sandy siltstone with dispersed clasts (1% or less)
>>109-111 cm: Sharp contact at 109 cm transitioning to moderately sorted sandstone interbed
>>111-146 cm: Grading from sandstone to sandy siltstone
>>146-150 cm: Siltstone with <25% sand in matrix
*Section 6
0-143 cm: Massive gray sandy siltstone with dispersed clasts (1% or less)
>>0-17 cm: Siltstone with <25% sand in matrix
138-143 cm: Moderately sorted sand

30 R1,2,3,4,5,6,CC (267.8 to 276.7 mbsf)
*Section 1
0-150 cm: Gray sandy siltstone with dispersed clasts
*Section 2
0-27 cm: Gray sandy siltstone with dispersed clasts
27-150 cm: Gray silty sandstone with dispersed clasts
*Section 3
0-33 cm: Gray silty sandstone with dispersed clasts
33-56 cm: Gray sandy siltstone with dispersed clasts; gradational boundaries
56-150 cm: Gray silty sandstone with dispersed clasts
*Section 4
0-150 cm: Gray silty sandstone with dispersed clasts
*Section 5
0-150 cm: Gray silty sandstone with dispersed clasts
*Section 6
0-124 cm: Gray silty sandstone with dispersed clasts
>>30-50 cm: Bed with poorer sorting and increased mud matrix
*Section CC
0-13 cm: Gray silty sandstone with dispersed clasts
13-18 cm: Missing

31 R1,2,3,4 (277.4 to 283.2 mbsf)
*Section 1
0-150 cm: Gray silty sandstone with dispersed clasts (<1%)
*Section 2
0-150 cm: Gray silty sandstone with dispersed clasts (<1%)
>>107-112 cm: Cemented patch
*Section 3
0-150 cm: Gray silty sandstone with dispersed clasts (<1%)
>>33-48 cm: Very large cobble
*Section 4
0-128 cm: Gray silty sandstone with dispersed clasts (<1%)

32 R1,2,3,4 (287.1 to 293.1 mbsf)
*Section 1
0-5 cm: Gray silty sandstone with dispersed clasts (1% or less); sharp lower contact
5-150 cm: Gray silty sandstone with dispersed clasts (~1% clasts); slightly more fine-grained matrix than top 5 cm of section 1
>>38 cm: Coal clast
>>133 cm: Coal clast
>>147 cm: Coal clast
*Section 2
0-150 cm: Gray silty sandstone with dispersed clasts (~1% clasts)
>>9.5 cm: Coal clast
>>84 cm: Coal clast
*Section 3
0-150 cm: Gray silty sandstone with dispersed clasts (~1% clasts)
>>107 cm: Coal clast
*Section 4
0-150 cm: Gray silty sandstone with dispersed clasts (~1% clasts)

33 R1,2,3,4,5,6 (296.7 to 305.2 mbsf)
*Section 1
0-150 cm: Gray silty sandstone with dispersed clasts (<1%)
>>51 cm: Coal clast
*Section 2
0-150 cm: Gray silty sandstone with dispersed clasts (<1%)
>>121 cm: Coal clast
>>133 cm: Coal clast
*Section 3
0-150 cm: Gray silty sandstone with dispersed clasts (<1%)
>>140 cm: Coal clast
*Section 4
0-89 cm: Gray silty sandstone with dispersed clasts (<1%)
89-115 cm: Sandy mudstone with a few scattered coarse sand grains
115-150 cm: Missing (sampled)
*Section 5
0-150 cm: Gray sandy siltstone with dispersed clasts
*Section 6
0-9 cm: Gray sandy siltstone with dispersed with clasts (mud matrix increasing with depth towards sharp lower contact)
9-90 cm: [See Figure 26 in Hambrey et al. (1991)]

34 R1,2,3,4,5,6,CC (306.3 to 315.2 mbsf)
*Section 1
0-130 cm: Gray muddy interlaminated sandstone and siltstone with dispersed clasts (<1%, granules only). Lamination is rhythmic. Siltstone laminae are 1 mm to 2 cm thick; sand laminae are typically 0.5 cm thick.
>>89 cm: Coal clast
>>109 cm Coal clast

130-150 cm: Gray sandy mudstone with dispersed clasts (<1%)

*Section 2
0-150 cm: Gray sandy mudstone with dispersed clasts (<1%); sand in matrix increasing towards section 5
*Section 3
0-150 cm: Gray sandy mudstone with dispersed clasts (<1%)
>>18 cm: Coal clast
>>25 cm: Coal clast
>>94 cm: Coal clast
*Section 4
0-150 cm: Gray sandy mudstone with dispersed clasts (<1%)
*Section 5
0-80 cm: Gray sandy mudstone with dispersed clasts (<1%)
80-150 cm: Convoluted and controrted light brownish gray poorly sorted sandstone and dark brownish gray to black mudstone with common dark brown wood fragments
*Section 6
0-120 cm: Convoluted and controrted light brownish gray poorly sorted sandstone and dark brownish gray to black mudstone with common dark brown wood fragments
>>35-37 cm: Wood fragment (~1.5 cm)
>>87-89 cm: Wood fragment (~1.5 cm)
*Section CC
0-12 cm: Convoluted and controrted light brownish gray poorly sorted sandstone and dark brownish gray to black mudstone with common dark brown wood fragments
12-17 cm: Missing

Site 739, Hole C

24 CC (169.0 to 169.16 mbsf)
*Section CC
0-5.5 cm: Missing
5.5-11.5 cm: Clast rich sandy diamictite; dark gray and more clay rich diamictite than lighter gray and silitier underlying diamictite units (26 and below)
11.5 cm-15.5 cm: Clasts

25 R1 (173.6 to 174.9 mbsf)
*Section 1
Note: Core section heavily fractured
0-11 cm: Dark gray clast poor sandy diamictite
>>11 cm: Clasts along contact
11-122 cm: Clast poor light gray muddy diamictite, friable; 3-4% clasts
39 cm: Yellow staining
59 cm: Yellow staining
85-87 cm: Yellow staining
109-110 cm: Yellow staining

26 R1,2,3,CC (183.2 to 188.0 mbsf)
*Section 1
0-48 cm: Light gray sandy diamictite, ~5% clast (clast rich), massive
>>0-15 cm: Large banded gneiss
48-150 cm: Light gray muddy diatom bearing clast poor diamictite
>>48-109 cm: Visible variation in sand percentage of matrix; weakly stratified
>>128-130 cm: Wispy wavy lamination (inclined)
>>140-145 cm: Wispy wavy lamination (horizontal)
*Section 2
0-70 cm: Stratified clast poor muddy diamictite and sandy mudstone w/ dispersed clasts
>>0-30 cm: Intensely stratified
70-150 cm: Structureless clast poor muddy diamictite
>>73 cm: Yellow staining
*Section 3
0-115 cm: Massive clast poor sandy diamictite; clasts ~1%
>>21 cm: Shell fragment
>>43-55 cm: Soft sediment deformation
115-150 cm: Stratified clast poor sandy diamictite
*Section CC
2-16 cm: Clast poor sandy diamictite
>>13 cm: Laminae visible at a core break
>>16 cm: Inclined (erosive?) contact
16-30 cm: Deformed clast poor muddy diamictite; ~2% clasts (aligned to sediment)

27 R1,CC (192.9 to 193.9 mbsf)
*Section 1
0-80 cm: Light gray diatom-rich sandy mudstone w/ dispersed clast (< 1%)

>>Weakly laminated (core is heavily fractured), but at 9-15 cm very clearly visible in well preserved section.
*Section CC
0-15 cm: Light gray diatom-rich sandy mudstone w/ dispersed clast (< 1%)
>>1 cm: Shell fragment
>>5 cm: Foram? fragment

28 R1,2,3,4,5,CC (202.2 to 209.6 mbsf)
*Section 1
0-150 cm: Light gray clast poor (3% clasts) muddy diamictite
>>0-108 cm: Weakly stratified diatom bearing section with 2-5 mm light colored muddy laminae
>>108 cm: Wispy laminae
*Section 2
0-150 cm: Light gray clast poor (3% clasts) muddy diamictite
>>121-136 cm: Steeply inclined sand and diamict laminae (of unequal width across the core)
*Section 3
0-115 cm: Light gray clast poor (3% clasts) muddy diamictite
>>14 cm: Shell fragment
>>25 cm: Shell fragment
*Section 4
0-150 cm: Light gray clast poor (3% clasts) muddy diamictite
>>72 cm: Cemented fracture
>>118 cm: Shell fragment
>>138.5 cm: Shall fragment
*Section 5
0-77 cm: Light gray clast poor (~1% or less clasts) muddy diamictite
>>32 cm: Wispy laminae
>>51 cm: Shell fragment
*Section CC
0-35 cm: Light gray clast poor (3% clasts) muddy diamictite
>>10 cm: Shell fragment
>>24-31 cm: Missing

29 R1,2,3,4,5,CC (212.2 to 219.3 mbsf)
*Section 1
0-150 cm: Light gray clast poor muddy diamictite with contorted laminae
*Section 2
0-150 cm: Light gray clast poor muddy diamictite with contorted laminae
>>24-33 cm: Planar mm-cm scale semi-horizontal lamination
*Section 3
0-150 cm: Light gray clast poor muddy diamictite with contorted laminae
>>8-68 cm: Planar mm-cm scale semi-horizontal lamination

*Section 4
0-150 cm: Light gray clast poor muddy diamictite with contorted laminae; some granule sized coal fragments in working half
>>100 cm: Shell layer

*Section 5
0-113 cm: Light gray clast poor muddy diamictite with contorted laminae
>>19 cm: Shell fragment
>>26-31 cm: Clast surrounded by material with noticeably greater sand fraction
>>74-84 cm: Steeply inclined bedding and folding
*Section CC
0-29 cm: Light gray clast poor muddy diamictite with contorted laminae
>>15-18 cm: Stratification only slightly inclined

30 R1,2,3,4,5,6,CC (221.8 to 230.2 mbsf)
*Section 1
0-150 cm: Light gray clast poor muddy diamictite w/ interbeds of sandy mud w/ dispersed clasts, most well stratified; clasts 1-2%, some section < 1%. Stratfication consists of interlaminated siltier and sandier *sandy siltstone*, w/ individual laminae typically 2-10 mm.
>>101 cm: Shell cast and fragments
*Section 2
0-150 cm: Light gray clast poor muddy diamictite w/ interbeds of sandy mud w/ dispersed clasts, most well stratified; clasts 1-2%, some section < 1%. Stratfication consists of interlaminated siltier and sandier *sandy siltstone*, w/ individual laminae typically 2-10 mm.
>>13-16 cm: Bowed up laminae
*Section 3
0-150 cm: Light gray clast poor muddy diamictite w/ interbeds of sandy mud w/ dispersed clasts, most well stratified; clasts 1-2%, some sections < 1%. Stratfication consists of interlaminated siltier and sandier *sandy siltstone*, w/ individual laminae typically 2-10 mm.
>>93-94 cm: Carbonate? or Silica? cemented patch (white, hard) or laminae of coarse sand
*Section 4:
0-136 cm: Light gray clast poor muddy diamictite w/ interbeds of sandy mud w/ dispersed clasts, most well stratified; clasts 1-2%, some sections < 1%. Stratfication consists of interlaminated siltier and sandier *sandy siltstone*, w/ individual laminae typically 2-10 mm.
>>65-136 cm: Inclined rhythmic lamination, with some laminae thicker than 10 mm (No core break at 65 cm; laminae become contorted above this point)
>>136 cm: Sharp, inclined contact between rhythmically stratified facies and underlying structureless diamictite
136-150 cm: Massive light gray clast poor muddy diamictite; clasts 1-2%
*Section 5
0-150 cm: Massive light gray clast poor muddy diamictite; clasts 1-2%
>>0-19 cm: Inclined bedding

>>114-150 cm: Semi-horizontal lamination
*Section 6
0-88 cm: Light gray clast poor muddy diamictite; clasts 1-2%
>>0-62 cm: Semi-horizontal lamination

31 R1,2,3,4,5,CC (231.4 to 238.0 mbsf)
*Section 1
0-150 cm: Light gray clast poor muddy diamictite w/ stratification. Beds primarily contorted and some steeply inclined. Matrix appears silty.
>>0-26 cm: Semi-horizontal weak stratification
>>67-102 cm: Contorted/convolute bedding; darker gray color
>>102-150 cm: Core material becoming bimodal sandier and more clayey, not as silty
*Section 2
0-150 cm: Light gray clast poor muddy diamictite w/ stratification. Beds primarily contorted and some steeply inclined; clasts ~3%.
>>5-6 cm: Horizontal lamina 0.5 cm thick cemented at core break
>>46-150 cm: Contorted and convolute bedding with lighter and darker gray laminae
*Section 3
0-115 cm: Lighter gray and siltier massive clast poor muddy diamictite with some contorted beeding; clasts ~1%
115-150 cm: Missing (Sampled)
*Section 4
0-150 cm: Lighter gray and siltier massive clast poor muddy diamictite with some contorted beeding; clasts ~1%
*Section 5
0-103 cm: Lighter gray and siltier massive clast poor muddy diamictite with some contorted beeding; clasts ~1%
>>11 cm: Shell fragment
*Section CC
0-16 cm: Lighter gray and siltier massive clast poor muddy diamictite with some contorted beeding; clasts ~1%
16-22 cm: Missing

32 R1, CC (241.1 to 242.3 mbsf)
Note: More sand in core material matrix than in previous core
*Section 1
0-103 cm: Light gray clast poor sandy diamictite; granule sized fragments of coal in working half
>>10-12 cm: Macrofossil sample taken (Larsen) #11811
>>17 cm: Horizontal mm scale lamina
>>44 cm: Horizontal mm scale lamina
>>84 cm: Horizontal mm scale lamina
>>80-103 cm: Sandy mudstone in working half
*Section CC
0-7 cm: Light gray clast poor sandy diamictite
7-12 cm: Missing

33 R1,2,3,4,5,6,CC (250.7 to 259.3 mbsf)
*Section 1
0-150 cm: Light gray clast poor muddy diamictite, with silty matrix and abundant contorted laminae and inclinded bedding; clasts ~1%

*Section 2
0-56 cm: Light gray clast poor muddy diamictite, with silty matrix and abundant contorted laminae and inclinded bedding; clasts ~1%
56-99 cm: Light greenish gray diatom rich silty claystone w/ dispersed clasts; sharp inclinded upper and lower contacts with sand bed on top
99-150 cm: Light to dark gray clast poor muddy and sandy diamicitite; clasts ~1-2%. Darker contorted laminae and beds have higher sand content in the matrix.
*Section 3
0-116 cm: Light to dark gray clast poor muddy and sandy diamicitite; clasts ~1-2%. Darker contorted laminae and beds have higher sand content in the matrix; sharp lower contact.
116-150 cm: Medium gray horizontally stratified clast poor sandy diamictite; ~3% clasts
*Section 4
0-150 cm: Light to dark gray clast poor muddy diamictite with commonly contorted bedding
*Section 5
0-150 cm: Light to dark gray clast poor muddy diamictite with commonly contorted bedding
>>93-100 cm: Boudinage of mud laminae
*Section 6
0-94 cm: Light to dark gray clast poor muddy diamictite with commonly contorted bedding
>>29-34 cm: Synsedimentary microfault (normal)
*Section CC
0-16 cm: Light to dark gray clast poor muddy diamictite with commonly contorted bedding

34 R1,2,3,4,5,CC (260.4 to 267.4 mbsf)
*Section 1
0-150 cm: Light gray clast poor diatom bearing muddy diamictite and sandy silt w/ dispersed clasts; clasts ~1% or less
>>0-21 cm: Lighter colored area; less and
>>14 cm: Shell fragment in working half
>>93-98 cm: Clast/coarse sand cluster
>>119-123 cm: Clast/coarse sand cluster
>>113-146 cm: Dark gray colored area with contorted bedding
*Section 2
0-113 cm: Light gray structureless clast poor muddy diamictite (less clast poor than previous section) with some shell fragments
113-115 cm: Diatom bearing (20%) clayey silt w/ dispersed clasts; weakly stratified
115-150 cm: Missing (Sampled)

*Section 3
0-83 cm: Diatom bearing (20%) clayey silt; weakly stratified
>>27-39 cm: Granule sized clasts
>>71-73 cm: One large outsized clast
83-150 cm: Massive light gray diatom bearing clast poor sandy diamictite; ~1% clasts
*Section 4
0-150 cm: Massive light gray diatom bearing clast poor sandy diamictite; ~1% clasts
*Section 5
0-19 cm: Massive light gray diatom bearing clast poor sandy diamictite; ~1% clasts
19-91 cm: Stratified light gray diatom bearing clast poor muddy diamictite
>>26-29 cm: Horizontal laminae
>>66-92 cm: Shell fragments in working half; possible forams and/or worm tubes
>>71-91 cm: Horizontal laminae
*Section CC
0-7 cm: Stratified light gray diatom bearing clast poor muddy diamictite
7-12 cm: Missing

35 R1,2,3,4 (270.0 to 275.4 mbsf)
*Section 1
0-75 cm: Light gray diatom-bearing sandy siltstone w/ dispersed clasts; clasts <1%
75-150 cm: Light and dark gray clast poor sandy diamictite w/ contorted bedding
>>76-93 cm: Dark sand rich beds
*Section 2
0-48 cm: Light and dark gray clast poor sandy diamictite w/ contorted bedding
48 cm-150 cm: Light gray diatom bearing sandy siltstone w/ dispersed clasts; clasts <1%
*Section 3
0-150 cm: Light gray diatom bearing sandy siltstone w/ dispersed clasts; clasts <1%
>>70-72 cm: Wispy laminae
>>141-150 cm: Contorted laminae
*Section 4
0-48 cm: Light gray diatom bearing sandy siltstone w/ dispersed clasts; clasts <1%
48-75 cm: Massive light gray clast poor sandy diamictite; clasts 2-3%
>>48 cm: Two larger clasts at top of the unit, up to 6 cm in diameter (other clasts in unit are up to 1 cm)
*Section CC
0-16 cm: Massive light gray clast poor sandy diamictite; clasts 2-3%
16-21 cm: Missing

36 R1,2,3,4,5,CC (279.7 to 287.3 mbsf)
*Section 1
0-67 cm: Light gray clast poor sandy diamictite with abundant coarse sand in matrix; clasts 1-2%
67-75 cm: Light gray mudstone with common clasts and sand laminae up to 5 mm thick at the base of unit
75-150 cm: Light gray clast poor diatom bearing muddy diamictite; clasts 2-3%
*Section 2
0-150 cm: Light gray clast poor diatom bearing muddy diamictite; clasts 2-3%

>>107-114 cm: Wispy laminae
*Section 3
0-150 cm: Light gray clast poor diatom bearing muddy diamictite; clasts 2-3%
>>72 cm: Wispy lamina
>>135-138: Clast cluster; clasts up to 8 mm in size
*Section 4
0-150 cm: Light gray clast poor diatom bearing muddy diamictite; clasts 2-3%
>>56-150 cm: Clasts <1% and reduced sand fraction
*Section 5
0-141 cm: Light gray clast poor diatom bearing muddy diamictite; clasts 2-3%
>>0-19 cm: Clasts <1% and reduced sand fraction
*Section CC
0-19 cm: Light gray clast poor diatom bearing muddy diamictite; clasts 2-3%
>>5-19 cm: Clasts <1% and reduced sand fraction

37 R1 (289.3 to 290.3 mbsf)
*Section 1
0-5 cm: Massive light gray clast poor muddy diamictite; clasts ~1%. Sharp planar contact at 5 cm.
5-99 cm: Light gray clast rich diamictite; clasts ~5% near top of section and decreasing towards bottom
>>35-37 cm: Wispy laminae, sandy, ~2 mm thick
>>74-75 cm: Coarse sand laminae, ~5 mm thick

38 R1,2,3,4 (298.9 to 303.7 mbsf)
*Section 1
0-150 cm: Massive light gray clast-poor muddy diamictite; clasts variable (1-3%) and variations occur in sand % of matrix
96-150 cm: Higher sand %
*Section 2
0-150 cm: Massive light gray clast-poor muddy diamictite; clasts variable (1-3%) and variations occur in sand % of matrix
*Section 3
0-150 cm: Massive light gray clast-poor muddy diamictite; clasts variable (1-3%) and variations occur in sand % of matrix
*Section 4
0-26 cm: Massive light gray clast-poor muddy diamictite; clasts variable (1-3%) and variations occur in sand % of matrix

39 R1,2,3,4,CC (308.6 to 313.6 mbsf)
*Section 1
0-150 cm: Light gray silty clay with common clasts; clasts 2-3%, less than 25% sand
>>49-128 cm: Millimeter-scale planar laminae
*Section 2
0-12 cm: Light gray silty clay with common clasts; clasts 2-3%, less than 25% sand
12-18 cm: Massive light gray clast poor muddy diamictite; clasts 3-5%
18-150 cm: Massive light gray clast poor sandy diamictite; clasts 3-5%

*Section 3
0-150 cm: Massive light gray clast poor sandy diamictite; clasts 3-5%
*Section 4
0-32 cm: Massive light gray clast poor sandy diamictite; clasts 3-5%
*Section CC
0-14 cm: Massive light gray clast poor sandy diamictite; clasts 3-5%
14-19 cm: Missing

40 R1,2 (318.2 to 319.9 mbsf)
*Section 1
0-37 cm: Light gray clast poor sandy diamictite; ~2-3% clasts
37-49 cm: Carbonate mixed with carbonate cemented sandy diamictite; deformed
49-150 cm: Brownish gray clast poor sandy diamictite; ~2-3% clasts. Finer sand in matrix than compared to 0-37 cm
>>135 cm: Mudstone intraclast
>>148 cm: Mudstone intraclast
*Section 2
0-12 cm: Light gray clast poor sandy diamictite

41 R1 (327.8 to 332.6 mbsf)
*Section 1
0-150 cm: Brownish gray clast poor sandy diamictite; clasts ~1-2%
*Section 2
0-115 cm: Brownish gray clast poor sandy diamictite; clasts ~1-2%
>>64 cm: Elongate clast; aligned c-axis to horizontal plane
115-150 cm: Missing (sampled)
*Section 3
0-150 cm: Brownish gray clast poor sandy diamictite; clasts ~1-2%
*Section CC
0-27 cm: Brownish gray clast poor sandy diamictite; clasts ~1-2%

42 R1,2,CC (337.5 to 340.5 mbsf)
Note: Regularly spaced drilling disturbances (dark bowed bands) in sections 2 and CC
*Section 1
0-150 cm: Light brownish gray clast poor diamictite; clasts 1-2%
>>57-59 cm: Clast cluster
*Section 2
0-130 cm: Light brownish gray clast poor diamictite; clasts 1-2%
*Section CC
0-17 cm: Light brownish gray clast poor diamictite; clasts 1-2%
17-22 cm: Missing

43 R1,CC (347.1 to 348.9 mbsf)
*Section 1
0-150 cm: Light brownish gray clast poor sandy diamictite; clasts 1-2%

*Section CC
6-22cm: Light brownish gray clast poor sandy diamictite; clasts 2%. Lithology same as section 1, only more sand in matrix.
22-26 cm: Missing

44 R1,2 (356.8 to 359.8 mbsf)
*Section 1
0-150 cm: Light to medium gray clast poor sandy diamicite; clasts 1-2%
*Section 2
0-141 cm: Light to medium gray clast poor sandy diamicite; clasts 1-2%

45 CC (366.5 to 366.8 mbsf)
*Section CC
0-21: Gray clast poor sandy diamictite
>>7-18 cm: Dark bowed band
21-26: Missing

46 R1,2,CC (376.2 to 378.4 mbsf)
Note: Regularly spaced drilling disturbances (dark bowed bands) in sections 2 and CC
*Section 1
0-150 cm: Massive gray clast poor sandy diamictite; clasts 1-2%
*Section 2
0-55 cm: Massive gray clast poor sandy diamictite; clasts 1-2%
*Section CC
0-14 cm: Massive gray clast poor sandy diamictite; clasts 1-2%
14-18 cm: Missing

47 R1 (385.9 to 386.8 mbsf)
Note: Regularly spaced drilling disturbances (dark bowed bands) at 41-44 cm and 60-93 cm
*Section 1
0-93 cm: Gray clast poor sandy diamictite; clasts 1-2%
>>86-87 cm: Yellowish lamina 1 cm thick (micrite)

48 R1,2 (395.6 to 398.1 mbsf)
*Section 1
0-150 cm: Massive Gray clast poor sandy diamictite; clasts 1-2%
*Section 2
0-94 cm: Massive Gray clast poor sandy diamictite; clasts 1-2%

Core 49 missing.

50 R1,2 (414.9 to 417.0 mbsf)
Note: Regularly spaced drilling disturbances (dark bowed bands) in section 1 and 2
*Section 1
0-150 cm: Gray clast poor sandy diamictite; clasts 1-2%

*Section 2
0-59 cm: Gray clast poor sandy diamictite; clasts 1-2%

51 R1,2 (424.5 to 426.7 mbsf)
*Section 1
0-150 cm: Gray clast poor sandy diamictite; clasts ~1%
*Section 2
0-69 cm: Gray clast poor sandy diamictite; clasts ~1%
>>50-52 cm: Fine grained calcareous lamina (<1 cm) and deformed by drilling

52 R1,2,CC (434.2 to 426.6 mbsf)
*Section 1
0-150 cm: Gray clayey silty sand with dispersed clasts (<1%)
>>21 cm: Rounded quartzite pebble
*Section 2
0-50 cm: Gray clayey silty sand with dispersed clasts (<1%)
50-60 cm: Transition to light gray clayey silt with a few dispersed granule sized clasts
60-76 cm: Light gray clayey silt with a few dispersed granule sized clasts

*Section CC
0-8 cm: Light gray clayey silt with a few dispersed granule sized clasts
8-13 cm: Missing

53 R1,CC (439.2 to 440.7 mbsf)
*Section 1
0-150 cm: Gray clayey silty sand with dispersed clasts (1% or less). Granule sized gravel only.
*Section CC
0-18 cm: Gray clayey silty sand with dispersed clasts (1% or less). Granule sized gravel only.
18-25 cm: Missing

54 R1,CC (443.9 to 445.8 mbsf)
*Section 1
0-150 cm: Brownish gray clayey silty sand with dispersed clasts (<1%)
*Section CC
0-35 cm: Brownish gray clayey silty sand with dispersed clasts (<1%)
35-40 cm: Missing

55 R1,2,CC (448.9 to 451.1 mbsf)
*Section 1
0-150 cm: Gray clayey silty sand with dispersed clasts (<1%)
*Section 2
0-15 cm: Gray clayey silty sand with dispersed clasts (<1%)
15-23 cm: Yellowish moderately sorted cemented fine sand
23-29 cm: Poorly sorted muddy sand with coarse sand grains

29-41 cm: Silt and clay bearing limestone with coarse sand grains dispersed throughout with intraclasts
41-48 cm: Gray clayey silty sand with dispersed clasts
*Section CC
0-14 cm: Gray clayey silty sand with dispersed clasts
14-20 cm: Missing

56 R1,CC (453.5 to 454.5 mbsf)
*Section 1
0-65 cm: Gray clayey silty sand with dispersed clasts (<1%)
*Section CC
0-25 cm: Gray clayey silty sand with dispersed clasts (<1%)
25-30 cm: Missing

57 R1,CC (458.5 to 459.5 mbsf)
*Section 1
0-72 cm: Gray clayey silty sand with dispersed clasts (1% or less)
*Section CC
0-22 cm: Gray clayey silty sand with dispersed clasts (1% or less)
22-27 cm: Missing

58 R1,2,CC (463.2 to 466.3 mbsf)
*Section 1
0-150 cm: Gray clayey silty sand with dispersed clasts (1% or less)
*Section 2
0-43 cm: Gray clayey silty sand with dispersed clasts (1% or less)
43-88 cm: Sandy clayey siltstone
88-139 cm: Gray clayey silty sand with dispersed clasts (<1%)
*Section CC
0-18 cm: Gray clayey silty sand with dispersed clasts (<1%)
18-24 cm: Missing

59 R1 (468.2 to 469.0 mbsf)
0-70 cm: Gray clayey silty sand with dispersed clasts (<1%)

60 R1 (472.9 to 474.4 mbsf)
0-4 cm: Brownish gray calcareous sandy mudstone or sandy muddy limestone with dispersed clasts
4-134 cm: Gray clayey silty sand with dispersed clasts
134-140 cm: Brownish gray calcareous sandy mudstone or sandy muddy limestone with dispersed clasts

Core 61 missing.

62 CC (482.6 to 482.7 mbsf)
0-6 cm: Brownish gray calcareous sandy mudstone or sandy muddy limestone with dispersed clasts
6-8 cm: Gray clayey silty sand with dispersed clasts
8-13 cm: Missing

APPENDIX C: GEOCHEMICAL ANALYSIS

TABLES

ACCURACY AND PRECISION

Table C.1. Average normalized weight percent major element (oxide) values based on three runs and eight replicates for sample 1166R1 104-106. Accuracy (%RSE) and precision ([2 X STDV/AVG] X 100) is shown.

	SiO2	TiO2	Al2O3	Fe2O3	MnO	MgO	CaO	Na2O	K2O	P2O5
Average	70.35	0.76	18.14	5.30	0.03	1.57	0.62	0.56	2.50	0.13
Standard Dev	0.431	0.007	0.353	0.161	0.002	0.047	0.055	0.052	0.067	0.015
Standard Error	0.153	0.003	0.125	0.057	0.001	0.017	0.020	0.018	0.024	0.005
%RSE	0.22	0.34	0.69	1.07	2.89	1.06	3.17	3.29	0.94	3.95
Precision	1.23	1.92	3.89	6.06	16.32	6.01	17.93	18.63	5.33	22.36

Table C.2. Average normalized weight percent major element (oxide) values based on three runs and eight replicates for USGS geochemical reference standard MAG-1. Accuracy (%RSE) and precision ([2 X STDV/AVG] X 100) is shown.

	SiO2	TiO2	Al2O3	Fe2O3	MnO	MgO	CaO	Na2O	K2O	P2O5
Average	57.58	0.85	19.27	8.23	0.11	3.57	1.70	4.52	3.99	0.18
Standard Dev	0.668	0.013	0.402	0.126	0.003	0.062	0.054	0.089	0.088	0.017
Standard Error	0.236	0.005	0.142	0.045	0.001	0.022	0.019	0.031	0.031	0.006
%RSE	0.41	0.55	0.74	0.54	0.88	0.61	1.12	0.70	0.78	3.26
Precision	2.32	3.12	4.18	3.06	4.97	3.47	6.35	3.94	4.40	18.45

SAMPLE MAJOR AND TRACE ELEMENTS

Table C.3. Normalized weight percent of major elements (oxides) for seven samples selected from ODP Sites 739, 742, and 1166

	1166 24R2 29-31	1166 16R1 104-106	742 34R6 72-74	742 28R1 58-60	742 22R2 103-105	739 55R2 10-12	739 32R1 99-101
SiO2	66.13	70.64	65.83	75.10	73.12	71.02	72.99
TiO2	0.85	0.75	0.98	0.76	0.77	0.71	0.71
Al2O3	24.21	18.04	24.24	14.12	15.71	14.00	13.28
Fe2O3	3.06	5.27	3.40	4.17	4.70	5.08	5.14
MnO	0.02	0.02	0.02	0.04	0.04	0.13	0.06
MgO	0.44	1.56	0.68	0.97	1.14	1.15	2.03
CaO	0.22	0.55	0.21	0.46	0.40	4.00	1.24
Na2O	0.38	0.52	0.37	0.63	0.52	0.52	1.18
K2O	4.60	2.54	4.18	3.65	3.50	3.27	3.25
P2O5	0.09	0.11	0.09	0.10	0.09	0.10	0.12
Total	100.00	100.00	100.00	100.00	100.00	100.00	100.00

Table C.4. Trace elements (ppm) for seven samples selected from ODP Sites 739, 742, and 1166

	1166 24R2 29-31	1166 16R1 104-106	742 34R6 72-74	742 28R1 58-60	742 22R2 103-105	739 55R2 10-12	739 32R1 99-101
Ba	774.79	511.60	982.03	724.56	706.85	663.56	1095.13
Cr	98.82	107.04	99.19	57.34	73.34	99.26	70.47
Ni	28.41	47.34	35.65	37.90	36.58	40.37	29.44
Sc	15.31	14.00	16.77	10.69	11.81	13.86	12.36
Sr	137.08	121.74	170.56	132.68	129.71	154.05	123.04
V	135.10	111.43	151.89	81.28	86.33	113.65	85.12
Y	27.56	27.64	33.53	29.65	28.31	29.99	26.59
Zr	368.61	161.73	410.81	261.79	214.98	254.97	246.89

APPENDIX D: MICROTEXTURE ANALYSIS

TABLES

Table D.1. Ranked counts of grain shape and surface textures for quartz grains from seven samples recovered from ODP Sites 1166, 742, and 739. Sphericity ranked 1-2 and roundness ranked 1-6 per Powers (1953), and mechanical/chemical textures ranked 1-4 per Newsome and Ladd (1999).

	Rank	Grain Shape		Mechanical Textures												Chemical Textures			
		sphericity	roundness	small conchoidal fractures	large conchoidal fractures	straight steps	arcuate steps	large breakage blocks	fractured plates	edge abrasion	mechanical/impact pits	straight grooves	curved grooves	irregular depressions	cracks	rounded edges	solution pits	adhering particles	silica precipitation overgrowths
1166L	1	26	0	12	12	19	20	21	35	19	12	17	21	12	17	6	6	2	5	26
1166 24R2	2	14	8	24	23	18	18	15	5	17	24	23	19	18	23	17	23	26	18	12
29-31	3		22	4	4	2	2	4	0	4	4	0	0	10	0	16	8	12	12	2
	4		9	0	1	1	0	0	0	0	0	0	0	0	0	1	3	0	5	0
	5		1																	
	6		0																	
1166U	1	23	0	9	14	22	17	27	31	25	10	28	29	19	30	2	0	1	0	19
1166 16R1	2	17	1	22	15	16	20	13	8	15	28	11	11	20	10	17	17	38	6	21
104-106	3		26	9	11	2	3	0	1	0	2	1	0	1	0	21	21	1	24	0
	4		13	0	0	0	0	0	0	0	0	0	0	0	0	0	2	0	10	0
	5		0																	
	6		0																	
742L	1	28	0	10	18	22	23	15	28	16	7	23	28	7	23	5	1	1	0	25
742 34R6	2	12	4	16	11	18	17	22	12	21	29	16	12	27	17	20	19	30	9	15
72-74	3		28	14	11	0	0	3	0	3	4	1	0	6	0	14	16	7	10	0
	4		8	0	0	0	0	0	0	0	0	0	0	0	0	1	4	2	21	0
	5		0																	
	6		0																	
742M	1	27	1	6	11	21	30	14	12	18	0	9	22	18	5	2	0	8	0	32
742 28R1	2	13	0	31	24	18	10	26	26	22	40	31	18	22	35	13	10	32	2	8
58-60	3		36	2	4	1	0	0	2	0	0	0	0	0	0	25	29	0	11	0
	4		3	1	1	0	0	0	0	0	0	0	0	0	0	0	1	0	27	0
	5		0																	
	6		0																	
742U	1	23	0	5	8	23	21	24	10	13	0	18	33	15	5	0	0	0	0	15
742 22R2	2	11	1	26	19	11	13	10	24	21	32	16	1	19	29	29	20	21	0	19
103-105	3		30	3	7	0	0	0	0	0	2	0	0	0	0	4	14	13	6	0
	4		2	0	0	0	0	0	0	0	0	0	0	0	0	1	0	0	28	0
	5		1																	
	6		0																	
739L	1	31	0	14	15	26	23	19	12	3	0	9	20	12	9	5	0	2	0	20
739 55R2	2	9	2	23	20	14	14	19	26	34	40	31	20	28	31	23	11	38	0	19
10-12	3		30	3	5	0	3	2	2	3	0	0	0	0	0	5	29	0	9	1
	4		8	0	0	0	0	0	0	0	0	0	0	0	0	7	0	0	31	0
	5		0																	
	6		0																	
739U	1	32	0	7	14	16	16	9	4	1	0	0	16	0	3	2	0	4	0	8
739 32R1	2	7	2	30	17	22	22	30	34	35	39	39	23	39	36	11	5	35	2	28
99-101	3		30	2	7	1	1	0	1	3	0	0	0	0	0	25	34	0	3	3
	4		6	0	1	0	0	0	0	0	0	0	0	0	0	1	0	0	34	0
	5		1																	
	6		0																	

Table D.2. Ranked counts of grain shape and surface textures converted to percentages for quartz grains from seven samples recovered from ODP Sites 1166, 742, and 739. "Sum 2-4" for mechanical/chemical textures is percent presence (frequency) of individual textures on surface of grain, where rank 1 for mechanical/chemical textures is effectively percent absence (less than 2% present in given surface area).

	Rank		Grain Shape			Mechanical Textures														Chemical Textures			
			sphericity	roundness		small conchoidal fractures	large conchoidal fractures	straight steps	arcuate steps	large breakage blocks	fractured plates	edge abrasion	mechanical/impact pits	straight grooves	curved grooves	irregular depressions	cracks	rounded edges		solution pits	adhering particles	silica precipitation	overgrowths
1166L	1		65	0		30	30	48	50	53	88	48	30	43	53	30	43	15		15	5	13	65
1166 24R2	2		35	20		60	58	45	45	38	13	43	60	58	48	45	58	43		58	65	45	30
29-31	3			55		10	10	5	5	10	0	10	10	0	0	25	0	40		20	30	30	5
	4			23		0	3	3	0	0	0	0	0	0	0	0	0	2.5		7.5	0	13	0
	5			3	Sum 2-4 ->	70	70	53	50	48	13	53	70	58	48	70	58	85		85	95	88	35
	6			0																			
1166U	1		58	0		23	35	55	43	68	78	63	25	70	73	48	75	5		0	2.5	0	48
1166 16R1	2		43	3		55	38	40	50	33	20	38	70	28	28	50	25	43		43	95	15	53
104-106	3			65		23	28	5	8	0	3	0	5	2.5	0	2.5	0	53		53	2.5	60	0
	4			33		0	0	0	0	0	0	0	0	0	0	0	0	0		5	0	25	0
	5			0	Sum 2-4 ->	78	65	45	58	33	23	38	75	30	28	53	25	95		100	98	100	53
	6			0																			
742L	1		70	0		25	45	55	58	38	70	40	18	58	70	18	58	13		2.5	2.5	0	63
742 34R6	2		30	10		40	28	45	43	55	30	53	73	40	30	68	43	50		48	75	23	38
72-74	3			70		35	28	0	0	8	0	8	10	2.5	0	15	0	35		40	18	25	0
	4			20		0	0	0	0	0	0	0	0	0	0	0	0	2.5		10	5	53	0
	5			0	Sum 2-4 ->	75	55	45	43	63	30	60	83	43	30	83	43	88		98	98	100	38
	6			0																			
742M	1		68	3		15	28	53	75	35	30	45	0	23	55	45	13	5		0	20	0	80
742 28R1	2		33	0		78	60	45	25	65	65	55	100	78	45	55	88	33		25	80	5	20
58-60	3			90		5	10	3	0	0	5	0	0	0	0	0	0	63		73	0	28	0
	4			8		3	3	0	0	0	0	0	0	0	0	0	0	0		2.5	0	68	0
	5			0	Sum 2-4 ->	85	73	48	25	65	70	55	100	78	45	55	88	95		100	80	100	20
	6			0																			
742U	1		68	0		15	24	68	62	71	29	38	0	53	97	44	15	0		0	0	0	44
742 22R2	2		32	3		76	56	32	38	29	71	62	94	47	3	56	85	85		59	62	0	56
103-105	3			88		9	21	0	0	0	0	0	5.9	0	0	0	0	12		41	38	18	0
	4			6		0	0	0	0	0	0	0	0	0	0	0	0	2.9		0	0	82	0
	5			3	Sum 2-4 ->	85	76	32	38	29	71	62	100	47	3	56	85	100		100	100	100	56
	6			0																			
739L	1		78	0		35	38	65	58	48	30	8	0	23	50	30	23	13		0	5	0	50
739 55R2	2		23	5		58	50	35	35	48	65	85	100	78	50	70	78	58		28	95	0	48
10-12	3			75		8	13	0	8	5	5	8	0	0	0	0	0	13		73	0	23	3
	4			20		0	0	0	0	0	0	0	0	0	0	0	0	18		0	0	78	0
	5			0	Sum 2-4 ->	65	63	35	43	53	70	93	100	78	50	70	78	88		100	95	100	50
	6			0																			
739U	1		82	0		18	36	41	41	23	10	3	0	0	41	0	8	5.1		0	10	0	21
739 32R1	2		18	5		77	44	56	56	77	87	90	100	100	59	100	92	28		13	90	5.1	72
99-101	3			77		5	18	3	3	0	3	8	0	0	0	0	0	64		87	0	7.7	8
	4			15		0	3	0	0	0	0	0	0	0	0	0	0	2.6		0	0	87	0
	5			3	Sum 2-4 ->	82	64	59	59	77	90	97	100	100	59	100	92	95		100	90	100	79
	6			0																			